

**A MECHANISTIC-EMPIRICAL APPROACH FOR EVALUATING THE EFFECT OF
DIAMOND GRINDING AND THIN OVERLAY ON PREDICTED PAVEMENT
PERFORMANCE**

By

Ronell Joseph H. Eisma

A THESIS

Submitted to
Michigan State University
in partial fulfillment of the requirements
for the degree of

Civil Engineering - Master of Science

Spring 2016

ABSTRACT

A MECHANISTIC-EMPIRICAL APPROACH FOR EVALUATING THE EFFECT OF DIAMOND GRINDING AND THIN OVERLAY ON PREDICTED PAVEMENT PERFORMANCE

By

Ronell Joseph H. Eisma

Advancements in pavement management practice require evaluating the performance of pavement preservation treatments using performance-related characteristics. However, state highway agencies face the challenge of developing performance-based relationships between quality characteristics of pavement preservation treatments and expected pavement performance. The objective of this study is to develop and evaluate a mechanistic-empirical procedure which can be used to relate the performance of surface smoothing pavement preservation treatments to a roughness-related, profile-based index. The profiles for pavement sections treated with diamond grinding and thin overlay treatments were obtained and the impact of these treatments on roughness was evaluated using the International Roughness Index (IRI) and the Dynamic Load Index (DLI). The effects of these treatments on the pavement profile, the dynamic loads experienced by the pavement, and predicted pavement performance were also observed. Using the proposed mechanistic-empirical procedure, the results of this study demonstrate that is possible to relate changes in IRI and DLI, as a result of surface smoothing treatments, to the expected pavement performance. The performance-based relationships obtained from this procedure can be used in the development of performance-related specifications.

For those whom I believe, believe in me.

TABLE OF CONTENTS

LIST OF TABLES	vi
LIST OF FIGURES	viii
CHAPTER 1: Introduction	1
1.1 Background	1
1.2 Performance specifications	1
1.3 Developing performance-based relationships	2
1.4 Pavement roughness indices	3
1.5 Problem statement, hypothesis, and objectives	4
1.6 Scope	5
CHAPTER 2: Literature Review	7
2.1 Pavement preservation and smoothing treatment performance	7
2.2 Studies on the impact of heavy vehicle characteristics on pavement damage	9
2.3 Dynamic load simulation	14
2.4 Evaluating pavement profile characteristics and surface roughness	16
2.5 Mechanistic-empirical pavement performance analysis	19
2.6 Mechanistic-empirical procedure for developing performance-based relationships ..	21
2.7 Long term pavement performance database	23
CHAPTER 3: Data Synthesis	25
3.1 Pavement section selection	25
3.2 Collection of pavement properties	27
CHAPTER 4: Data Analysis	32
4.1 Procedure for evaluating the change in profile roughness index	34
4.2 Simulating axle load spectra representative of WIM data	35
4.3 Simulating dynamic axle loads using TruckSim	37
4.4 Procedure for predicting pavement performance using MEPDG	40
4.5 Summary of data analysis procedure	43
CHAPTER 5: Diamond Grinding Results and Discussion	44
5.1 Effect of diamond grinding on pavement profile	44
5.2 Effect of diamond grinding on pavement dynamic load	48
5.3 Effect of diamond grinding on predicted pavement performance	52
CHAPTER 6: Thin Overlay Results and Discussion	59
6.1 Effect of thin overlay on pavement profile	59
6.2 Effect of thin overlay on pavement dynamic load	63

6.3 Effect of thin overlay on predicted pavement performance.....	67
CHAPTER 7: Summary, Conclusions, Recommendations	74
7.1 Summary of findings.....	74
7.2 Conclusions.....	78
7.3 Recommendations.....	81
APPENDICES	84
Appendix A Concrete pavement profile elevations and PSD	85
Appendix B Asphalt pavement profile elevations and PSD	93
Appendix C Concrete pavement dynamic axle load spectra	100
Appendix D Asphalt pavement dynamic axle load spectra	105
Appendix E Concrete pavement predicted performance	110
Appendix F Asphalt pavement predicted performance	118
REFERENCES	122

LIST OF TABLES

Table 2.1: Tractor semi-trailer properties evaluated by Gillespie et al. (8, 19).....	11
Table 2.2: Impact of truck properties on pavement damage (8).....	12
Table 2.3: Impact of site factors on pavement damage (8).....	13
Table 2.4: LTPP GPS experiments (34)	24
Table 2.5: LTPP SPS experiments (34)	24
Table 3.1: LTPP SDR 28.0 data sources.....	30
Table 3.2: Summary of concrete pavement sections used in analysis	31
Table 3.3: Summary of asphalt pavement sections used in analysis	31
Table 4.1: Threshold values for determining SLE.....	42
Table 5.1: Summary of concrete pavement sections used in analysis	44
Table 5.2: Change in DLC of single axle load spectra due to diamond grinding.....	49
Table 5.3: Validation of single axle Cl. 9 loads for diamond grinding	49
Table 5.4: Change in DLC of tandem axle load spectra due to diamond grinding.....	50
Table 5.5: Validation of tandem axle Cl. 9 loads for diamond grinding	50
Table 5.6: Count of diamond ground pavement sections by SLE performance	53
Table 6.1: Summary of asphalt pavement sections used in analysis	59
Table 6.2: Change in DLC of single axle load spectra due to thin overlay	64
Table 6.3: Validation of single axle Cl. 9 loads for thin overlay.....	65
Table 6.4: Change in DLC of tandem axle load spectra due to thin overlay	65
Table 6.5: Validation of tandem axle Cl. 9 loads for thin overlay.....	65

Table 6.6: Count of thin overlain pavement sections by SLE performance	68
------------------------------------------------------------------------------	----

LIST OF FIGURES

Figure 2.1: Rigid body model of tractor-semitrailer (8)	15
Figure 3.1: Summary count of sections to be shortlisted ¹	25
Figure 3.2: Shortlisted count of pavement sections used in data analysis	27
Figure 4.1: General procedure for mechanistic-empirical analysis	34
Figure 4.2: General example for SLE calculation	42
Figure 5.1: IRI before and after diamond grinding	45
Figure 5.2: DLI before and after diamond grinding	46
Figure 5.3: IRI versus DLI for all diamond ground sections	46
Figure 5.4: Section 42-3044 change in profile elevations due to diamond grinding	47
Figure 5.5: Section 42-3044 change in PSD due to diamond grinding	47
Figure 5.6: Section 27-3009 change in profile elevations due to diamond grinding	47
Figure 5.7: Section 27-3009 change in PSD due to diamond grinding	48
Figure 5.8: Roughness index vs change in DLC of tandem axles for diamond grinding	51
Figure 5.9: Roughness index vs change in DLC of tandem axles for diamond grinding	51
Figure 5.10: Section 42-3044 change in simulated dynamic axle loads due to diamond grinding	52
Figure 5.11: Section 27-3009 change in simulated dynamic axle loads due to diamond grinding	52
Figure 5.12: Effect of diamond grinding on predicted faulting performance	56
Figure 5.13: Effect of diamond grinding on predicted cracking performance	57

Figure 5.14: Effect of diamond grinding on predicted roughness	57
Figure 5.15: Comparison of effective and ineffective diamond grinding treatment.....	58
Figure 6.1: IRI before and after thin overlay	60
Figure 6.2: DLI before and after thin overlay	60
Figure 6.3: IRI versus DLI for all diamond ground sections	61
Figure 6.4: Section 49-A310 change in profile elevations due to thin overlay	62
Figure 6.5: Section 49-A310 change in PSD due to thin overlay	62
Figure 6.6: Section 32-B310 change in profile elevations due to thin overlay.....	63
Figure 6.7: Section 32-B310 change in PSD due to thin overlay	63
Figure 6.8: Roughness index vs change in DLC of single axles for thin overlay.....	66
Figure 6.9: Roughness index vs change in DLC of tandem axles for thin overlay	66
Figure 6.10: Section 49-A310 change in simulated dynamic axle loads for thin overlay	67
Figure 6.11: Section 32-B310 change in simulated dynamic axle loads for thin overlay	67
Figure 6.12: Effect of thin overlay on predicted rutting performance	71
Figure 6.13: Effect of thin overlay on predicted roughness performance	72
Figure 6.14: Comparison of effective and ineffective thin overlay treatment.....	73
Figure A.1: 6-3010 profile analysis results.....	85
Figure A.2: 13-3017 profile analysis results.....	85
Figure A.3: 27-4050 profile analysis results.....	86
Figure A.4: 42-3044 profile analysis results.....	86
Figure A.5: 46-3010 profile analysis results.....	87
Figure A.6: 55-3009 profile analysis results.....	87
Figure A.7: 4-7614 profile analysis results.....	88

Figure A.8: 16-3017 profile analysis results	88
Figure A.9: 49-C431 profile analysis results	89
Figure A.10: 8-3032 profile analysis results	89
Figure A.11: 27-3009 profile analysis results	90
Figure A.12: 38-3006 profile analysis results	90
Figure A.13: 42-9027 profile analysis results	91
Figure A.14: 20-3015 profile analysis results	91
Figure A.15: 31-3028 profile analysis results	92
Figure A.16: 39-9006 profile analysis results	92
Figure B.1: 16-B310 profile analysis results	93
Figure B.2: 16-C310 profile analysis results	93
Figure B.3: 53-A310 profile analysis results	94
Figure B.4: 20-B310 profile analysis results	94
Figure B.5: 4-C310 profile analysis results	95
Figure B.6: 4-A310 profile analysis results	95
Figure B.7: 32-B310 profile analysis results	96
Figure B.8: 49-A310 profile analysis results	96
Figure B.9: 49-B310 profile analysis results	97
Figure B.10: 17-B310 profile analysis results	97
Figure B.11: 53-C310 profile analysis results	98
Figure B.12: 18-A310 profile analysis results	98
Figure B.13: 20-A310 profile analysis results	99
Figure B.14: 32-A310 profile analysis results	99

Figure C.1: 6-3010 95 th percentile axle load spectra	100
Figure C.2: 13-3017 95 th percentile axle load spectra	100
Figure C.3: 27-4050 95 th percentile axle load spectra	100
Figure C.4: 42-3044 95 th percentile axle load spectra	101
Figure C.5: 46-3010 95 th percentile axle load spectra	101
Figure C.6: 55-3009 95 th percentile axle load spectra	101
Figure C.7: 4-7614 95 th percentile axle load spectra	102
Figure C.8: 16-3017 95 th percentile axle load spectra	102
Figure C.9: 49-C431 95 th percentile axle load spectra.....	102
Figure C.10: 8-3032 95 th percentile axle load spectra	103
Figure C.11: 27-3009 95 th percentile axle load spectra	103
Figure C.12: 38-3006 95 th percentile axle load spectra	103
Figure C.13: 42-9027 95 th percentile axle load spectra	104
Figure C.14: 31-3028 95 th percentile axle load spectra	104
Figure C.15: 39-9006 95 th percentile axle load spectra	104
Figure D.1: 16-B310 95 th percentile axle load spectra	105
Figure D.2: 16-C310 95 th percentile axle load spectra	105
Figure D.3: 53-A310 95 th percentile axle load spectra	105
Figure D.4: 20-B310 95 th percentile axle load spectra	106
Figure D.5: 4-C310 95 th percentile axle load spectra	106
Figure D.6: 4-A310 95 th percentile axle load spectra	106
Figure D.7: 32-B310 95 th percentile axle load spectra	107
Figure D.8: 49-A310 95 th percentile axle load spectra	107

Figure D.9: 49-B310 95 th percentile axle load spectra	107
Figure D.10: 17-B310 95 th percentile axle load spectra	108
Figure D.11: 53-C310 95 th percentile axle load spectra	108
Figure D.12: 18-A310 95 th percentile axle load spectra	108
Figure D.13: 20-A310 95 th percentile axle load spectra	109
Figure D.14: 32-A310 95 th percentile axle load spectra	109
Figure E.1: 6-3010 predicted performance	110
Figure E.2: 13-3017 predicted performance	110
Figure E.3: 27-4050 predicted performance	111
Figure E.4: 42-3044 predicted performance	111
Figure E.5: 46-3010 predicted performance	112
Figure E.6: 55-3009 predicted performance	112
Figure E.7: 4-7614 predicted performance	113
Figure E.8: 16-3017 predicted performance	113
Figure E.9: 49-C431 predicted performance	114
Figure E.10: 8-3032 predicted performance	114
Figure E.11: 27-3009 predicted performance	115
Figure E.12: 38-3006 predicted performance	115
Figure E.13: 42-9027 predicted performance	116
Figure E.14: 20-3015 predicted performance	116
Figure E.15: 31-3028 predicted performance	117
Figure E.16: 39-9006 predicted performance	117
Figure F.1: 16-B310 predicted performance.....	118

Figure F.2: 16-C310 predicted performance.....	118
Figure F.3: 53-A310 predicted performance	118
Figure F.4: 20-B310 predicted performance.....	118
Figure F.5: 4-C310 predicted performance.....	119
Figure F.6: 4-A310 predicted performance	119
Figure F.7: 32-B310 predicted performance.....	119
Figure F.8: 49-A310 predicted performance	119
Figure F.9: 49-B310 predicted performance.....	120
Figure F.10: 17-B310 predicted performance.....	120
Figure F.11: 53-C310 predicted performance.....	120
Figure F.12: 18-A310 predicted performance	120
Figure F.13: 20-A310 predicted performance	121
Figure F.14: 32-A310 predicted performance	121

CHAPTER 1: Introduction

1.1 Background

The development and connection of large scale pavement networks is integral in streamlining nationwide commerce and communication. The challenge for highway agencies exists in the maintenance and repair of these pavement networks while maintaining serviceability for all road users. The significant costs associated with pavement reconstruction and rehabilitation has highlighted the need to practice pavement preservation, which incorporates low-cost preventive maintenance strategies in pavement network management plans. Currently, agencies in the United States and Canada are striving to extend the knowledge found in research of sustainable highway practice beyond construction and into pavement preservation and maintenance (1).

Highway agencies are interested in developing a suite of pavement performance indicators that can be used to predict pavement preservation treatment performance. Since preservation treatments that are used correctly can be more cost-effective than rehabilitation or reconstruction, most highway agencies now implement sophisticated pavement management systems by developing curves to track and predict future conditions of a pavement. The general consensus in improving pavement management systems is to incorporate a performance-based funding policy where management decisions are based on pavement performance, and that performance measures are quantifiable and outcome-driven (2).

1.2 Performance specifications

The shift to pavement preservation practice led to the development of performance specifications while minimizing management costs. The traditional approach to highway construction was the use of end-result specifications, i.e. the contractor performs the required

work based on predefined plans and specifications. However, the disadvantage of this approach is that the majority of the risk associated with construction lies with the agency while failing to incentivize the contractor to deliver better quality work than prescribed (3, 4). To address this issue, highway agencies started implementing performance specifications in highway construction. These specifications are based on performance-related parameters that are typically measurable during construction, and relax the requirements on construction methods to give the contractor freedom to achieve the desired specifications. The contractor is then awarded a payment equivalent to the quality of the work achieved, and can also be incentivized for work above quality or receive reduced pay for poor quality work. Such pay adjustments are substantiated by the performance-based relationships developed as part of the specification.

1.3 Developing performance-based relationships

There is a lack of widely accepted guidelines for establishing these specifications for preservation treatments. A typical performance specification will describe desired levels or thresholds of key material and construction characteristics that are correlated with fundamental engineering properties and can be used to predict performance (5, 6). Ideally, these characteristics are measurable at the time of construction, or in this case, application of a preservation treatment. However, pavement preservation treatments typically do not alter the structural capacity of the pavement structure and therefore limit the amount of quantifiable pavement characteristics which can be measured during construction. Therefore, it is important to not only identify a suitable quality characteristic that justifies the suitability of a preservation treatment, but also develop a quantifiable relationship between the characteristic and predicted or measured pavement performance.

1.4 Pavement roughness indices

Road surface roughness is a commonly monitored pavement characteristic that is used to evaluate the ride quality of pavements. Pavement roughness describes the variation of irregularities along the surface of the pavement in the longitudinal direction (7). Previous research has established that roughness is closely associated with vehicle operating costs as well as vehicle dynamic load experienced by pavements (8, 9). Therefore, if all other site factors remain constant, a pavement surface that maintains its smoothness over time is expected to: 1) reduce costs associated with maintenance and vehicle wear, 2) experience less load-related damage, and 3) ensure the safety and comfort of road users.

The development of profilographs and profilometers from the 1960s to early 1990s has long-since spurred the initiative of highway agencies to collect pavement profile data to assess pavement roughness and ensure the proper placement of asphalt and concrete pavements (10). Such efforts have resulted in the development of numerous profile-based indices based on vehicle response models. Such indices include the International Roughness Index (IRI) which is used by 84 percent of highway agencies to monitor smoothness over time (11). IRI is a response-based measure developed from passenger car. However, the significant impact of heavy vehicle load on pavement fatigue encouraged the development of a profile-based index which considers variations in pavement response due to dynamic truck loads. The Dynamic Load Index (DLI), was later developed to capture the variance in the frequencies of a pavement profile which are associated with vehicle and axle bounce of heavy vehicles (12).

1.5 Problem statement, hypothesis, and objectives

Pavement roughness is a metric that can be used to describe the effectiveness of pavement preservation treatments in improving surface smoothness. State of the practice surveys identify diamond grinding and thin asphalt overlay application as two common smoothening treatments (1). Profile-based indices IRI and DLI are used to quantify the change in roughness due to these treatments, and are proposed as candidate quality characteristics that may be related to predicted pavement performance.

If relationships can be established between the changes in the measureable quality of a pavement and the predicted performance of the same pavement, a comprehensive performance-related specification may be developed for surface smoothening preservation treatments. The evaluation to relate pavement roughness to predicted performance is done in this thesis by considering of the following hypotheses:

- A change in surface roughness will impact the dynamic load directly, that is, a reduction in roughness is expected to reduce dynamic loads experienced by the pavement, and vice versa.
- An approach that utilizes the change in dynamic load spectra to predict the change in pavement performance due a diamond grinding or thin overlay treatment can be developed.
- If the change in pavement performance can be quantified, it is possible that a relationship can be developed between a change in a profile-based index (IRI or DLI) and predicted performance measures associated with concrete and asphalt pavements.

In order to test the above hypotheses, the following objectives were met:

1. Extract profile elevation data from several pavement sections known to have experienced smoothing treatment and calculate the IRI and DLI before and after treatment to determine the change in roughness due to treatment.
2. Evaluate the change in dynamic load response before and after the treatment.
3. Determine the variations in profile characteristics before and after the treatment, i.e. physical profile elevation changes and profile signal variations
4. Develop a mechanistic-empirical procedure that uses the change in dynamic axle load for establishing a relationship between the change in roughness and a change in predicted performance due to both diamond grinding and thin overlay treatments.
5. Describe the results using the information obtained from profile analyses, and information related to material-related, construction, and climactic properties of pavement sections.

1.6 Scope

Chapter 1 of this thesis provides background information that describes the need for performance-based relationships for pavement preservation treatments for use in the development of performance-related specifications.

Chapter 2 documents a literature review that describes the concept of pavement preservation and highlights the need for developing relationships between preservation treatment quality characteristics and pavement performance. It also provides background on vehicle dynamics and the relationship with road roughness, and expands on the profile-based indices IRI and DLI. Chapter 2 also presents an overview of the mechanistic-empirical design guide,

including the types of inputs required for asphalt and concrete pavements, and where there exists a potential for introducing dynamic load spectra as inputs to evaluate a change in performance.

Chapter 3 provides a synthesis of the data obtained for the pavement profiles evaluated for this research and reasons for shortlisting the number of sections evaluated from a larger subset. The sections were obtained from the Long Term Pavement Performance (LTPP) monitoring database.

Chapter 4 describes the data analysis procedure adopted for this research. It includes the procedure for: 1) evaluating the change in roughness index, 2) simulating the dynamic load response of the pavement, and 3) predicting pavement performance using the dynamic axle load.

Chapters 5 and 6 present the results of the analysis and discussion of results for diamond grinding and thin overlay treatments, respectively. For each chapter, the comparison of IRI and DLI relationships with performance are shown, and the results are discussed.

Chapter 7 summarizes the findings of this research and discusses the potential for using the relationships developed between profile-based roughness-related indices and pavement performance in performance-related specifications for pavement preservation treatments.

The Appendix contains the following for all pavement sections: (1) before and after treatment pavement profiles and PSDs, (2) before and after treatment single and tandem dynamic axle load spectra, 3) before and after treatment of MEPDG performance prediction results.

CHAPTER 2: Literature Review

2.1 Pavement preservation and smoothening treatment performance

Pavement preservation is a proactive approach for managing existing pavements and involves applying preventive treatments or actions on a pavement in the early stage of its life. An effective preservation program can extend the life of a pavement network, improve network-level pavement performance, reduce user and agency costs, and ensure road safety for the public (13). There are numerous factors that can impact the performance of preservation treatments, including traffic levels, climate, and pavement condition. These factors are part of the treatment selection criteria used by highway agencies (14). An increase in repeated loads can accelerate the propagation of load-related distresses on the pavement. As a result, a pavement that is unable to withstand expected traffic will lead to an ineffective use of pavement preservation treatments. Climate is another site factor which can impact treatment performance since pavement materials are susceptible to changes in the environment. Emulsion-based treatments are especially sensitive to temperature and humidity, and weather-related effects such as precipitation or extreme temperatures can contribute to pavement failure (14). The existing pavement conditions also have a significant impact on preservation treatment performance. Since the concept of preservation is to apply a treatment when the pavement is in good condition, incorrect treatment timing can result in poor performance (13). It is important to consider these site factors when examining and explaining the performance of preservation treatments.

Pavement performance measures can be structural or functional in nature. The former measures are associated with pavement distresses which compromise the structural capacity of the pavement system as a whole. The latter measures are related to ride quality and road user safety associated with surface smoothness and friction (15). Since preservation treatments do not

significantly modify the structural capacity of a pavement, the quality characteristics used to determine treatment effectiveness are based on the functional properties of pavement. The ride quality of a pavement is a commonly measured property to describe and monitor the surface roughness of pavements. Although numerous preservation treatments can impact the ride quality of a pavement, two common treatments that are specifically designed to provide a smoother pavement surface are diamond grinding and thin overlay for concrete and asphalt pavements, respectively.

The diamond grinding procedure removes a thin layer ($3/16$ to $1/4$ inches) from the surface of jointed plain concrete pavement (JPCP) using diamond saw blades. This treatment results in a smooth, level surface and generally reduces surface noise while improving surface friction. Although diamond grinding can reduce the roughness caused by excessive faulting at joints, faulting will most likely reoccur if the load transfer at joints is not restored (*14*). Thin overlay treatments involve placing a thin hot-mix asphalt layer (0.75 to 1.5 inches thick) composed of asphalt binder and aggregate over an existing pavement surface (*14*). This treatment is used to address surface conditions including minor cracking, raveling, friction loss, bleeding, and primarily roughness. The asphalt overlay renews the pavement surface and is expected to reduce roughness and improve ride quality, but the performance of asphalt material can vary depending on the mix design, the climate in which the pavement is located, and the severity of the existing distresses.

Surveys of current practice indicate that the typical ranges of life extension are 8 to 15 years for diamond grinding and 3 to 23 years for thin overlay (*14, 16, 17*). The large ranges of service life extension may be attributed to the dependence of these treatments on the site factors mentioned previously. Diamond grinding and thin overlay treatments are applied primarily to

improve the functional performance of a pavement in terms of surface roughness. However, early research in pavement dynamics demonstrated that level of roughness of a pavement can be related to the amount of dynamic load it experiences, which can be linked fatigue or load-related damage.

2.2 Studies on the impact of heavy vehicle characteristics on pavement damage

Numerous past research efforts have established that the characteristics of heavy vehicles are significant contributors to the progression of various pavement distresses. This is an important consideration because the vast amount of traffic on national roadways consists of heavy truck traffic. Early vehicle population surveys conducted by Cebon et al. found that although tractor-semitrailers represent about 30 percent of all registered heavy vehicles in the United States, these same trucks compose approximately 70 percent of heavy truck highway mileage (18). Common tractor semi-trailer configurations range from three to five axles and can be categorized in Federal Highway Administration (FHWA) heavy vehicle Classes 6 through 9 (19). From the late 1980s onward, the prevalence of heavy truck traffic on roadway networks led to progressive research efforts to describe the pavement damaging impacts of dynamic load caused by heavy vehicles. Several of the early theoretical studies related vehicles and road surface interactions using two analysis groups: “whole-life models” (20, 21) and “single vehicle pass” (18, 22-24) evaluations.

The studies performed using “whole-life models” were validated using the AASHO road test. The “whole-life models” were used to predict pavement structure and surface profile deterioration due to applied dynamic wheel loads using empirical relationships between wheel loads and changes in road surface profile. Ullidtz et al. and Papagiannakis et al. successfully reproduced the AASHO results and Papagiannakis et al. found that the inclusion of dynamic



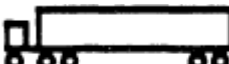
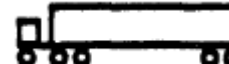
analysis considerably improved the accuracy of damage prediction (20, 21). Papagiannakis quantified that consideration of dynamic vehicle load added 17 to 22 percent theoretical damage caused by walking-beam truck suspensions and 6 to 8 percent additional damage caused by air truck suspensions. The studies performed by Monismith et al., O'Connell et al., and Cebon et al. incorporated the "single vehicle pass" analysis method to determine the incremental change in road damage due to one pass of a vehicle. Monismith found that the theoretical damage increase caused by dynamic loads for tandem suspensions when compared to the damage due to static wheel loads alone increased by 19 to 37 percent (22). O'Connell concluded that dynamic wheel loads typically resulted in up to 25 percent increase in theoretical pavement damage, which can be improved by careful suspension design (23). Cebon determined that dynamic wheel loads are most likely to have a greater influence on pavement fatigue life and asserted that road deterioration is governed by damage at the worst location (95th percentile) rather than the average value of the road surface (18, 24). Cebon further concluded that theoretical fatigue damage due to dynamic loads was found to be up to four times that of the damage due to static loads at the worst locations, under conditions of typical highway speeds and surface roughness.

A comprehensive study performed in 1992 by Gillespie, Karamihas, Cebon, et al. simulated vehicle and pavement interactions to determine the influence of truck and site properties on pavement fatigue and permanent deformation (rutting) (8). This study utilized analytical methods and existing mechanistic models of trucks and pavement structures to develop a comprehensive vehicle and roadway simulation system. This system provided a means to accurately model the complex interactions between truck, tire, and pavement properties to evaluate the impact of numerous truck and site factors on fatigue and rutting damage. For the purposes of evaluating the trends in pavement damage in response to truck characteristics, a

baseline matrix of fifteen truck configurations that represent the primary size and weight variables was established. A sample taken from this matrix of the properties for tractor-semitrailer trucks considered in the study evaluated by Gillespie et al. are summarized in Table 2.1. Tables 2.2 and 2.3 summarize the findings of this study with regards to the impact of various truck and site factors on pavement damage.

In this study, Gillespie et al concluded that the maximum axle loads on heavy vehicles are the primary contributors to fatigue damage on both rigid and flexible pavements (8). Truck steer axles in particular with more than 10 kip loads on conventional tires are more damaging than 20 kip axles on dual tires. Furthermore, the dynamic loads caused by interaction between the truck and pavement increased fatigue damage on rigid and flexible pavements. In the best conditions, the consideration of dynamic vehicle loads induced 25 to 50 percent more damage than static loads, and in the worst case scenarios, generated four times as much damage than that induced by static loads. (8). For most typical truck suspensions evaluated in the study, it was found that rough pavements experienced damage at a higher rate than smooth pavements.

Table 2.1: Tractor semi-trailer properties evaluated by Gillespie et al. (8, 19)

Truck configuration	Configuration name	FHWA Class	GVW (kips)	Axle loads (kips)	Wheelbases ¹ (feet)
	3-axle tractor-semitrailer	6	52	12/20/2020	10/36
	4-axle tractor-semitrailer	7	66	12/20/1934	12/36
	5-axle tractor-semitrailer	8	80	12/34/34	10/36
	5-axle tractor-semitrailer	9	80	14/33/33	10/36

¹Wheelbases to tandem centers where tandem spreads were set at 52 inches.

Table 2.2: Impact of truck properties on pavement damage (8)

Truck property	Impact on pavement fatigue and permanent deformation
Static axle load	Axle loads have the greatest impact on damage due to power-law relationship between load and fatigue. Relative fatigue damage varies with the assumed power law exponent but the axle load remains the dominant factor in impacting fatigue for all reasonable exponent values.
Gross vehicle weight (GVW)	Due to the linear relationship between permanent deformation and weight, GVW has a direct impact on rutting. Fatigue damage for both rigid and flexible pavement varies significantly over the range of GVWs examined, but the findings conclude fatigue is not systemically related to GVW but depends more on the maximum axle load on each vehicle combination.
Suspension type	The stiffness properties of single-axle suspension typically exhibit minimal variation which results in only a second-order influence on fatigue. Tandem axle dynamics have a much greater influence on fatigue of rigid and flexible pavements. In practice, tandem axles do not produce equivalent damage to two single axles with equivalent loads due to inequalities in static load sharing that cause disproportionate distribution of fatigue onto the heavily loaded axle. Suspension type has minimal impact on flexible pavement rutting.
Axle spacing	Rigid pavements benefit from closer spacing of axles within axle groups. Due to stress interactions between axles, rigid pavements experience a reduction in fatigue damage with a reduction in axle spacing. Flexible pavement fatigue and deformation damage are largely not sensitive to axle spacing.
Tire inflation pressure	Tire pressure has a moderate impact on rigid pavement fatigue and greatly impacts fatigue damage of flexible pavements. Tire inflation has a minimal influence on permanent deformation.
Tire configuration	The heavily loaded conventional tire on the steer axle is the configuration found to be the largest contributor to damage in both fatigue and permanent deformation.
Vehicle speed	Vehicle speed increases peak dynamic wheel loads on rigid pavements. Compared to the static loading case at zero speed, normal road speed (45 to 65 miles/hour) resulted in 1.5 to 2 times greater fatigue damage on a road of moderate roughness (160 inches/mile). For flexible pavements, the increase in dynamic load with increased speed was compensated by shorter duration of the applied axle load, resulting in fairly constant fatigue increase with speed for most cases. Rutting decreases at high speed due to decreasing load times.

Table 2.3: Impact of site factors on pavement damage (8)

Site factors	Impact on pavement fatigue and permanent deformation
Roughness	Road roughness excites truck axle loads and increases fatigue damage. Rough ¹ pavements increase serviceability damage at a rate 1.5 times greater than smooth ² pavements. Roughness does not significantly affect rutting damage on flexible pavements.
Pavement temperature	The temperature gradient in the slab contribute to curling stresses which can add to stress caused by moving vehicles. An increase in temperature gradient within rigid pavement slab of 1°F per slab inch increases fatigue damage by a factor of 10 over that of zero-gradient condition for most trucks. Pavement temperature greatly affects flexible pavement properties, particularly rutting damage which can increase with increasing temperature.
Layer thickness and subgrade strength	Pavement layer thicknesses and subgrade strength have a high influence on fatigue and rutting, comparable to the magnitude of influence of axle load on damage.

¹IRI = 240 inches/mile and ²IRI = 80 inches/mile

Previous vehicle dynamics studies concluded that the dynamic axle loads caused by heavy vehicles are influential contributors to the damage experienced by pavements and will play a key role in the prediction of pavement performance. Furthermore, the impact of dynamic loads on fatigue-related damage is exacerbated by an increase in pavement surface roughness. The study performed by Gillespie et al. did not establish functional relationships between the factors and damage due to the interaction between variables (8). The relative damage values determined for each variable may change if the nominal level of another variable is altered. However, it is important to consider the effect of such factors when developing performance-based relationships between pavement roughness and performance.

The many research efforts that evaluated the damage on roads due to dynamic loads required a measure of the magnitude of dynamic variation of heavy vehicle loads. Cebon et al. performed sensor studies of weigh-in-motion (WIM) load data of trucks and showed that, assuming “perfectly accurate” sensors, the expected standard deviation of the error in static load estimation for a wheel is the root mean squared of the dynamic tire force (25). The study later

performed by Gillespie, Karamihas, Cebon et al utilized a previously-established dimensionless variable known as the Dynamic Load Coefficient (8):

$$DLC = \frac{\sigma}{\bar{F}} \quad 2.1$$

Where σ is the standard deviation of the distribution of dynamic loads of a typical truck axle and \bar{F} is the mean of the same distribution. The DLC is a simple measure of the variation of dynamic axle loads for a specific combination of road roughness and speed. The axles of a truck moving on smoother road are theoretically expected to have DLC values nearer to zero (8).

2.3 Dynamic load simulation

As part of past research efforts to study the interactions between heavy vehicle loads and pavements, several computer models were developed to simulate the dynamic load response of trucks. Accurate modeling of heavy vehicle characteristics provides a means to simulate dynamic loads while retaining the freedom of adjusting vehicle properties to determine relationships between truck properties and pavement response. For the purpose of predicting dynamic load, Gillespie et al. considered the vehicle as several rigid bodies constituting lumped masses connected by compliant links (8). The suspension systems at each axle of the vehicle support the “primary mass”, or the “sprung mass”, which is considered rigid with mass properties located at the center of gravity and moment of inertia concentrated about the center of gravity in the pitch plane. The “unsprung masses” that are relevant to dynamic load are concentrated at each truck axle, consisting of the axle, brakes, steering knuckle, wheels, and portions of the suspension.

An example model of a 5-axle tractor-semitrailer truck is shown in Figure 2.1. As seen in this figure, the full vehicle consists of a spring-and-dashpot system connecting the sprung and unsprung masses. Together, the tractor and trailer sprung masses have three degrees of freedom:

bounce of the tractor, pitch of the tractor, and pitch of the trailer. Each of the axles also retains a bounce component, totaling eight degrees of freedom for the model presented in Figure 2.1. This model is treated as planar and allows only pitch rotation as seen by an observer from the side of the planar model.

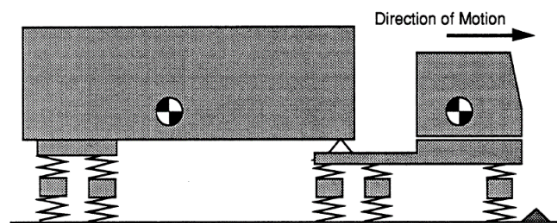


Figure 2.1: Rigid body model of tractor-semitrailer (8)

Several computer programs were developed to model relevant truck properties in order to simulate dynamic vehicle loads on pavements. The earliest models developed were NASTRAN, ADAMS, and DADS but were later deemed inefficient due to their generality (8). Research institutions such as MIT, the University of Cambridge, and the University of Michigan Transportation Research Institute (UMTRI) developed special-purpose programs that can evaluate a vehicle model with all pertinent degrees of freedom while eliminating extraneous ones to develop a more efficient modeling program. In particular is the UMTRI Pitch-Plane Model which evaluates all relevant parameters of vehicle behavior and is designed to accept measured road profiles as input (8). This model was intended to be a design tool for studying the effects of components of trucks on ride forces, including dynamic loads experienced by the pavement. UMTRI has since developed the original model for use in TruckSim™, a modern comprehensive tool which can simulate the dynamic behavior of heavy vehicles (26).

TruckSim is an integrated set of computer modeling tools that can simulate and analyze the dynamic behavior of trucks, busses, and tractor-trailer combinations under different test conditions (26). The software uses detailed nonlinear tire and spring models and major kinetic

and compliance relationships for the simulation of suspension and steering systems of heavy highway vehicles. Furthermore, the kinematic and dynamic equations established during the development of the software were determined to be valid for full nonlinear motion of rigid bodies. The main inputs of the software consist of truck properties such as axle configurations, axle loads, and vehicle speed, longitudinal profile elevations, and the type of simulation module. The two simulation modules present in the software are “2D Ride and Dynamic Pavement Load” and “3D Handling and Roll”. The 2D module predicts vehicle vibrations due to road roughness and the resulting dynamic pavement response due to those vibrations while the 3D module predicts directional and roll response to driver steering. This feature is pertinent to the development of performance-based relationships between roughness and pavement performance for the management of pavement networks. To conduct the analysis presented in this study, TruckSim version 3.2 was used and additional documentation was consulted which clearly outlines the simulation procedure (27).

2.4 Evaluating pavement profile characteristics and surface roughness

A measure of pavement surface condition was first introduced by the American Association of State Highway Officials (AASHO). This study concluded with the development of the present serviceability rating (PSR) and later the present serviceability index (PSI) (28). The PSR and PSI concepts relate pavement failure to public satisfaction of ride quality on a scale of 0 to 5, with 5 representing an ideal level of surface smoothness. These early findings encouraged research into evaluation of various roughness measurement methods to replicate the AASHO test results. Researchers concluded that the measurements of the different technologies could be unified under a single standardized roughness measurement, and this led to the development of the International Roughness Index (IRI) (29). The IRI was developed by measuring the response of a

quarter-car model in terms of suspension deflection and dividing it by the distance traveled, resulting in a profile index in units of slope that captures the magnitude of vertical change in elevation over the length of a profile. A higher IRI value indicates a rougher pavement, and vice versa. A survey of U.S. highway agencies conducted in 1999 found that 84 percent of agencies use IRI to monitor pavement smoothness over time, indicating its widespread acceptance as a pavement roughness measure (30).

IRI was originally designed using the response of passenger cars. However, as mentioned previously, the load due to heavy vehicles significantly influences pavement fatigue damage. In the early 1990s, studies performed by the OECD Scientific Expert Group IR6 established that the dynamic aspect of heavy vehicles, i.e. vehicle bounce and axle bounce, occur at specific frequency ranges of a pavement profile evaluated as a signal response (31). The findings of the OECD experiments showed that vehicle bounce occurs in the range of 1.5 to 4 Hz (22 to 59 feet at a speed of 60 miles per hour) and that axle bounce occurs between 8 and 15 Hz (6 to 11 feet at 60 miles per hour). Lee and Chatti developed a new roughness index called the Dynamic Load Index (DLI) that captures profile characteristics corresponding to these wavelengths which are responsible for the dynamic response of a pavement experiencing heavy vehicle loads (12). DLI is presented in the final calibrated form in Equation 2.2 below.

$$DLI = \sqrt{V_1 + 14V_2} \quad 2.2$$

Where V_1 is the variance of profile elevation in the frequency range of 1.5 to 4.0 Hz and V_2 is the variance of elevation in the frequency range of 8.0 to 15 Hz.

The DLI was designed to incorporate the truck response function and the power spectral density (PSD) of a surface profile to represent the standard deviation of truck response. A significant component of the research performed by Chatti et al. involved the signal-based

analysis of pavement profiles. Since the elevation changes in a profile represent response variations over time, these same elevations can be evaluated as random signals which are described by the profile itself or its associated statistical properties. The Power Spectral Density (PSD) function, used in early pavement dynamics studies (8, 32), utilizes the Fourier Transform technique to decompose the profile signal into a series of sine wave amplitudes. The PSD function represents the interaction of these amplitudes with spatial frequency, expressed as wave number in cycles per foot or wavelength. The PSD of any given length of road profile is unique, and describes how variance in amplitude is distributed over wave number.

The amplitude of the PSD can be expressed in terms of elevation or slope. The evaluation of the PSD in conjunction with variations in surface elevation can provide insight into changes in physical profile characteristics. Previous studies have determined that long wavelengths identified in a profile signal are indicative of high amplitude in the variation of elevations along a pavement profile (7, 8, 32). By examining the variations in in road profile PSD due to varying vehicle loads, Chatti et al. was able to evaluate the ability of DLI to describe the ranges of dynamic load experienced by a pavement in comparison to IRI as well as the agency-based Ride Quality Index (RQI) used by the Michigan Department of Transportation (MDOT). TruckSim vehicle modeling software was used to perform the simulations. Chatti et al found that variation in DLI correlated very well with dynamic loads, and was more effective at describing this variation than IRI or RQI. Therefore, DLI can be considered as profile-based roughness measurement index to supplement IRI in the development of performance-based relationships between road roughness, dynamic load, and predicted performance due to smoothening treatments. Furthermore, evaluating the signal-based characteristics of a profile can provide valuable insight into its behavior in response to heavy vehicle loads.

2.5 Mechanistic-empirical pavement performance analysis

The use of mechanistic-empirical pavement design over traditional empirical methods is advantageous for many reasons. Primarily, mechanistic-empirical design incorporates stress-strain responses which can better characterize pavement behavior and therefore increase design reliability. The AASHTO Mechanistic-Empirical Pavement Design Guide (MEPDG) is the established procedure for the mechanistic-empirical design and analysis of rigid and flexible pavement and led to the development of AASHTO MEPDG and AASHTOWare Pavement ME analysis software (33). MEPDG/Pavement ME software accepts a comprehensive suite of inputs that represent properties known to impact the performance of pavements which pertain to traffic, climate, construction material properties, and pavement geometry. A tool for predicting the performance of pavements is available through the use of MEPDG/Pavement ME software through accurate representation of key parameters pertaining to pavement structure and environment. The AASHTO design guide software accepts input values at three levels of detail (33):

- Level 1 – Very good knowledge of the desired pavement-related property
- Level 2 – Modest knowledge of the desired pavement-related property
- Level 3 – Poor knowledge of the desired pavement-related property

The levels represent how well a user can define characteristics related to pavement properties or environmental factors that are pertinent to the AASHTO models used to predict pavement performance. In order to accurately predict the performance of a designed pavement section, Level 1 and 2 inputs for construction, material, environment, and traffic must be utilized when possible.

High level inputs (1 or 2) for traffic characteristics are necessary for accurately evaluating the impact of surface smoothing treatments on pavement performance. The preservation treatments of interest in this study are diamond grinding and thin overlay, which are designed to reduce pavement surface roughness. This reduction in roughness is expected to cause a reduction in the dynamic load experienced by the pavement as concluded by previous studies on vehicle dynamics and truck-pavement interactions. If Level 1 or Level 2 traffic knowledge is present for truck traffic volumes and weights on a given pavement section, the incremental damage calculation utilizing expected traffic should increase in accuracy which will be reflected in pavement performance prediction. The following are the traffic data collected for the design procedure (33).

- Base year truck-traffic volume
- Vehicle operational speed
- Truck-traffic directional and lane distribution factors
- Vehicle class distribution
- Axle load distribution factors
- Axle and wheel base configurations
- Tire characteristics and inflation pressure
- Truck lateral distribution factor
- Truck growth factors

The TruckSim program described in Section 2.3 will simulate the dynamic response of a given axle load combination on a select pavement profile. The result of the TruckSim simulation is a series dynamic loads which represent the varying dynamic response of each axle in the model vehicle along the pavement profile. This subset is the dynamic response for a single pass for a

truck with a unique axle load combination. As discussed, Cebon et al. concluded the road damage is governed by the worst location (95th percentile) as opposed to the average value of the road surface. Therefore, it is reasonable to assume that the 95th percentile of the dynamic loads simulated by TruckSim is adequately representative of damage caused by the vast range of dynamic response simulated along the pavement.

2.6 Mechanistic-empirical procedure for developing performance-based relationships

Based on the MEPDG/Pavement ME design procedures and the known impact of heavy vehicle loads on pavement damage, a mechanistic-empirical procedure is proposed for evaluating the change in dynamic load on the pavement due to surface smoothing treatment. This procedure is outlined below:

1. Obtain the raw elevation profile data for a pavement section known to experience the desired surface treatments (diamond grinding or thin overlay), before and after the treatment was performed.
2. Collect detailed pavement axle load data from pavement monitoring databases that specify gross-vehicle weights or weights of axles observed on a pavement in the year of treatment, categorized into a series of axle load groups. This information provides a distribution of static axle loads applied to the pavement in the year of treatment.
3. Generate a new population of trucks of a reasonable, fixed number that are representative of the static axle load distribution in Step 2. It is necessary that the static axle loads obtained in Step 2 are defined by axle type since the TruckSim software accepts load inputs by individual types when modeling a vehicle.
4. Use each of the axle load combinations of the simulated population in Step 3 to perform multiple runs of the dynamic load simulation procedure in TruckSim. Each axle load

combination must be tested for dynamic response on the pavement profile in a “before treatment” state. Each axle load combination from the same population must then be re-tested on the pavement profile that corresponds to an “after treatment” state.

5. Synthesize the resulting dynamic load results of Step 4 into two sets of axle load spectra that represent the dynamic loads experienced by the pavement before and after the treatments. As determined by Cebon et al., it is appropriate to take the 95th percentile of the entire dynamic response of a single run to represent the dynamic axle loads for that specific truck (axle load combination). These 95th percentile axle loads can then be combined to create single and tandem axle load spectra.
6. Perform the MEPDG prediction analysis using the appropriate pavement material and environmental properties, while incorporating the single and tandem axle load spectra from Step 5 as inputs in the axle load distribution component of the software, i.e. predict pavement performance using dynamic loads before treatment and repeat the performance prediction for dynamic loads after treatment, keeping all other pavement properties constant. The slight variation in this procedure is for the case of simulating thin overlay treatment, where an additional layer of asphalt should be added to the pavement structure in MEPDG/Pavement ME that is equivalent to the thickness of the actual overlay applied on the section.
7. Observe and evaluate the change in predicted performance. A change in performance can be attributed to the change in axle load spectra. The change in axle load spectra is due to a change in pavement profile elevations, which correspond to change in pavement surface roughness. The potential exists for relating profile-indices which describe surface roughness (IRI, DLI) to pavement performance.

2.7 Long term pavement performance database

The LTPP program was established to study the behavior of pavement sections across the nation and evolved into a comprehensive pavement monitoring database maintained by the Federal Highway Administration (FHWA) (34). The LTPP database is organized into two main categories of study: General Pavement Studies (GPS) and Specific Pavement Studies (SPS). The fundamental difference between the two are that GPS studies consist of existing pavements while SPS experiments evaluated test sections using different treatment factors in comparison to a control section. A description of the GPS and SPS sections can be seen in Table 2.4 and 2.5.

In general, each GPS and SPS section is a 500-foot monitored portion with a 50-foot sampling section at each end (34). GPS test sections have a maintenance control zone 500-feet before the monitored section, and 250 feet beyond the monitoring section. The SPS sections consist of multiple treated sections in a single project, each 500-foot in length, and separated by a maintenance control zone between each treated segment. The pavement sections in the LTPP database have been constructed according to highway agency specifications and subjected to regular traffic loading. Therefore, the use of LTPP data from in-service pavements provides the advantage of realistic simulation of pavement performance when using the MEPDG/Pavement ME design approach that requires inputs of pavement construction, material, and site properties.

Table 2.4: LTPP GPS experiments (34)

GPS-1	Asphalt Concrete (AC) Pavement on Granular Base
GPS-2	Asphalt Concrete Pavement on Bound Base
GPS-3	Jointed Plain Concrete Pavement (JPCP)
GPS-4	Jointed Reinforced Concrete Pavement (JRCP)
GPS-5	Continuously Reinforced Concrete Pavement (CRCP)
GPS-6	Asphalt Concrete Overlay on AC Pavement
GPS-6A	Existing AC Overlay of AC Pavement (at the start of the program)
GPS-6B	AC Overlay Using Conventional Asphalt of AC Pavement–No Milling
GPS-6C	AC Overlay Using Modified Asphalt of AC Pavement–No Milling
GPS-6D	AC Overlay on Previously Overlaid AC Pavement Using Conventional Asphalt
GPS-6S	AC Overlay of Milled AC Pavement Using Conventional or Modified Asphalt
GPS-7	AC Overlay on PCC Pavement
GPS-7A	Existing AC Overlay on PCC Pavement
GPS-7B	AC Overlay Using Conventional Asphalt on PCC Pavement
GPS-7C	AC Overlay Using Modified Asphalt on PCC Pavement
GPS-7D	AC Overlay on Previously Overlaid PCC Pavement Using Conventional Asphalt
GPS-7F	AC Overlay Using Conventional or Modified Asphalt on Fractured PCC Pavement
GPS-7R	Concrete Pavement Restoration Treatments With No Overlay
GPS-7S	Second AC Overlay, Which Includes Milling or Geotextile Application, on PCC Pavement With Previous AC Overlay
GPS-9	Unbonded PCC Overlay on PCC Pavement

Table 2.5: LTPP SPS experiments (34)

SPS-1	Strategic Study of Structural Factors for Flexible Pavements
SPS-2	Strategic Study of Structural Factors for Rigid Pavements
SPS-3	Preventive Maintenance Effectiveness of Flexible Pavements
SPS-4	Preventive Maintenance Effectiveness of Rigid Pavements
SPS-5	Rehabilitation of AC Pavements
SPS-6	Rehabilitation of Jointed Portland Cement Concrete (JPCC) Pavements
SPS-7	Bonded PCC Overlays of Concrete Pavements
SPS-8	Study of Environmental Effects in the Absence of Heavy Loads
SPS-9P	Validation and Refinements of Superpave Asphalt Specifications and Mix Design Process
SPS-9A	Superpave Asphalt Binder Study
SPS-9C	AC overlay on CRCP
SPS-9J	AC overlay on JPCC
SPS-9N	New AC Pavement Construction

CHAPTER 3: Data Synthesis

3.1 Pavement section selection

The Long Term Pavement Performance (LTPP) database was used as the primary source of data for this study. The design of experiments in the LTPP database varied, and it was necessary to first identify the pavement sections which were treated with diamond grinding and thin overlay.

The first step was to narrow down the experiment evaluation to a reasonable subset of pavement sections on which diamond grinding and thin overlay were performed. Based on this criteria, the SPS 3, SPS 4, SPS 6, and JPCP and JRCP sections of the GPS experiments were evaluated.

Figure 3.1 shows the number of sections identified from these experiments that were known to be treated with thin overlay and diamond grinding, separated by LTPP climatic zone.

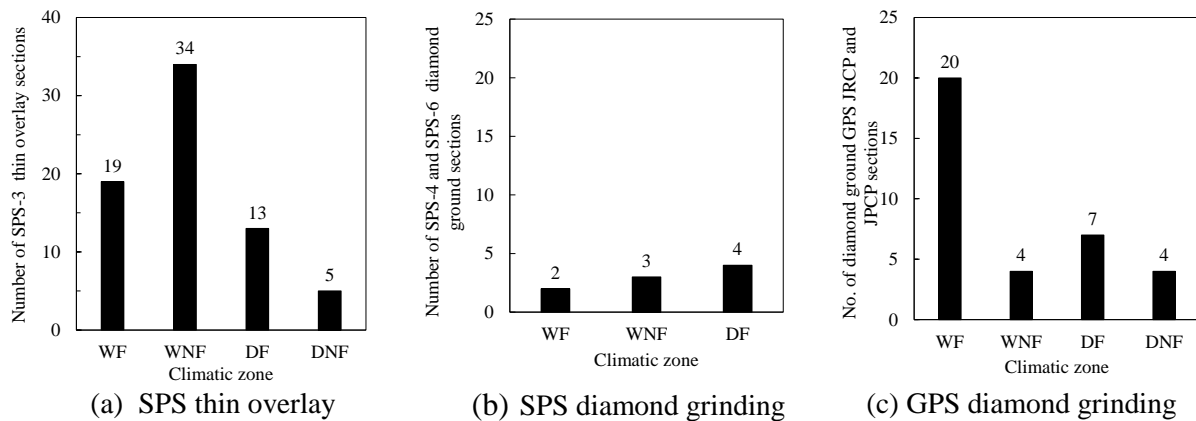


Figure 3.1: Summary count of sections to be shortlisted¹

¹WF, WNF, DF, DNF = Wet Freeze, Wet No-Freeze, Dry Freeze, Dry No-Freeze climate.

The pavement sections identified in Figure 3.1 were then shortlisted based on the following criteria:

1. The profile data must be available and in the *.erd file format. Profile monitoring data before and after the treatment were needed to evaluate the impact of the treatment on a change in pavement profile. The FHWA administration switched from DNC 690 profilers

to T-6600 profilers in 1996 to rectify this problem (35) but many of the raw profile data were difficult to interpret because of the archaic format.

2. The impact of other maintenance treatments must be minimized. An effort was made to select pavement sections where only diamond grinding and thin overlay were applied. This was not a difficult criterion to meet for thin overlay sections since the SPS-3 experiment was specifically designed to include segments solely treated with thin overlay. However, the first selection criterion significantly reduced the number of available pavement sections. As a result, to augment the number of rigid pavement sections evaluated, four sections were considered in the analysis provided that additional treatments were not substantial. These select few sections with additional treatments are summarized below:

- Section 13-3017 - grinding applied in May 2000 and “partial depth patching other than at joint” applied in May 2001, but no profile data were available between these time periods.
- Section 20-3015 - “transverse joint sealing”, “lane-shoulder longitudinal shoulder joint sealing” and “full depth transverse joint repair patch” were applied.
- Section 38-3006 - “joint load transfer restoration” was applied.
- Section 39-9006 - “full depth transverse joint repair patch” and “joint load transfer restoration” were applied.

3. The change in the monitored roughness before and after treatment is significant. Pavements that experienced little to no change in roughness were not considered in the analysis since these profiles may not significantly impact dynamic load. A few pavement sections were selected that showed an increase in roughness after treatment for the

potential to observe the impact of pavement properties or site characteristics on the change in dynamic load.

Figure 3.2 summarizes the number of pavement sections shortlisted from those identified in Figures 3.1.

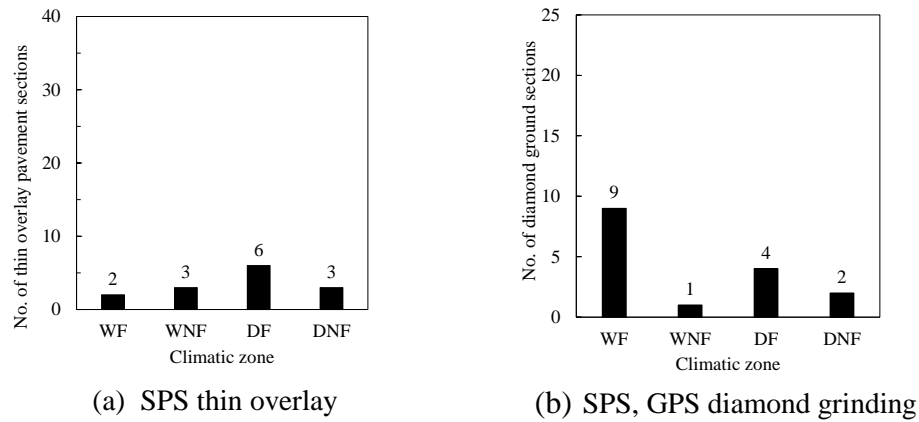


Figure 3.2: Shortlisted count of pavement sections used in data analysis

3.2 Collection of pavement properties

In order to perform the mechanistic-empirical procedure as proposed in Chapter 2, it was necessary to collect the appropriate profile, traffic, and construction data for each pavement section shortlisted in Figure 3.1. At the time this research was performed, the LTPP Standard Data Release number 28 (SDR 28.0) was used and the specific sources of obtained parameters are listed in Table 3.1. It was not always the case that the data required for the inputs into the mechanistic-empirical design was readily available. The LTPP data were evaluated to examine any shortcomings in availability to be addressed:

- Traffic - The MEPDG models require traffic volume adjustment factors and axle distributions for single, tandem, tridem, and quad axles as part of its inputs. This traffic data were available for all pavement sections in three main forms: weigh-in-motion (WIM), automatic vehicle classification (AVC) and vehicle counts. WIM data are presented as tabulated numbers of axles observed within axle groups, with each load

group covering a specific load interval. AVC data are the number of vehicles counted over time by vehicle type, and vehicle counts are simply the number of vehicles counted with time. WIM data were most compatible for performing this analysis. However, since the WIM information consisted of counts with fixed axle bins, these counts were used to simulate a spectra consisting of unique axle load combinations that represent the original WIM load distribution experienced by that pavement section.

- **Material and construction** - MEPDG design procedures require general material inputs such as pavement layer thicknesses and various strength and mix design properties. However, certain essential inputs were not always available in the LTPP database. Several instances were discovered that lacked entries for exact aggregate gradations for pavement layers, certain thermal properties of concrete, erodibility or friction loss information of concrete slab, joint sealant types, select asphalt mix design parameters, and assorted properties of soil sublayers. Whenever and wherever this information was available, it was used as the input parameters in the MEPDG design software. However, from a pavement management and developmental approach standpoint, as is the purpose of this study, it will be difficult and at times impractical to always seek Level 1 material information that could only be obtainable at the time of construction of these projects. The MEPDG software provides default values for all material properties as determined through national calibration representing Level 3 inputs (33). Provided these values were reasonable, these calibrated default properties were selected as inputs.
- **Environment** - The MEPDG software contains a database of climatic data for a multitude of locations in the United States. The pavement sections selected for analysis have GPS coordinates which can be used for interpolation of climatic information specific to each

site. However, the exact depth to the groundwater table specifically at all sites was not available. A depth of 10 feet was assumed for all climatic generation files under the assumption that the performance predictions will be compared between sections and that the focus of this study is development of an approach rather than developing new pavement design.

The major inputs required in MEPDG analysis were reviewed and compared with the data available for the pavements to be evaluated in this project. The available data and required inputs were grouped into three categories (traffic, material and construction, environment) and the shortcomings in the data were identified. Several strategies were proposed for missing data elements and these strategies are outlined above. Utilizing the data sources summarized in Table 3.1 and strategies for addressing data shortcomings described earlier, the proposed mechanistic-empirical procedure can be performed for all the pavement sections shortlisted. Tables 3.2 and 3.3 summarize the concrete and asphalt pavement sections used in this analysis.

Table 3.1: LTPP SDR 28.0 data sources

Parameter	Database source location	Usage
before and after pavement profiles	LTPP AIMS Data	Pavement profile elevations .ERD format
truck traffic axle loads	TRF_MONITOR_AXLE_DISTRIB	distributions for axle group generation
concrete pavement construction properties for MEPDG inputs	PCC_MIX_DESIGN	cement mix design, water-cement ratio, cement type
	INV_PCC_STEEL	steel reinforcement measurements
	INV_PCC_JOINT	joint spacing
	INV_PCC_STR	compressive strength test results
	UNBOUND_LAYER_PROPERTIES	unbound layer type (layers above subgrade)
	SECTION_LAYER_STRUCTURE	layer thicknesses and layer type (material codes)
	PCC_AGG_PROP	aggregate properties
	PCC_AGG_GRADATION	aggregate gradation
	Vol.1 MATERIAL_TEST - L05B	layer thicknesses
	LTPP Infopave.com	construction and treatment dates, GPS for climate
asphalt pavement construction properties for MEPDG inputs	AC_BINDER_PROP	Viscosity, Pen_77, Pen_39
	AC_MIX_PROP	GMM, GMB, PB, air voids, effective binder content
	SUBGRADE_PROPERTIES	subgrade type
	UNBOUND_LAYER_PROPERTIES	unbound layer type (layers above subgrade)
	SECTION_LAYER_STRUCTURE	layer thicknesses and layer type (material codes)
	AC_AGG_PROP	aggregate properties
	AC_AGG_GRADATION	aggregate gradation
	Vol.1 MATERIAL_TEST - L05B	layer thicknesses
	LTPP Infopave.com	construction and treatment dates, GPS for climate

Table 3.2: Summary of concrete pavement sections used in analysis

No.	Section ID	State	Monitoring Age (years)			Climate Zone	AAWD ²	FI ³	AADTT ⁴	Slab thickness (in)	Subgrade type
			Before	Application ¹	After						
1	6-3010	CA	9.03	10.24	11.69	DNF	55	0	4088	8.8	A-6
2	13-3017	GA	10.04	10.99	11.47	WNF	118	15	2702	9.9	A-5
3	27-4050	MN	15.73	18.92	20.82	WF	95	1452	220	8	A-3
4	42-3044	PA	10.73	10.91	11.11	WF	186	263	3864	12.7	A-2-4
5	46-3010	SD	9.84	9.88	10.81	WF	98	1055	418	9.3	A-2-4
6	55-3009	WI	10.97	11.74	11.76	WF	128	609	356	8.2	A-6
7	4-7614	AZ	12.47	14.00	14.47	DNF	36	0	1743	10	A-2-4
8	16-3017	ID	18.17	18.95	19.92	DF	89	345	748	10	A-4
9	49-C431	UT	6.98	7.73	7.78	DF	96	396	1087	9.8	A-1-b
10	8-3032	CO	17.83	18.77	20.96	DF	95	346	289	8.6	A-1-a
11	27-3009	MN	13.07	14.10	15.04	WF	119	1022	2812	7.5	A-6
12	38-3006	ND	14.76	19.84	21.00	DF	195	1417	416	8.4	A-4
13	42-9027	PA	10.91	11.08	11.28	WF	138	285	3864	12.2	A-2-4
14	20-3015	KS	12.48	13.75	14.36	WF	73	261	932	9.2	A-6
15	31-3028	NE	17.23	18.82	19.22	WF	92	449	609	8.2	A-7-6
16	39-9006	OH	13.43	13.58	14.55	WF	134	307	3073	9.4	A-1-b

Note: ¹Age at the time of treatment application, ²Average annual wet days, ³Freezing index, ⁴Average annual daily traffic, ⁵AASHTO soil classification

Table 3.3: Summary of asphalt pavement sections used in analysis

No.	Section ID	State	Monitoring age (years)			Climate Zone	AAWD ²	FI ³	AADTT ⁴	Overlay thickness (in)	Subgrade type ⁵
			Before	Application ¹	After						
1	16-B310	ID	0.01	0.12	0.21	DF	112	627	532	1.1	A-1-b
2	16-C310	ID	0.01	0.12	0.22	DF	98	642	356	1.2	A-1-b
3	53-A310	WA	0.01	0.02	0.34	DF	128	282	294	1.8	A-1-b
4	20-B310	KA	0.00	0.50	0.57	WF	85	195	300	1.5	A-7-6
5	4-C310	AR	0.21	0.20	1.03	DNF	60	1	475	1.6	A-2-6
6	4-A310	AR	0.22	0.34	1.05	DNF	26	1	350	1.2	A-2-6
7	32-B310	NE	0.03	0.16	0.15	DF	66	310	801	1.5	A-4
8	49-A310	UT	0.00	0.01	0.18	DF	79	315	160	1	A-2-4
9	49-B310	UT	0.01	0.01	0.18	DF	113	278	160	1.7	A-2-4
10	17-B310	IL	0.49	1.05	1.51	WF	123	630	312	1.2	A-4
11	53-C310	WA	0.02	0.00	0.49	WNF	198	23	184	1.1	A-1-a
12	18-A310	IN	0.83	0.51	1.80	WF	123	182	1384	1	A-4
13	20-A310	KA	0.00	0.42	0.58	WF	83	253	129	1.2	A-7-6
14	32-A310	NE	0.73	0.71	0.83	DNF	51	101	113	1.1	A-7-6

Note: ¹Age at the time of treatment application, ²Average annual wet days, ³Freezing index, ⁴Average annual daily traffic, ⁵AASHTO soil classification

CHAPTER 4: Data Analysis

The mechanistic-empirical procedure proposed in Chapter 2 is reiterated here:

1. Obtain the raw elevation profile data for a pavement sections where the treatments diamond grinding or thin overlay were applied, before and after the treatment was performed.
2. Collect detailed axle load data from pavement monitoring databases that specify gross-vehicle weights or weights of axles observed on the pavement in the year of treatment. Categorize this data into a series of axle load groups. This information provides a historical distribution of static axle loads in the year of treatment.
3. Generate a new population of trucks of that are representative of the static axle load distribution in Step 2. It is necessary that the static axle loads obtained in Step 2 are defined by individual single and tandem axle loads since the TruckSim software accepts load inputs by axle type.
4. Use each of the axle load combinations of the simulated population in Step 3 to perform multiple runs of the dynamic load simulation in TruckSim. Each axle load combination must be tested for dynamic response on the before and after pavement profile. Each axle load combination from the same population must then be re-tested on the pavement profile that corresponds to an “after treatment” state.
5. Synthesize the resulting dynamic load spectra results of Step 4 into two sets of axle load spectra that represent the dynamic loads experienced by the pavement before and after the treatment. As determined by Cebon et al., it is appropriate to take the 95th percentile of the entire dynamic response of a single run to represent the dynamic axle loads for that

specific truck (axle load combination). These 95th percentile axle loads can then be combined to create single and tandem axle load spectra.

6. Perform the MEPDG performance prediction analysis using the appropriate pavement material and environmental properties, while incorporating the single and tandem axle load spectra from Step 5 as traffic inputs, i.e. predict pavement performance using dynamic loads before treatment and repeat the performance prediction for dynamic loads after treatment, keeping all other pavement properties constant. There is a slight variation in this procedure for the case of simulating thin overlay treatment, where an additional layer of asphalt equivalent to the thickness of the thin overlay added to the pavement structure in the MEPDG program.
7. Observe and evaluate the change in predicted performance measures. A change in performance can be attributed to the change in axle load spectra only. The change in axle load spectra is due to a change in pavement profile elevations, which correspond to change in pavement surface roughness. The potential exists for relating profile-indices which describe surface roughness (IRI, DLI) to predicted pavement performance.

The above approach is illustrated in Figure 4.1. Using this procedure, the impact of diamond grinding and thin overlay on pavement roughness, dynamic load, and predicted pavement performance was evaluated.

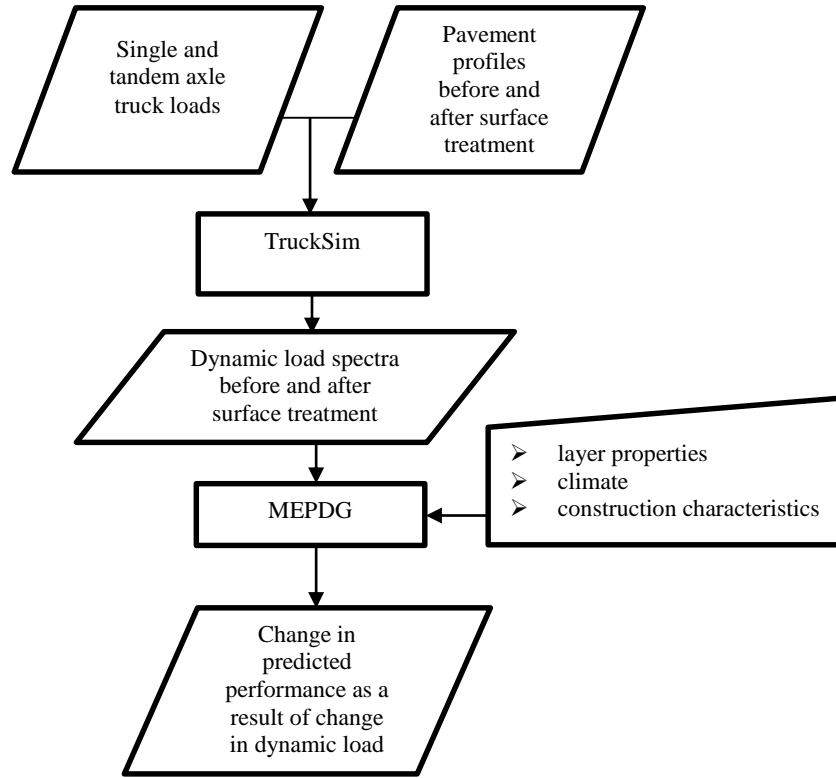


Figure 4.1: General procedure for mechanistic-empirical analysis

4.1 Procedure for evaluating the change in profile roughness index

This procedure is independent of the mechanistic-empirical analysis outlined in Figure 4.1.

However, it is necessary to perform this step to establish the change in roughness index, either ΔIRI or ΔDLI , as quality characteristics to be related to the predicted performance obtained from the mechanistic-empirical analysis. The change in profile indices were calculated using the equation below.

$$\Delta\text{Index} = \text{Index}(\text{before}) - \text{Index}(\text{after}) \quad (4.1)$$

Where:

ΔIndex = change in index ΔIRI (inches/mile) or ΔDLI (inches E-2)

$\text{Index}(\text{before})$ = IRI (inches/mile) or DLI (inches E-2) before treatment

$\text{Index}(\text{after})$ = IRI (inches/mile) or DLI (inches E-2) after treatment

By subtracting the profile index after treatment from the profile index before treatment, it is possible to correlate the “positive” or “negative” value of $\Delta Index$ with an effective or ineffective smoothing treatment. A positive change in index suggests a decrease in surface roughness after treatment, and a negative change in index indicates the roughness increased after treatment. To obtain the current IRI, the pavement profile data were evaluated using ProVAL version 3.5 engineering analysis software. The results of the ProVAL analysis correlated well with the observed (monitored) performance reported in the LTPP database.

The DLI for each section was also calculated using the calibrated DLI Equation 2.2 as shown in Chapter 2. The pavement profile elevations were converted to a frequency signal using fast Fourier transform procedure. The profile signals were then evaluated to identify the variance (V_1 and V_2 , Chapter 2) within critical wavelengths known to impact truck vehicle and axle bounce loads (6 to 11 feet and 22 to 59 feet, Chapter 2). The results of the ΔIRI and ΔDLI were compared to verify a correlation with the change in roughness of the pavement profile.

4.2 Simulating axle load spectra representative of WIM data

As described in Section 3.2 of Chapter 3, the WIM data of each pavement section were used to obtain axle load combinations representative of the traffic experienced by the section during the year the profile was monitored. A Monte Carlo simulation was used to create a distribution of approximately 300 single and tandem axle load combinations. This simulation was repeated to create a population of trucks for each pavement section. The rationale for simulation of 300 axle load combinations are presented below:

1. A single simulation run in TruckSim is typically a quick, semi-automated procedure which outputs the dynamic response along a pavement profile for a single set of axle loads. However, simulation of multiple axle load groups with the goal of developing

an axle spectrum of dynamic response will require numerous manual simulation runs. The total number of simulation runs for a single pavement profile will equal the number of axle load combinations multiplied by two, for the repeat evaluation between the before and after treatment states. As seen in the LTPP WIM database, any single given year traffic data may consist of 15,000 to 20,000 axle loads that are not combined into trucks, which translates to double that amount of simulation runs for a single pavement section.

To avoid tremendous manual computation effort, it was deemed reasonable to simulate an axle load distribution that is representative of the distribution in of the WIM data for each profile. Multiple initial trials were performed to evaluate WIM load spectra resulting from 1000, 500, 300 and 150 simulated axle-load-combinations (2000, 1000, 600, and 300 simulation runs) and the results of these trials showed the WIM load spectra only diverged significantly when less than 300 axle load combinations were used. Therefore, the simulation 300 representative axle load combinations were deemed appropriate for the analysis of a single pavement section.

2. Since a distribution of trucks was used to generate a new population of single and tandem axle loads, there were not always exactly 300 truck axle load combinations generated. However, provided that the exact number of combinations tested on a profile before smoothening were subsequently used to simulate dynamic response on a profile after smoothening treatment, it is appropriate to compare the change in dynamic response solely due to change in surface roughness.
3. The following additional considerations were made in the generation of axle load distributions. The limitations of the TruckSim software version used for this analysis

only allowed the simulation of truck configurations of FHWA Class 5, Class 9, and Class 12 heavy vehicles. As stated previously, Cebon et al. found that tractor semi-trailers (FHWA classes 6 through 9) compose 70 percent of the heavy vehicle traffic on U.S. highways.

Although it may be appropriate to conclude that Class 9 axle load distributions alone are sufficient for evaluating the effect of pavement roughness changes on dynamic vehicle loads, validation procedures were performed to compare the DLC generated by Class 9 distributions alone to combined Class 5, 9 and Class 12 truck traffic..

4.3 Simulating dynamic axle loads using TruckSim

The TruckSim software accepts single and tandem axle loads and the pavement profile elevations as inputs to simulate the dynamic behavior of trucks, busses, and tractor-trailer combinations under different test conditions (26). The software simulates the dynamic response of a pavement for a pass of a single truck with the given axle load combination along the specified profile. Diamond grinding and thin overlay are preservation treatments that modify profile elevations will impact the road roughness and, consequently, change the dynamic response. To evaluate the impact surface smoothening due to the treatment, a pair of simulation runs can be performed where the axle load combination remains constant as pavement profile is changed. After a series of runs for numerous axle load combinations, two sets of dynamic load spectra can be obtained which represent a change in dynamic truck response before and after surface treatment. The TruckSim procedure was repeated for each truck axle load combination and is described below:

1. Open TruckSim. Navigate to the “Runs” screen of the TruckSim software after initializing the program and select the Data Set to be the desired truck configuration to be tested through

the drop-down menu. For example, when testing a Class 9 truck, select “5-Axle semi-trailer (tandem) ride”.

2. At the same “Runs” screen, locate the “Simulation Input” section on the left-hand side of the screen. Select the desired pavement profile by selecting the “Pick ERD file” option under the drop-down menu for “Input: ERD File”. Navigate to the desired profile and select it.
3. Locate the “System” menu under the “Simulation Input” section on the left side of the “Runs” screen. Select “Go-To Data Set” from the drop down menu which will open the “loaded vehicle screen”. This screen will show the truck configuration based on the setting selected in Step 1. For example, the “5-Axle semi-trailer (tandem) ride” configuration will show required inputs for the load of the first single axle, combined load for the first tandem axle, and separate loads for the second tandem axle. Input the desired loads corresponding to each axle for a single axle load combination.
4. Check the remaining inputs by clicking the “Back” button on the top right corner of the “loaded vehicle screen” to return to the runs screen. Take note of the remaining inputs under the “Simulation Input” section. The vehicle speed by default is set to 60 miles per hour, which is within typical heavy truck speed limits. Under “Computation Parameters” the default step size is 0.001. This indicates that there will be approximately 1000 simulated responses for each axle load for a single pavement profile. Also, under “Computer Run” section, the simulation type is kept at the default “2D Ride”, indicating a 2-dimensional simulation of the left-wheelpath variations along the pavement profile.
5. Perform the simulation based on the inputs specified in steps 1 through 4 by selecting the Run Simulation button on the “Runs” screen. The resulting output file is by default located in

the Runs folder, which can be navigated through the explorer browser. The file has a .BIN extension and is labeled “98”.

6. Convert the output file “98.BIN” to an ASCII text file using a third party program. For this study, the program BinToASCII version 1.10 was used with a conversion Record setting of “[F]loat20” or “F20” in software notation.
7. Transfer the converted ASCII text into a spreadsheet program, such as Microsoft Excel. Convert the pasted text to columns delimited by commas. Based on the F20 conversion setting, the dynamic responses of the first through fifth axle loads (from the front to rear of the truck) will be located in columns U, V, W, X and Y respectively. Based on the software step size setting of 0.001, there will be approximately 1000 individual dynamic responses for a single truck axle load configuration simulated on a pavement profile.

The simulated dynamic response of each truck was characterized using the DLC (Equation 2.1, Chapter 2). The DLC of the variations in dynamic response of the single steer axle and tandem drive axle were calculated. The mean of these DLC values was determined for the whole population of trucks, before and after treatment, in order to characterize the change in dynamic response due to treatment. The formula to calculate ΔDLC was:

$$\Delta DLC = DLC(before) - DLC(after) \quad (4.2)$$

Where:

ΔDLC = change of mean DLC of steer or drive axle dynamic response due to treatment

$DLC (before)$ = mean DLC of steer or drive axle dynamic response before treatment

$DLC (after)$ = mean DLC of steer or drive axle dynamic response after treatment

4.4 Procedure for predicting pavement performance using MEPDG

The Mechanistic-Empirical Pavement Design Guide (MEPDG) is a mechanistic-empirical approach to predict pavement performance based on pavement structure, materials, climate, and traffic volume (33). The models in the MEPDG software predict performance measures over time as they relate to material behavior, pavement geometry, loading, and distress progression.

The software predicts the following performance measures:

- Rigid pavements: percent slab cracking, faulting (in), roughness (in/mile)
- Flexible pavements: alligator cracking (%), longitudinal cracking (foot/mile), thermal cracking (foot/mile), rutting (in), and roughness (in/mile).

The change in dynamic truck response obtained from TruckSIM can be used in-place of the typical axle load spectra inputs in order to reflect a change in predicted performance due to dynamic load. By doing so, the impact of a change in profile can be reflected in the change in predicted performance. The procedure for predicting the change in pavement performance due to a change in dynamic load is presented below:

1. Obtain all relevant construction and material-related information for a given pavement section. The Long-Term Pavement Performance database was used to obtain these properties (See Table 3.1, Chapter 3):
 - a. General information: time of pavement construction and treatment
 - b. Analysis parameters: initial IRI (IRI before and after treatment)
 - c. Traffic: AADTT, number of lanes, dynamic axle load distributions
 - d. Climate: Global Positioning System coordinates, elevation
 - e. Structure: Cement/HMA mix design material properties
 - f. Layers: Layer geometry, structural and material properties

2. Input all relevant properties of pavement section obtained from sources in Table 3.1.

The MEPDG axle load distribution inputs are the dynamic axle load distributions simulated in the procedure outlined in Section 4.3. The MEPDG input of initial IRI will be the measured “before treatment” state. Perform MEPDG analysis and record the resulting predicted performance over time.

3. Repeat Step 2, but with the initial IRI input as the “after treatment” IRI and the axle load input as the dynamic axle load distributions corresponding to truck response from the “after treatment” profile. Repeat the MEPDG analysis and record the resulting predicted performance over time.

4. Compare the two predicted performance curves obtained in Steps 2 and 3 and evaluate the service life extension (SLE) obtained as a result of change in profile smoothness. The SLE is calculated using Equation 4.3 seen below. The threshold values for each performance measure were chosen based on typical performance limits found in literature and pavement management practices (See Table 4.1). Note that for the threshold value of IRI, the SLE was calculated using the value of IRI prior to smoothing treatment.

Although typical thresholds for roughness when constructing new pavements exist, the timing for preservation treatments can vary. From a survey of state-of-practice in pavement smoothness treatments, this treatment timing was found to vary by agency(36). Therefore, when evaluating the life extension with respect to predicted roughness, it is pertinent to select the roughness at the time of treatment as the roughness threshold and consider the SLE as the time to reach this original precondition before treatment. An example of SLE calculation is shown in Figure 4.2.

$$SLE = TT_{After} - TT_{Before} \quad (4.3)$$

Where:

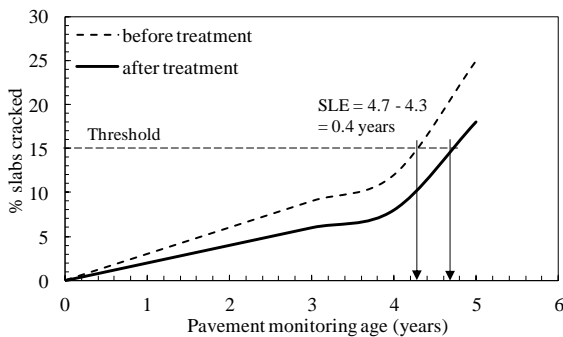
SLE = service life extension (years)

TT = Time to threshold (years)

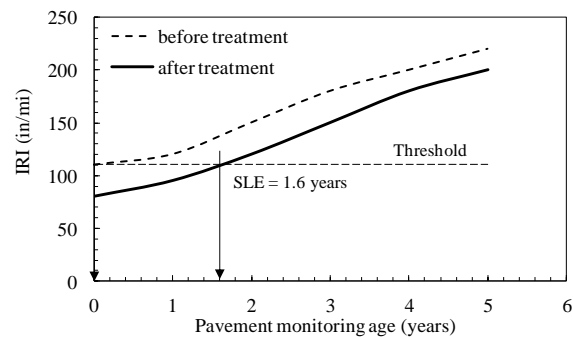
The sign of the resulting SLE naturally correlates between the result of an effective or ineffective treatment. A positive SLE value indicates an extension in pavement life, which should be indicative of the treatment reducing surface roughness, thus reducing dynamic load. An SLE that is zero or negative indicates the smoothing treatment was ineffective or unable to treat the roughness-related issues that may lead to higher load. Figure 4.2 shows a sample calculation for SLE for the general predicted performance measure and specifically for IRI.

Table 4.1: Threshold values for determining SLE

Pavement type	MEPDG performance measure	Threshold
Rigid	Fatigue cracking (%)	15
	Faulting (in)	0.15
	IRI (in/mi)	before treatment IRI
Flexible	Alligator cracking (%)	25
	Longitudinal cracking (ft/mi)	2000 feet per mile
	Thermal cracking (ft/mi)	1000 feet per mile
	Rutting (in)	0.25
	IRI (in/mi)	before treatment IRI



(a) SLE sample general calculation



(b) SLE sample calculation for IRI

Figure 4.2: General example for SLE calculation

4.5 Summary of data analysis procedure

A treatment applied to improve surface roughness (diamond grinding or thin overlay) is expected to change (smoothen) the pavement profile. An improvement in the critical wavelengths of a profile which impact truck body and axle bounce should result in lower dynamic loads on a pavement. This shift in dynamic load spectra can be captured through a simulation program such as TruckSim which accepts inputs of vehicle load and pavement profile.

The dynamic load spectra generated for a pavement profile before and after treatment as axle load distributions in MEPDG, a change in predicted performance can be observed that is directly a result of the change in load, due to the change in roughness, quantified by a change in roughness measuring indices IRI and DLI.

This procedure was used to examine the potential for a relationship between these profile-based indices and the predicted performance in terms of service life extension for each of the rigid and flexible pavement sections specified in Tables 3.2 and 3.3.

CHAPTER 5: Diamond Grinding Results and Discussion

This chapter presents the results in terms of the effects of diamond grinding on the following aspects:

- Change in pavement profile roughness and profile characteristics
- Change in truck dynamic response
- Change in pavement performance

The characteristics of each pavement section are reiterated here in Table 5.1 as a reference.

Table 5.1: Summary of concrete pavement sections used in analysis

No.	Section ID	State	Age (years)			Climate Zone	AAWD ²	FI ³	AADTT ⁴	Slab thickness (in)	Subgrade type
			Before	Application ¹	After						
1	6-3010	CA	9.03	10.24	11.69	DNF	55	0	4088	8.8	A-6
2	13-3017	GA	10.04	10.99	11.47	WNF	118	15	2702	9.9	A-5
3	27-4050	MN	15.73	18.92	20.82	WF	95	1452	220	8	A-3
4	42-3044	PA	10.73	10.91	11.11	WF	186	263	3864	12.7	A-2-4
5	46-3010	SD	9.84	9.88	10.81	WF	98	1055	418	9.3	A-2-4
6	55-3009	WI	10.97	11.74	11.76	WF	128	609	356	8.2	A-6
7	4-7614	AZ	12.47	14.00	14.47	DNF	36	0	1743	10	A-2-4
8	16-3017	ID	18.17	18.95	19.92	DF	89	345	748	10	A-4
9	49-C431	UT	6.98	7.73	7.78	DF	96	396	1087	9.8	A-1-b
10	8-3032	CO	17.83	18.77	20.96	DF	95	346	289	8.6	A-1-a
11	27-3009	MN	13.07	14.10	15.04	WF	119	1022	2812	7.5	A-6
12	38-3006	ND	14.76	19.84	21.00	DF	195	1417	416	8.4	A-4
13	42-9027	PA	10.91	11.08	11.28	WF	138	285	3864	12.2	A-2-4
14	20-3015	KS	12.48	13.75	14.36	WF	73	261	932	9.2	A-6
15	31-3028	NE	17.23	18.82	19.22	WF	92	449	609	8.2	A-7-6
16	39-9006	OH	13.43	13.58	14.55	WF	134	307	3073	9.4	A-1-b

Note: ¹Age at the time of treatment application, ²Average annual wet days, ³Freezing index, ⁴Average annual daily traffic, ⁵AASHTO soil classification

5.1 Effect of diamond grinding on pavement profile

The effect of diamond grinding on the pavement profile characteristics was evaluated by determining the change in profile index using Equation 4.1. The changes in indices are denoted as Δ IRI and Δ DLI. IRI was determined using ProVAL profile evaluation software and the results correlated well with the LTPP monitored IRI. DLI was determined using the procedure described in Chapter 2 and Equation 2.2. Figures 5.1 and 5.2 show the change in profile-based indices for the pavement sections before and after diamond grinding treatment.

Based on the change in profile-based indices, the diamond grinding treatment was generally effective in reducing roughness on the pavement sections, except for sections 8-3032 and 27-3009. An examination of the profile elevations for the sections which did experience a reduction in roughness index showed that the irregularities in the surface were largely removed. Furthermore, the successful treatments were able to reduce the general spectra of wavelengths present in the profiles, eliminating the presence of high frequencies of the profile elevations. The profile elevations of the sections which exhibited worse roughness after treatment showed that the elevations were not smoothed significantly. The change in PSD of section 8-3032 showed that there was generally no appreciable decrease in the entire range of profile wavelengths, which is reflected in the slight increase in profile indices seen in Figure 5.1 and 5.2. The PSD change in section 27-3009 showed a significant increase in the profile signal of all wavelengths, which translates to increased vehicle and axle bounce and expected increase in dynamic load response.

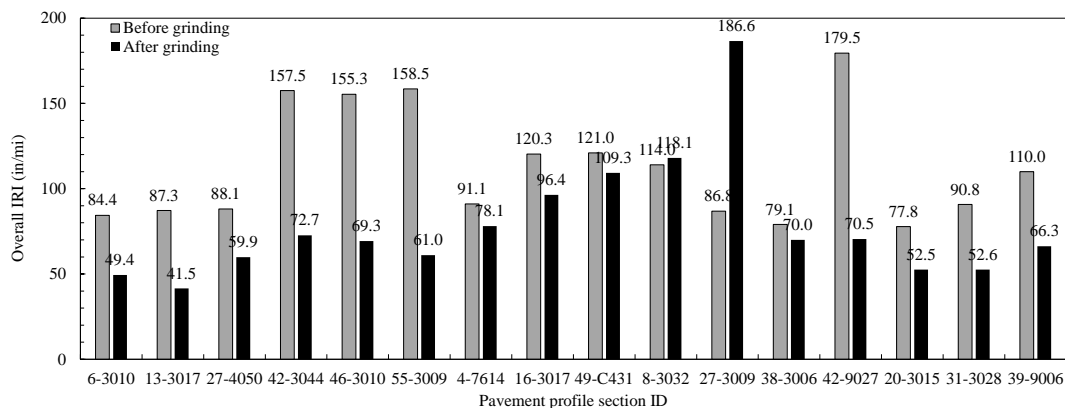


Figure 5.1: IRI before and after diamond grinding

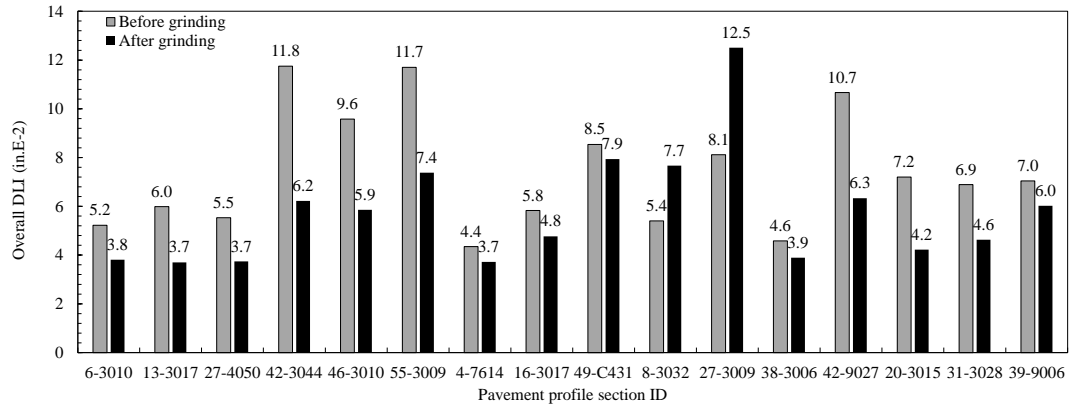


Figure 5.2: DLI before and after diamond grinding

The cause of poor treatment effectiveness can be for a variety of reasons not limited to climate or pavement construction issues. Diamond grinding must be performed in accordance with the International Grinding and Grooving Association (IGGA) specifications. Spacing of the diamond saw blades with respect to the hardness of aggregate can impact the resulting pavement texture and friction (14). Existing distress mechanisms are not addressed through slab stabilization or potential full-depth repairs prior to grinding may adversely affect treatment performance. Figure 5.3 shows the comparison of change in DLI versus change in IRI after grinding. As seen in this figure, DLI and IRI appear to correlate well with each other.

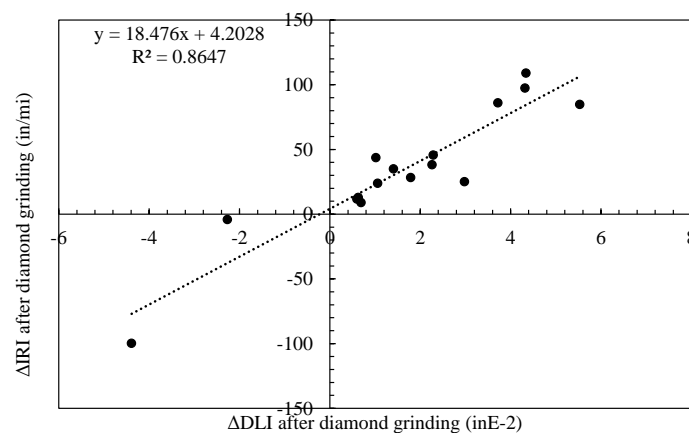


Figure 5.3: IRI versus DLI for all diamond ground sections

An example of the profile characteristics of a pavement section which exhibited improved surface smoothness (Section 42-3044) is shown in Figures 5.4 and 5.5. An example of the results of an ineffective diamond grinding treatment (Section 27-3009) is shown in Figures 5.6 and 5.7. The characteristics exhibited by these profiles align with the observed trends described earlier.

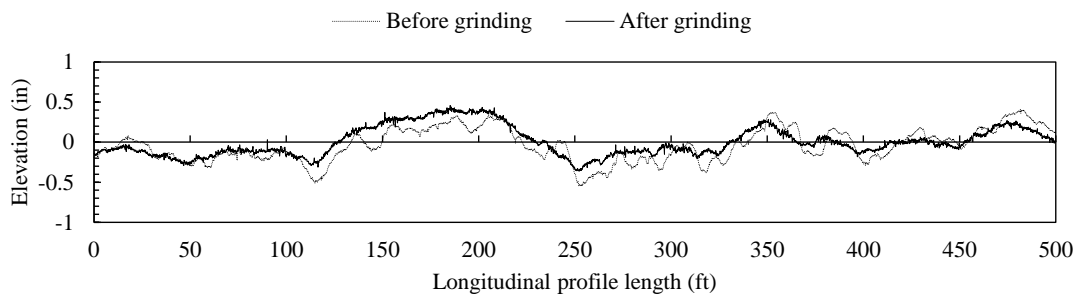


Figure 5.4: Section 42-3044 change in profile elevations due to diamond grinding

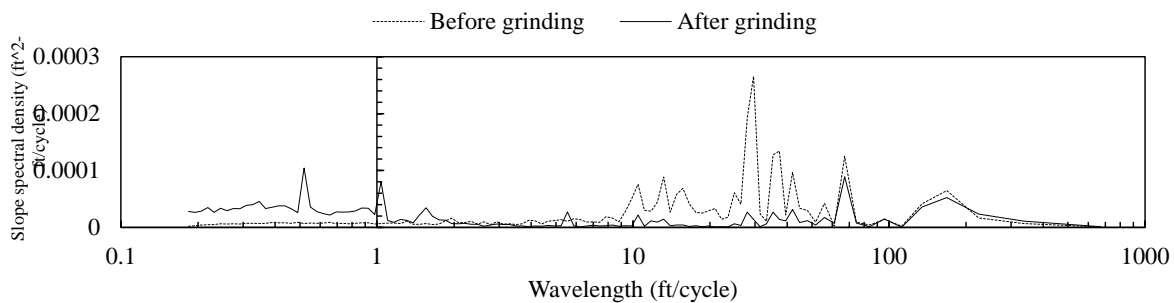


Figure 5.5: Section 42-3044 change in PSD due to diamond grinding

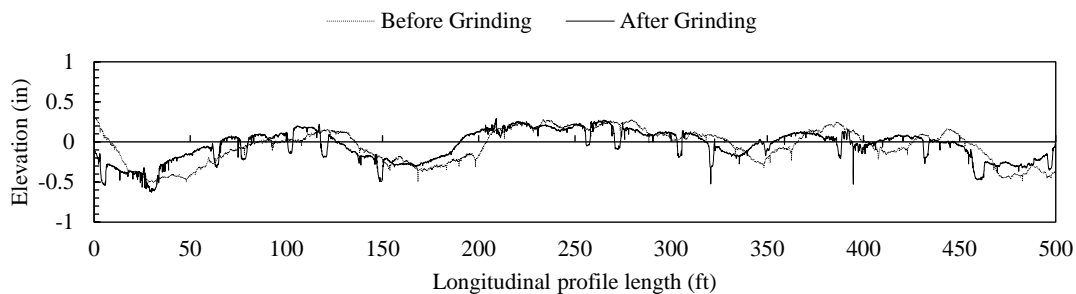


Figure 5.6: Section 27-3009 change in profile elevations due to diamond grinding

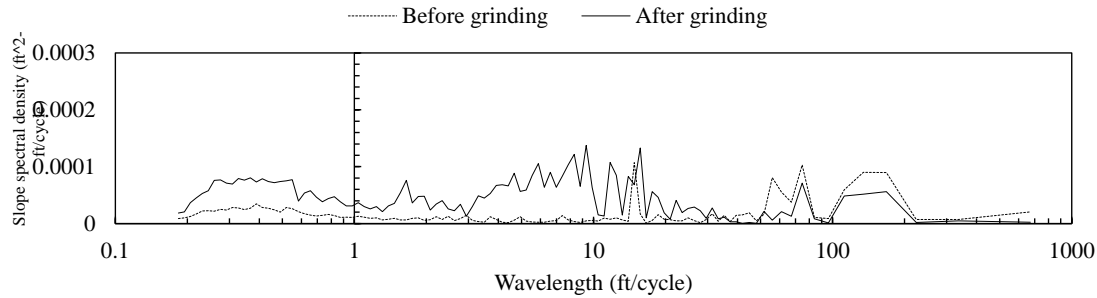


Figure 5.7: Section 27-3009 change in PSD due to diamond grinding

5.2 Effect of diamond grinding on pavement dynamic load

The effect of diamond grinding on dynamic loads experienced by the pavement was evaluated by determining the change in the Dynamic Load Coefficient (DLC) using Equation 4.2. To reiterate, these Δ DLC values were obtained by calculating the mean DLC of the entire dynamic response of single and tandem axle loads before and after treatment of the same pavement section. Tables 5.2 through 5.5 show the change in DLC for the pavement sections before and after diamond grinding treatment for the single and tandem axle load spectra, as well as the validation of Class 9 distributions compared to the combined Class 5, 9 and 12 distributions. Figures 5.8 and 5.9 show the Δ IRI and Δ DLI versus Δ DLC for single and tandem axles, respectively.

The validation test using Class 9 axle load distributions was performed for Section 42-3044. The results of these validation tests are shown in Tables 5.3 and 5.6. As seen in the percent difference between the mean changes in DLC, the difference is minimal, ranging from approximately 2.5 to 7.6 percent. As seen in Figures 5.8 and 5.9, there appears to be a relationship between the change in DLC and change in roughness. In general, an improvement (positive value) of change in profile index results in a greater positive change in DLC, which signifies a reduction in dynamic response experienced by the pavement. Furthermore, the linear regression models fit to the curves show that DLI has a better R^2 value with change in single axle

load DLC due to diamond grinding versus IRI (27.4% for DLI versus 19.8% for IRI). However, the IRI shows a slightly better fit for describing the change in tandem axle load DLC due to diamond grinding (27 % for DLI versus 27.9% for IRI). This suggests both indices can capture the relative change in dynamic load.

Table 5.2: Change in DLC of single axle load spectra due to diamond grinding

S. No	Section ID	State	Before treatment mean DLC (%)	After treatment mean DLC (%)	Δ DLC of mean single axle DLCs (%)
1	6-3010	UT	3.78	3.12	0.66
2	13-3017	IL	2.57	2.19	0.38
3	27-4050	NE	3.33	3.15	0.18
4	42-3044	IN	7.58	5.67	1.91
5	46-3010	KA	5.23	4.48	0.75
6	55-3009	NE	4.22	2.4	1.82
7	4-7614	KA	3.24	3.88	-0.64
8	16-3017	AR	4.87	4.21	0.66
9	49-C431	WA	7.16	6.64	0.52
10	8-3032	ID	3.87	3.58	0.29
11	27-3009	ID	5.19	6.09	-0.9
12	38-3006	AR	4.68	3.12	1.56
13	42-9027	OH	4.42	5.01	-0.6
14	20-3015	UT	7.44	6.44	1.01
15	31-3028	CO	4.44	2.8	1.64
16	39-9006	WA	4.68	3.59	1.09

Table 5.3: Validation of single axle Cl. 9 loads for diamond grinding

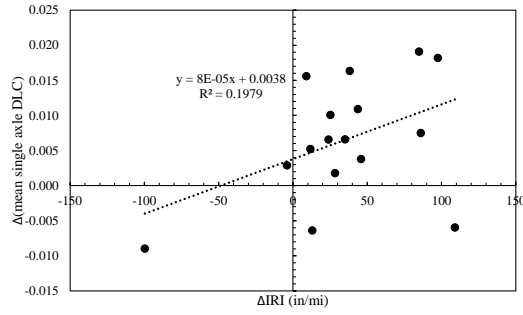
Vehicle class distributions	Section ID	State	Before treatment mean DLC	After treatment mean DLC	Δ DLC of mean single axle DLCs
Cl. 9	42-3044	IN	7.58	5.67	1.91
Cl. 5, 9, 12	42-3044	IN	7.96	6.19	1.77
				difference	0.14
				% difference	7.61

Table 5.4: Change in DLC of tandem axle load spectra due to diamond grinding

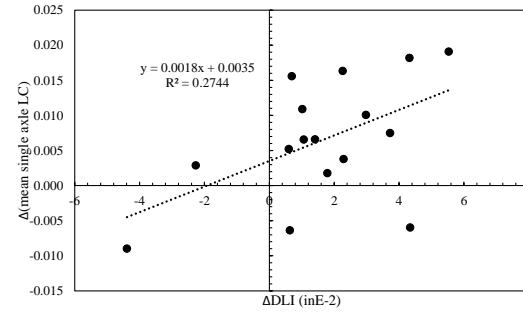
S. No	Section ID	State	Before treatment mean DLC (%)	After treatment mean DLC (%)	Δ DLC of mean tandem axle DLCs (%)
1	6-3010	UT	3.96	2.97	0.99
2	13-3017	IL	2.76	2	0.76
3	27-4050	NE	4.48	4	0.48
4	42-3044	IN	5.84	3.86	1.98
5	46-3010	KA	5.14	3.99	1.15
6	55-3009	NE	4.18	2.26	1.92
7	4-7614	KA	3.24	3.73	-0.49
8	16-3017	AR	3.96	3.55	0.41
9	49-C431	WA	5.07	5.02	0.05
10	8-3032	ID	3.97	3.4	0.57
11	27-3009	ID	4.06	5.16	-1.11
12	38-3006	AR	5.34	3.53	1.82
13	42-9027	OH	3.58	4.06	-0.48
14	20-3015	UT	7.81	7.57	0.24
15	31-3028	CO	3.63	2.38	1.25
16	39-9006	WA	5.39	3.89	1.49

Table 5.5: Validation of tandem axle Cl. 9 loads for diamond grinding

Vehicle class distributions	Section ID	State	Before treatment mean DLC	After treatment mean DLC	Δ DLC of mean single axle DLCs
Cl. 9	42-3044	IN	5.84	3.86	1.98
Cl. 5, 9, 12	42-3044	IN	5.34	3.41	1.93
				difference	0.05
				% difference	2.56

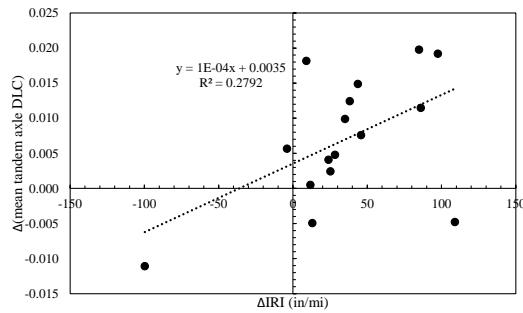


(a) Δ IRI vs single axle Δ DLC

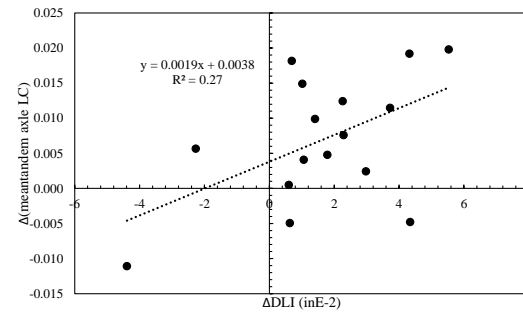


(b) Δ DLI vs single axle Δ DLC

Figure 5.8: Roughness index vs change in DLC of tandem axles for diamond grinding



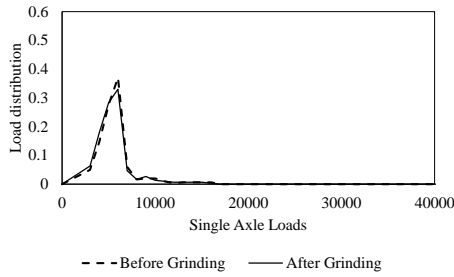
(a) Δ IRI vs tandem axle Δ DLC



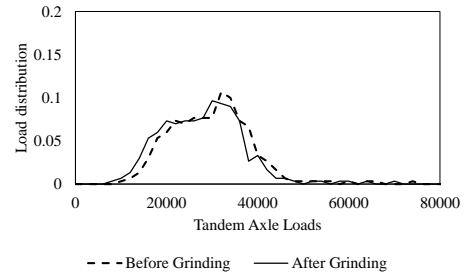
(b) Δ DLI vs tandem axle Δ DLC

Figure 5.9: Roughness index vs change in DLC of tandem axles for diamond grinding

The simulated dynamic load spectra of single and tandem axles corresponding to the pavement sections selected earlier which exhibited varying results after diamonding grinding treatment are shown in Figures 5.10 and 5.11 (sections 42-3044 and section 27-3009, respectively). As seen in Figure 5.10, there is a slight shift towards the lower loads of the spectra in both horizontal and vertical directions, demonstrating the impact of reduced roughness on dynamic load response. In contrast, Figure 5.11 shows a shift towards the higher loads of the spectra, signifying an increase in dynamic loads experienced by the pavement which is reflected in the worsening of pavement smoothness (increased profile-based roughness indices IRI and DLI).

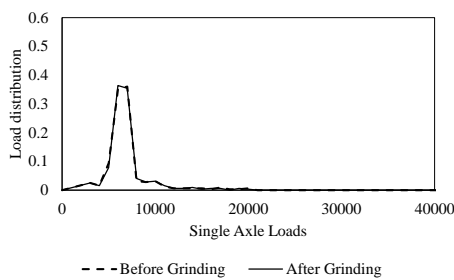


(a) Single axle dynamic load spectra

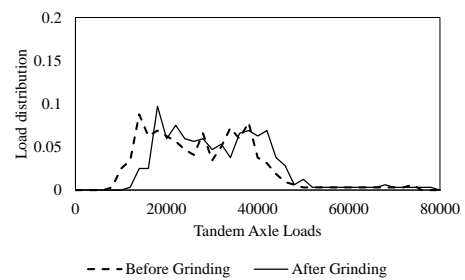


(b) Tandem axle dynamic load spectra

Figure 5.10: Section 42-3044 change in simulated dynamic axle loads due to diamond grinding



(a) Single axle dynamic load spectra



(b) Tandem axle dynamic load spectra

Figure 5.11: Section 27-3009 change in simulated dynamic axle loads due to diamond grinding

5.3 Effect of diamond grinding on predicted pavement performance

The effect of diamond grinding on the MEPDG predicted concrete pavement performance was evaluated by determining the Service Life Extension (SLE) as shown in Equation 4.2. To reiterate, the SLE is the change in time to a specified performance threshold for all other performance measures except predicted roughness. When estimating SLE due to predicted roughness, the difference in time to reach pre-condition (pre-treatment IRI) was considered. Figure 5.12 through 5.14 show the change in SLE for the pavement sections before and after diamond grinding treatment, for predicted faulting, fatigue cracking, and IRI, respectively. The results of the mechanistic-empirical performance prediction indicate that diamond grinding has varying levels of pavement performance depending on performance measure.

In the case of predicted faulting, the range of SLE was from -2.6 to 4.4 years. The SLE due to predicted fatigue cracking ranged from -0.8 to 14.4 years. The range of SLE due to predicted roughness was from 0 to 36 years. Recall that typical ranges of life extension found in current practice as a result of diamond grinding are 8 to 15 years, independent of performance measure.

Although the majority of cases where an improvement in profile smoothness resulted in increase in pavement life, the magnitude of this improvement varies by pavement section, and by the performance measure predicted. Table 5.6 shows a count of sections that fall into four categories of performance in terms of SLE range. As seen in this table, the predicted performance due to IRI captures a wider range of SLE in comparison to SLE obtained from other performance measures.

Table 5.6: Count of diamond ground pavement sections by SLE performance

SLE category	due to faulting	due to fatigue cracking	due to IRI
SLE > 10 years	0	1	4
SLE = 1-10 years	6	4	10
SLE = 0-1 year	7	8	2
SLE < 0 years	3	3	0

These counts suggest that using a profile-based index that is a measure of pavement roughness appears to predict the performance in terms of roughness, better than in terms of other performance measures. However, since roughness can impact dynamic load, a roughness based index is still capable of assessing an improvement in predicted load-related distresses, such as fatigue cracking. The SLE predicted due to fatigue cracking and IRI show a wide range of performance predicted is described as a result of a change in dynamic load inputs. Furthermore, pavement roughness is also impacted by the level of faulting present yet there is only a small range in SLE (-2.6 to 4.4 years) due to predicted faulting. This suggests that although profile smoothing treatments such as diamond grinding may address short-term faulting-related

roughness, profile-based roughness indices IRI and DLI that measure instantaneous surface smoothness may not capture the presence of underlying faulting mechanisms.

As seen in the variations of performance shown in Figures 5.12 to 5.14, the pavement sections which showed a small or negative change in IRI and DLI are largely located in the 0 to 1 year SLE range. Many that showed a significant change in IRI and DLI are on the higher end of the SLE range. Section 27-3009, which exhibited particularly rougher surface after treatment, is consistently on the negative end of the SLE spectrum, indicating this treatment reached a threshold sooner after ineffective grinding. These variations in predicted performance can be attributed to the variation in dynamic load response after treatment as well as the various material, construction, and environment-related factors corresponding to each pavement section.

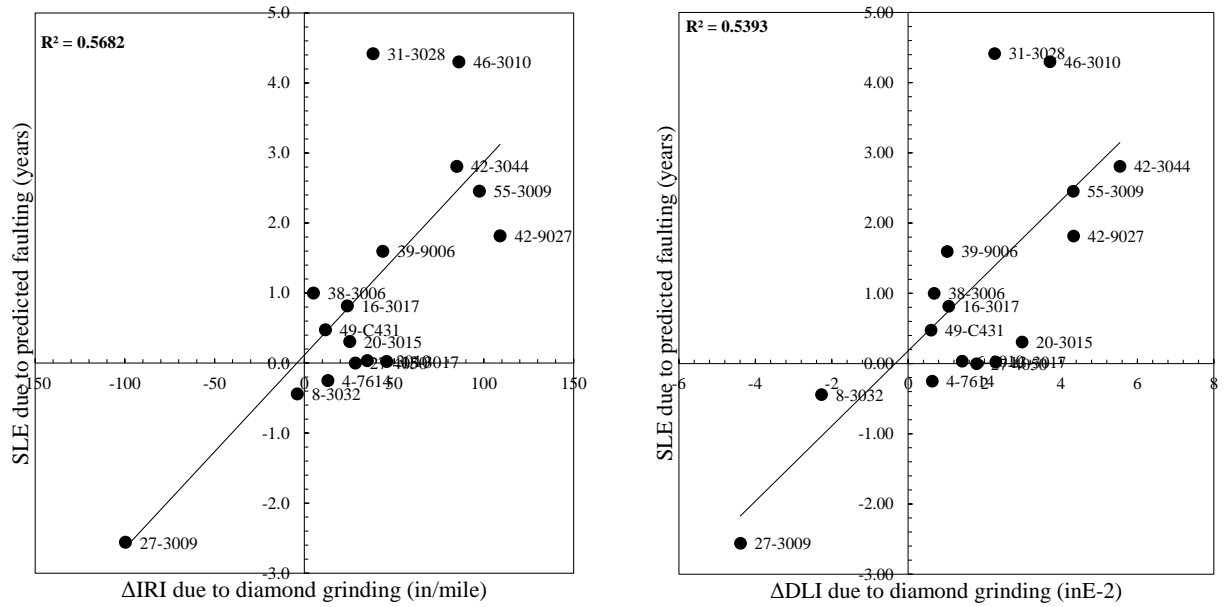
Below are some key observations from the mechanistic-empirical performance prediction with regards to pavement properties, site factors, and corresponding performance for the diamond ground pavement sections.

- The two pavement sections that showed an increase in IRI and DLI after treatment exhibited very poor performance in terms of SLE (due to predicted faulting, cracking, and IRI): 8-3032 (-0.4, -0.8, 0 years) and 27-3009 (-2.6, -0.3, 0 years). IRI and DLI were a good indicator for predicting poor performance for these sections.
- These same two sections (8-3032 and 27-3009) also have low slab thickness which can be attributed to higher load-related damage. Section 27-3009 has the lowest slab thickness out of all of the pavement sections (7.5 inches) and one of the highest Average Annual Daily Truck Traffic (AADT) levels (2812).
- There was no predicted cracking observed on five of the sections before treatment (6-3010, 13-3017, 4-7614, 49-C431, and 42-9027). The MEPDG fatigue cracking model

predicted no occurrence of fatigue cracking for these same sections after treatment. As a result, these five sections retained an SLE of zero years with respect to fatigue cracking performance. An examination of the actual LTPP monitored cracking for each of these sections showed there were no observed fatigue, longitudinal cracking, or transverse cracking at the time of treatment. This suggests that the mechanistic-modeling of these pavement sections was accurate in terms of predicting cracking, but also implies that SLE alone may misrepresent the effect of having no distress before or after treatment.

- The same five sections mentioned above did, however, exhibit the presence of faulting and high IRI prior to treatment date, according to LTPP monitoring data, and this may have prompted the reason for diamond grinding. This agrees with the presence of predicted faulting and IRI present in the MEPDG predicted performance.
- Excluding the sections which exhibited zero SLE in terms of predicted cracking specified above, the other sections that exhibited an SLE of 1 year or less, due to fatigue cracking and faulting, generally share similar characteristics. These sections either had high traffic levels (2800 to 4000 AADTT) or were located in climates with lower Average Annual Wet Days (AAWD) less than 100 days per year. As determined in the literature review, a concrete slab subjected to high temperatures or a rapid increase in thermal gradient across the slab interface can experience greater cracking over time due to slab curling and warping.

Figures 5.12 through 5.14 show that a performance-based relationship between profile indices can be developed using the proposed mechanistic-empirical procedure. IRI appears to somewhat better describe the change in performance measures than DLI, as seen in the relatively larger R^2 values.

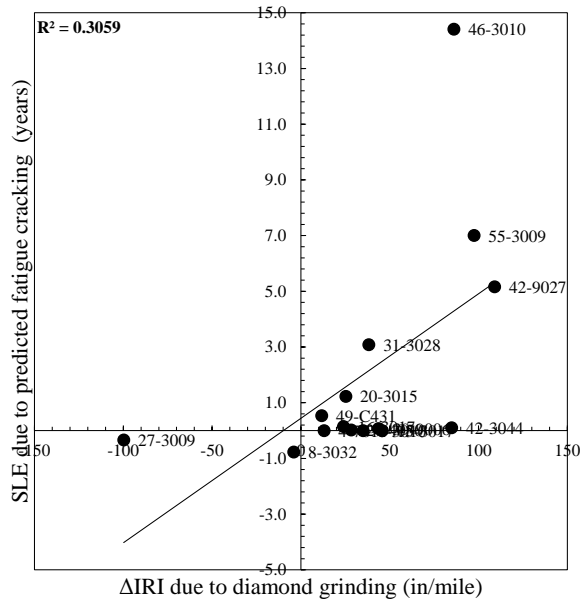


(a) Δ IRI vs SLE due to predicted faulting

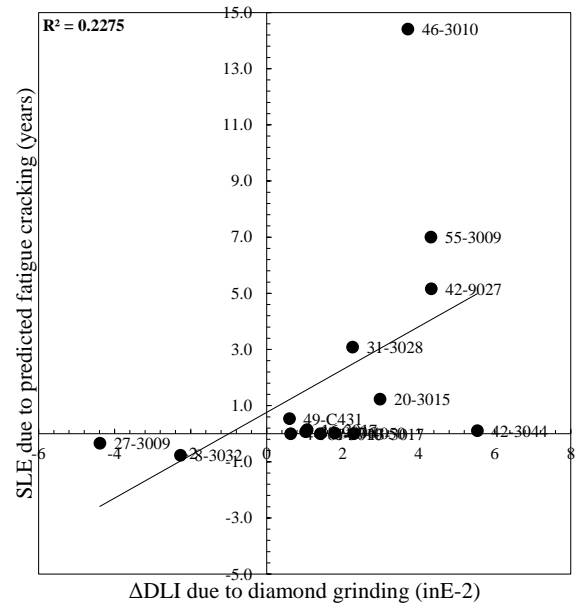
(b) Δ DLI vs SLE due to predicted faulting

Figure 5.12: Effect of diamond grinding on predicted faulting performance

In parallel to the examples of effective and ineffective diamond grinding treatment presented earlier, the impact of change in pavement roughness, and thus a change in dynamic load, on predicted performance is presented in Figure 5.15, for sections 42-3044 and 27-3009. The effect of reduction in roughness can be seen in Figures 5.15 a, b, and c as each reaches a lower level of predicted faulting, cracking, and IRI at the end of the design life. In contrast, these same performance measures all increase in Figures 5.15 d, e, and f; this can be attributed to an increase in profile roughness, which was caused by an increase in dynamic load.

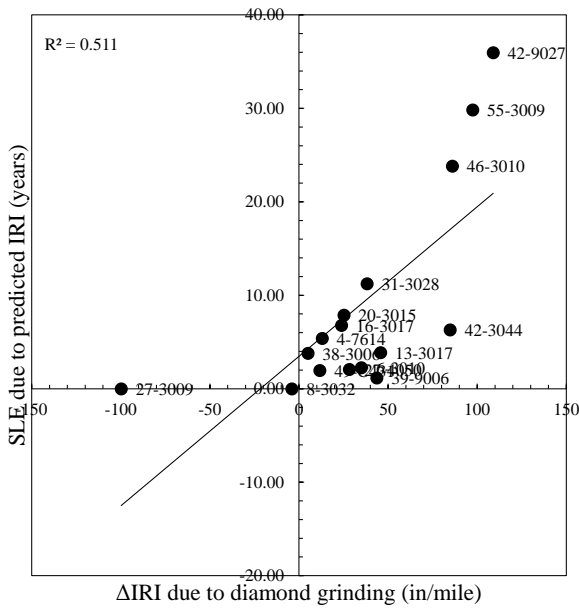


(a) Δ IRI vs SLE due to predicted cracking

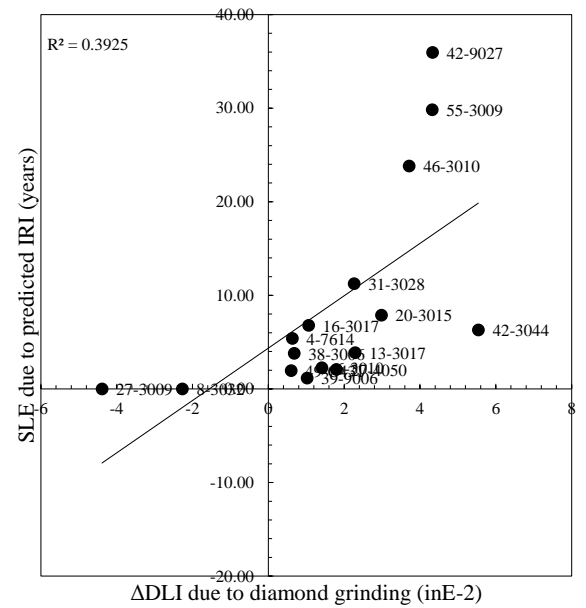


(b) Δ DLI vs SLE due to predicted cracking

Figure 5.13: Effect of diamond grinding on predicted cracking performance

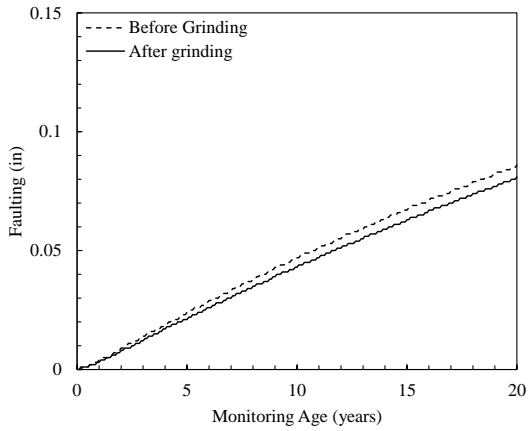


(a) Δ IRI vs SLE due to predicted IRI

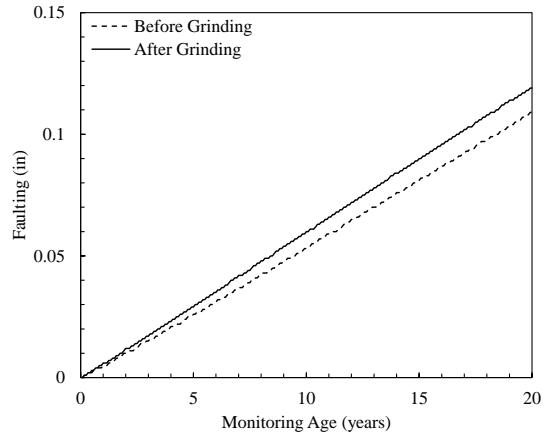


(b) Δ DLI vs SLE due to predicted IRI

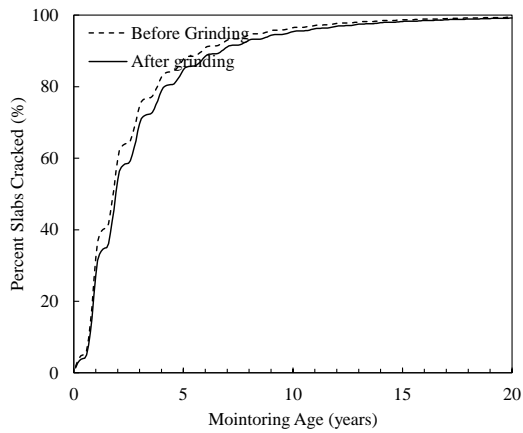
Figure 5.14: Effect of diamond grinding on predicted roughness



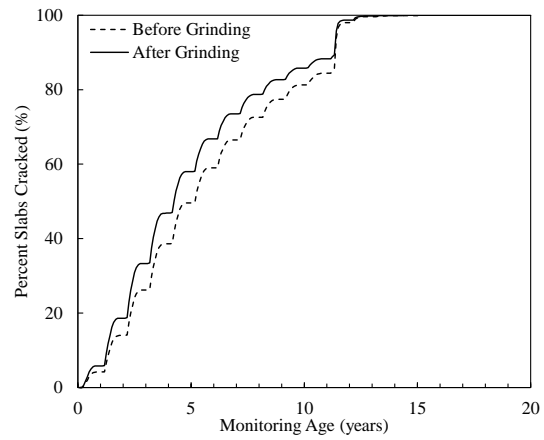
(a) 42-3044 faulting



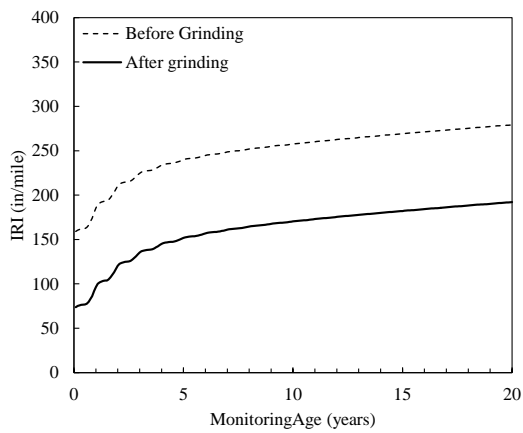
(b) 27-3009 faulting



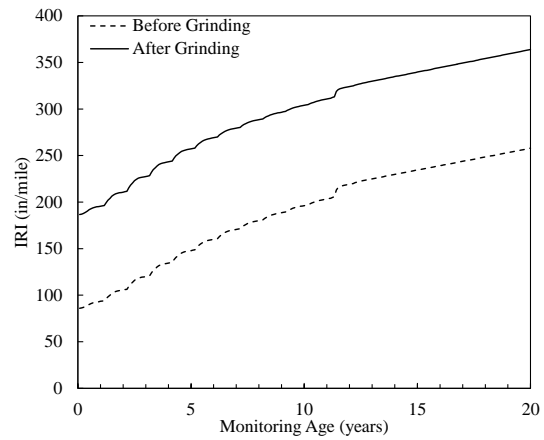
(c) 42-3044 cracking



(d) 27-3009 cracking



(e) 42-3044 IRI



(f) 27-3009 IRI

Figure 5.15: Comparison of effective and ineffective diamond grinding treatment

CHAPTER 6: Thin Overlay Results and Discussion

This chapter presents the results in terms of the effects of thin overlay on the following aspects:

- Change in pavement profile roughness and profile characteristics
- Change in truck dynamic response
- Change in pavement performance

The characteristics of each pavement section are reiterated here in Table 6.1 as a reference.

Table 6.1: Summary of asphalt pavement sections used in analysis

No.	Section ID	State	Monitoring age (years)			Climate Zone	AAWD ²	FI ³	AADTT ⁴	Overlay thickness (in)	Subgrade type ⁵
			Before	Application ¹	After						
1	16-B310	ID	0.01	0.12	0.21	DF	112	627	532	1.1	A-1-b
2	16-C310	ID	0.01	0.12	0.22	DF	98	642	356	1.2	A-1-b
3	53-A310	WA	0.01	0.02	0.34	DF	128	282	294	1.8	A-1-b
4	20-B310	KA	0.00	0.50	0.57	WF	85	195	300	1.5	A-7-6
5	4-C310	AR	0.21	0.20	1.03	DNF	60	1	475	1.6	A-2-6
6	4-A310	AR	0.22	0.34	1.05	DNF	26	1	350	1.2	A-2-6
7	32-B310	NE	0.03	0.16	0.15	DF	66	310	801	1.5	A-4
8	49-A310	UT	0.00	0.01	0.18	DF	79	315	160	1	A-2-4
9	49-B310	UT	0.01	0.01	0.18	DF	113	278	160	1.7	A-2-4
10	17-B310	IL	0.49	1.05	1.51	WF	123	630	312	1.2	A-4
11	53-C310	WA	0.02	0.00	0.49	WNF	198	23	184	1.1	A-1-a
12	18-A310	IN	0.83	0.51	1.80	WF	123	182	1384	1	A-4
13	20-A310	KA	0.00	0.42	0.58	WF	83	253	129	1.2	A-7-6
14	32-A310	NE	0.73	0.71	0.83	DNF	51	101	113	1.1	A-7-6

Note: ¹Age at the time of treatment application, ²Average annual wet days, ³Freezing index, ⁴Average annual daily traffic, ⁵AASHTO soil classification

6.1 Effect of thin overlay on pavement profile

The effect of thin overlay on the selected pavement profiles was evaluated by determining the change in profile index using Equation 4.1. The change in indices is denoted as ΔIRI and ΔDLI . IRI was determined by using ProVAL profile evaluation software, and it correlated well with the LTPP monitored IRI values. DLI was evaluated using Equation 2.2. Figures 6.1 and 6.2 show the change in profile-based indices for the pavement sections before and after thin overlay treatment.

Based on before and after comparison of profile-based indices, thin overlay was effective in reducing roughness except for a few sections: 32-B310, 4-A310, 16-C310, and 17-B310.

Section 32-B310 exhibited an increase in IRI after the treatment, but a marginal reduction in DLI

after treatment. Section 4-A310 exhibited a small increase in IRI after treatment, and a significant increase in DLI after treatment. Section 16-C310 exhibited a minor increase in DLI but a decrease in IRI after treatment. Lastly, section 17-B310 exhibited a small increase in IRI and a small decrease in DLI after treatment. Figures 6.1 and 6.2 illustrate these discrepancies.

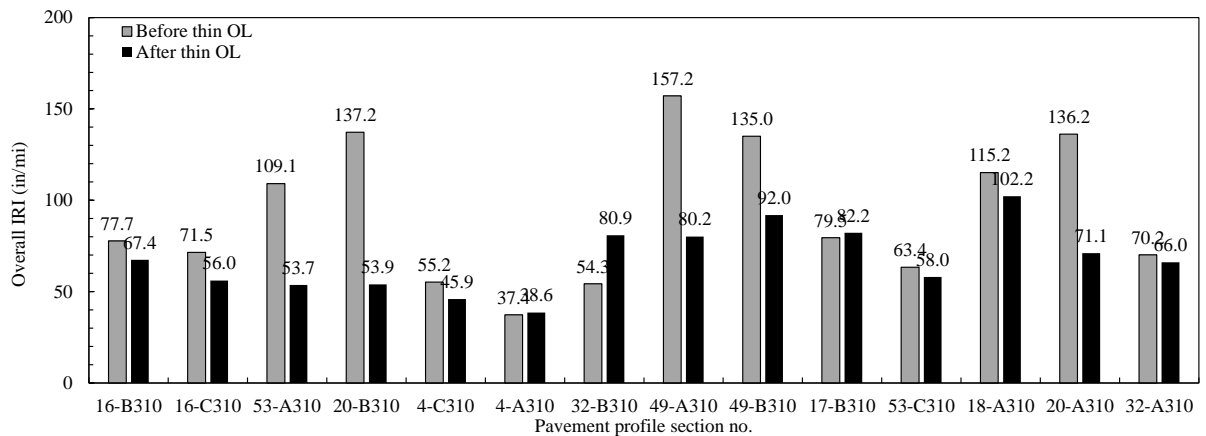


Figure 6.1: IRI before and after thin overlay

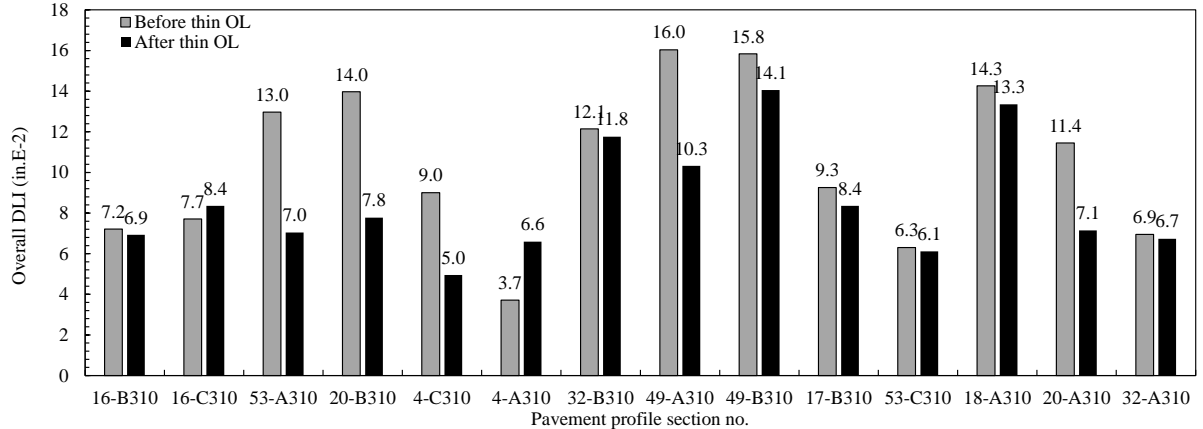


Figure 6.2: DLI before and after thin overlay

Figure 6.3 shows the relationship between the changes in DLI versus changes in IRI after thin overlay. As seen here, the correlation coefficient between the changes in roughness indices is 0.66. Recall that the coefficient of correlation R^2 for comparison of change in indices for

concrete pavement grinding was 0.86. These results suggest that IRI and DLI may correlate, though not as strongly in comparison to the change in profile index due to diamond grinding.

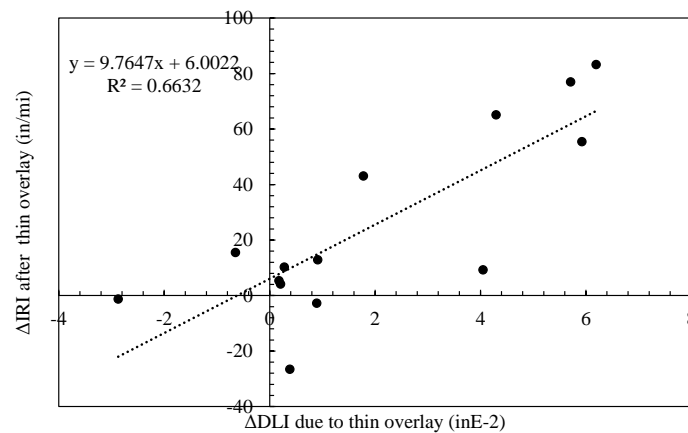


Figure 6.3: IRI versus DLI for all diamond ground sections

An examination of the profile elevations of sections 32-B310, 4-A310, 16-C310 and 17-B310 shows the presence of surface irregularities at the time of monitoring. The change in DLI of 4-A310 is the only Δ DLI among the four sections that agrees with worsened profile characteristics. The PSDs of sections 4-A310 and 32-B310 show that although the treatment was able to reduce the long wavelength characteristics of the profile, the shorter wavelengths were exacerbated. These short wavelengths correspond to high frequencies in the profile signal, which ultimately translates to increased vehicle bounce and an expected increase in dynamic load response. An examination of the PSD of sections 16-C310 and 17-B310 indicate that there was generally no appreciable decrease in the entire range of profile wavelengths, which is reflected in minimal change in profile indices as seen in Figures 6.1 and 6.2. These observations suggest the treatment on these sections was ineffective, either during application or in terms of treatment longevity.

The remaining profiles of pavement sections with agreeing IRI and DLI changes, and demonstrate an improvement in surface roughness, showed that surface irregularities were

mostly removed after treatment. The PSD signal of the sections that exhibited an improvement in surface smoothness also demonstrated a reduction in PSD signal across the range of wavelengths, which is beneficial in reducing overall frequency ranges that contribute to truck bounce and dynamic loads.

An example of the profile characteristics of a pavement section which exhibited improved surface smoothness (Section 49-A310) is shown in Figures 6.4 and 6.5. An example of the results of an ineffective thin overlay treatment (Section 32-B310) is shown in Figures 6.6 and 6.7. The characteristics exhibited by these profiles verify the observed trends described earlier.

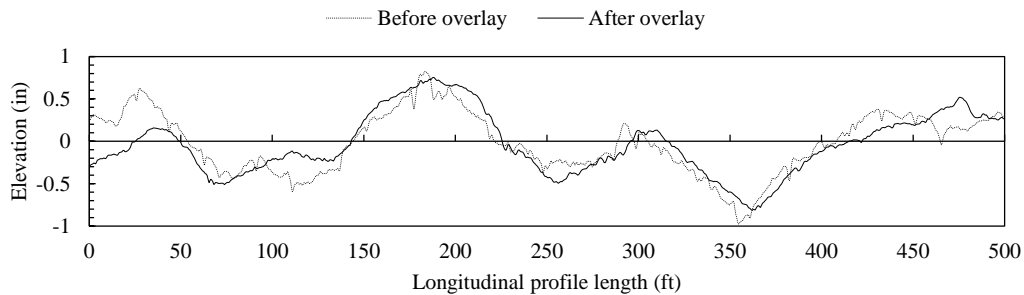


Figure 6.4: Section 49-A310 change in profile elevations due to thin overlay

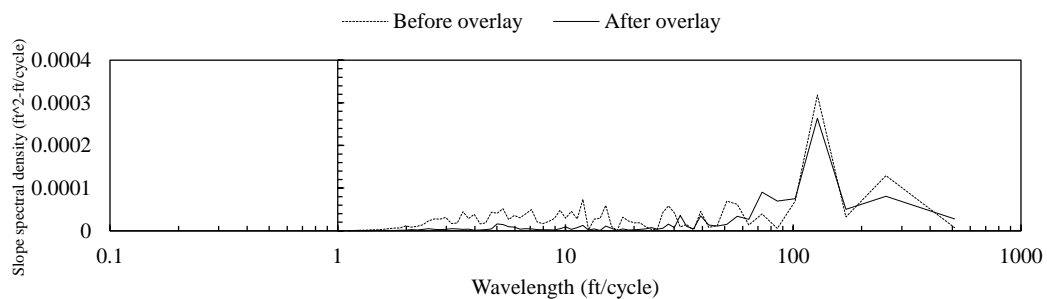


Figure 6.5: Section 49-A310 change in PSD due to thin overlay

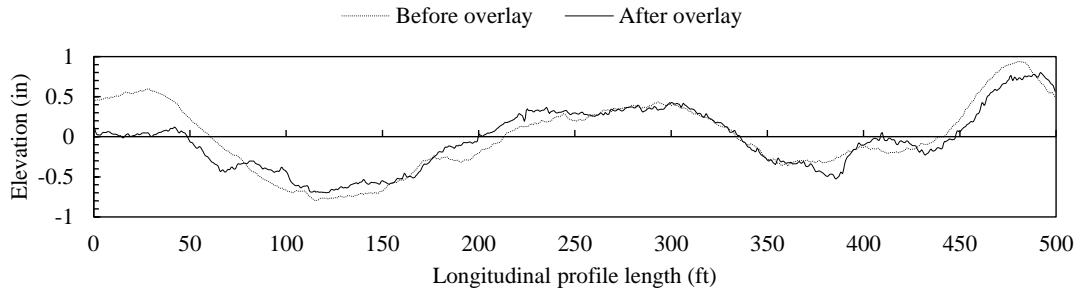


Figure 6.6: Section 32-B310 change in profile elevations due to thin overlay

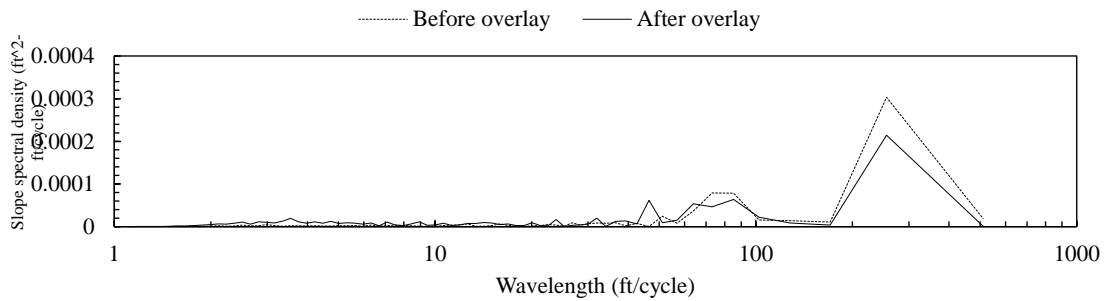


Figure 6.7: Section 32-B310 change in PSD due to thin overlay

6.2 Effect of thin overlay on pavement dynamic load

The effect of thin overlay applications on dynamic loads experienced by the pavements was evaluated by determining the change in the Dynamic Load Coefficient (DLC) using Equation 4.2. To reiterate, these Δ DLC values were obtained by calculating the mean DLC of the entire dynamic response of single and tandem axle loads before and after treatment of the same pavement section. Tables 6.2 through 6.5 show the change in DLC for the pavement sections before and after thin overlay application for the single and tandem axle load spectra, as well as the validation of Class 9 distributions compared to the combined Class 5, 9 and 12 distributions.

The validation test for using Class 9 axle load distributions was performed using Section 49-B310. The results of these validation tests are shown in Tables 6.3 and 6.6. As seen in the

percent difference between the mean changes in DLC, the difference is minimal, ranging from approximately 13.6 to 10.5 percent difference. Figures 6.8 and 6.9 show the potential for a relationship between the change in DLC and change in roughness. Generally, the results show a reduction in profile index as a result of thin overlay treatment corresponded with a reduction in the mean change in DLC. However, in contrast to the findings for diamond grinding, the linear regression models fit to the curves show lower coefficients of correlation, with a better value for IRI. For single axles, the correlation coefficient is 16% for IRI versus 1.6% for DLI. For tandem axles, the correlation coefficient is 25% for IRI versus 6.3% for DLI. This suggests that thin overlays do not significantly reduce dynamic loads.

Table 6.2: Change in DLC of single axle load spectra due to thin overlay

S. No	Section ID	State	Before treatment mean DLC (%)	After treatment mean DLC (%)	Δ DLC of mean single axle DLCs (%)
1	16-B310	UT	3.8	2.2	1.6
2	16-C310	IL	2.99	2.24	0.75
3	53-A310	NE	3.72	3.16	0.55
4	20-B310	IN	0.45	0.04	0.41
5	4-C310	KA	2.03	2.1	-0.07
6	4-A310	NE	2.36	1.5	0.86
7	32-B310	KA	2.24	2.66	-0.42
8	49-A310	AR	4.17	2.38	1.79
9	49-B310	WA	3.33	0.43	2.9
10	17-B310	ID	0.47	0.42	0.05
11	53-C310	ID	0.22	1.89	-1.67
12	18-A310	AR	0.25	0.21	0.04
13	20-A310	OH	0.31	0.19	0.12
14	32-A310	UT	2.38	2.36	0.02

Table 6.3: Validation of single axle Cl. 9 loads for thin overlay

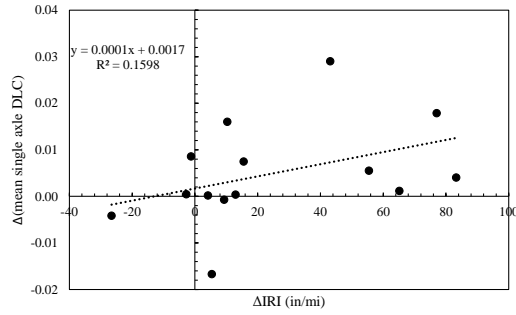
Vehicle class distributions	Section ID	State	Before treatment mean DLC (%)	After treatment mean DLC (%)	Δ DLC of mean single axle DLCs (%)
Cl. 9	49-B310	WA	3.33	0.43	2.9
Cl. 5, 9, 12	49-B310	WA	2.871	0.34	2.53
				difference	0.0037
				% difference	13.5962

Table 6.4: Change in DLC of tandem axle load spectra due to thin overlay

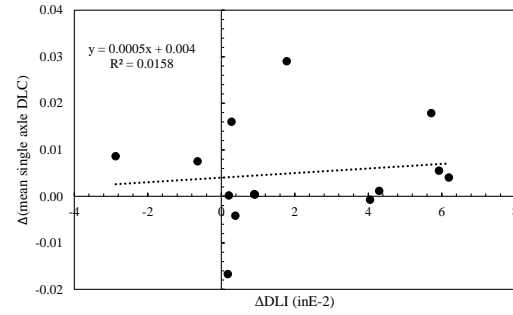
S. No	Section ID	State	Before treatment mean DLC (%)	After treatment mean DLC (%)	Δ DLC of mean tandem axle DLCs (%)
1	16-B310	UT	2.27	1.47	0.8
2	16-C310	IL	2.42	1.88	0.54
3	53-A310	NE	2.93	2.33	0.59
4	20-B310	IN	0.34	0.02	0.32
5	4-C310	KA	1.67	1.8	-0.13
6	4-A310	NE	1.78	1.44	0.34
7	32-B310	KA	1.97	2.41	-0.44
8	49-A310	AR	3.65	1.88	1.77
9	49-B310	WA	2.87	0.24	2.64
10	17-B310	ID	0.24	0.24	0
11	53-C310	ID	0.19	1.71	-1.52
12	18-A310	AR	0.45	0.29	0.16
13	20-A310	OH	0.38	0.19	0.2
14	32-A310	UT	2.54	2.44	0.09

Table 6.5: Validation of tandem axle Cl. 9 loads for thin overlay

Vehicle class distributions	Section ID	State	Before treatment mean DLC (%)	After treatment mean DLC (%)	Δ DLC of mean single axle DLCs (%)
9	49-B310	WA	2.87	0.24	2.64
9	49-B310	WA	2.59	0.22	2.37
				difference	0.0026
				% difference	10.4612

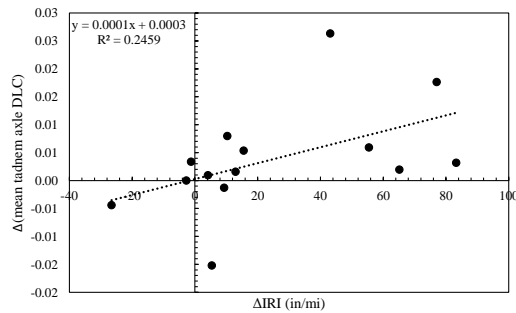


(a) Δ IRI vs single axle Δ DLC

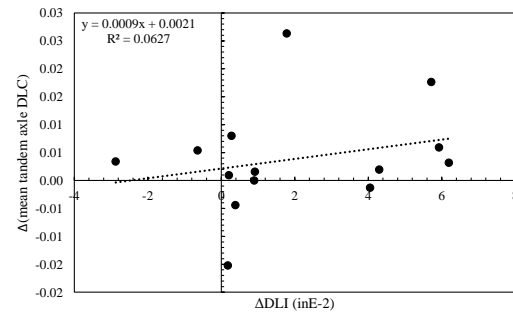


(b) Δ DLI vs single axle Δ DLC

Figure 6.8: Roughness index vs change in DLC of single axles for thin overlay



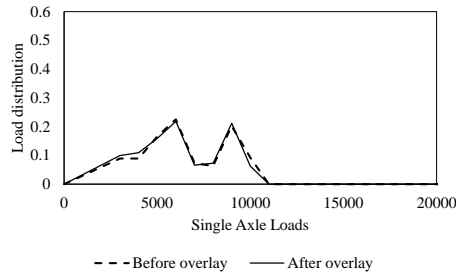
(a) Δ IRI vs tandem axle Δ DLC



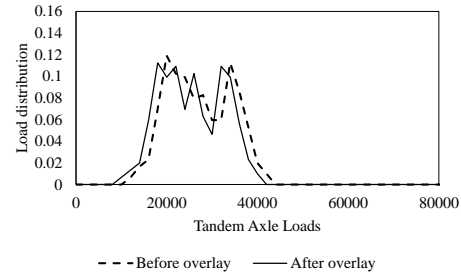
(b) Δ DLI vs tandem axle Δ DLC

Figure 6.9: Roughness index vs change in DLC of tandem axles for thin overlay

The simulated dynamic load spectra of single and tandem axles corresponding to the pavement sections exhibiting different results after thin overlay treatment are shown in Figures 6.10 and 6.11 (sections 49-A310 and section 32-B310, respectively). As seen in Figure 6.10, the shift in load spectra to the lower end of the spectrum is more pronounced for tandem axle load distributions; this demonstrates the impact of an effective thin overlay. In contrast, Figure 6.11 shows a shift towards the higher end of the spectrum, indicative of the increase in profile roughness as a result of an ineffective treatment.

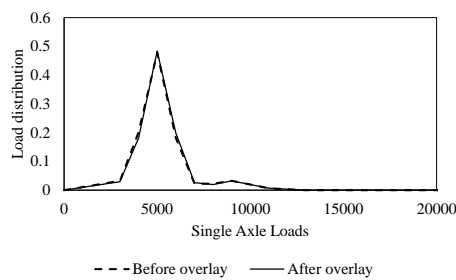


(a) Single axle dynamic load spectra

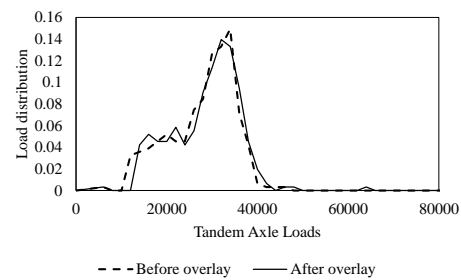


(b) Tandem axle dynamic load spectra

Figure 6.10: Section 49-A310 change in simulated dynamic axle loads for thin overlay



(a) Single axle dynamic load spectra



(b) Tandem axle dynamic load spectra

Figure 6.11: Section 32-B310 change in simulated dynamic axle loads for thin overlay

6.3 Effect of thin overlay on predicted pavement performance

The effect of thin overlay on the MEPDG predicted asphalt pavement performance was evaluated by determining the change in Service Life Extension (SLE) as shown in Equation 4.2. To reiterate, the SLE is the change in the time for a performance measure to reach a specified threshold for all other performance measures except predicted roughness. When estimating SLE due to predicted roughness, the difference in time to reach pre-condition (pre-treatment IRI) was calculated.

Upon performing the evaluation of SLE in terms of various types of cracking, rutting, and IRI, the most reliable conclusions could only be determined from the SLE due to predicted IRI. The predicted performance for cracking were highly variable and the correlations observed

between the change in dynamic load and the change in predicted SLE due to rutting were weaker. It is questionable to draw direct conclusions from the rutting performance, because the phenomenon of permanent deformation (i.e., rutting) in asphalt pavements is attributed to gross vehicle weights rather than dynamic loads.

Figure 6.12 and 6.13 show the SLE for the pavement sections before and after thin overlay, for predicted rutting and IRI, respectively. The results of the mechanistic-empirical performance prediction indicate that thin overlay has a varying effect on pavement performance, and this variance is much more pronounced than the change in predicted performance observed due to diamond grinding, as seen in Chapter 5.

In the case of predicted rutting, the range of SLE was from 0.2 to 16.5 years. The SLE due to predicted IRI ranged from 0 to 50 years. Recall that in Chapter 2, the typical ranges of life extension in current practice as a result of thin overlay treatments are 3 to 23 years, which suggests the predicted values fall above the typical ranges. Table 6.6 shows a count of sections that fall into four ranges of SLE performance. Despite most of the pavement sections exhibiting an improvement in roughness, the magnitude of SLE change also varies by pavement section, much like what was observed with diamond grinding treatments. However, this discrepancy does not seem to exist between performance measures, with a seemingly equally distributed spread of SLE between predicted rutting and IRI.

Table 6.6: Count of thin overlain pavement sections by SLE performance

SLE category	due to rutting	due to IRI
SLE > 10 years	5	5
SLE = 1-10 years	3	4
SLE = 0-1 year	6	5
SLE < 0 years	0	0

The variations of performance can be seen in Figures 6.12 and 6.13. As seen in these figures, the predicted performance due to rutting as a result of thin overlay treatment exhibits significant variation across all change of profile indices. In some cases, profiles with a low positive ΔIRI (sections 32-B310 and 32-A310) resulted in up to 8 years less life extension compared to sections with a larger positive ΔIRI (sections 49-B310 and 49-A310). Moreover, the correlation between ΔIRI and ΔDLI with predicted SLE due to rutting is not as significant.

The profile-based indices appear to have a better characterization of predicted SLE performance due to predicted IRI. The trends in Figure 6.13 show a better relationship between the magnitudes of improvement in profile index to a corresponding improvement in IRI performance using a linear regression model. It is evident from this model that a lower change in ΔIRI or ΔDLI will result in lower life extension due to predicted roughness. These observations suggest that the change in dynamic load due to thin overlay is better correlated to a change in predicted roughness, in comparison to the performance predicted for cracking and rutting.

Below are key observations from the mechanistic-empirical performance prediction with regards to pavement properties, site factors, and corresponding performance for the thin overlain pavement sections. Although predicted alligator cracking, longitudinal cracking, and thermal cracking were evaluated in the analysis, the inability to draw any conclusions when evaluating service life extensions due to these performance measures were due to the following reasons:

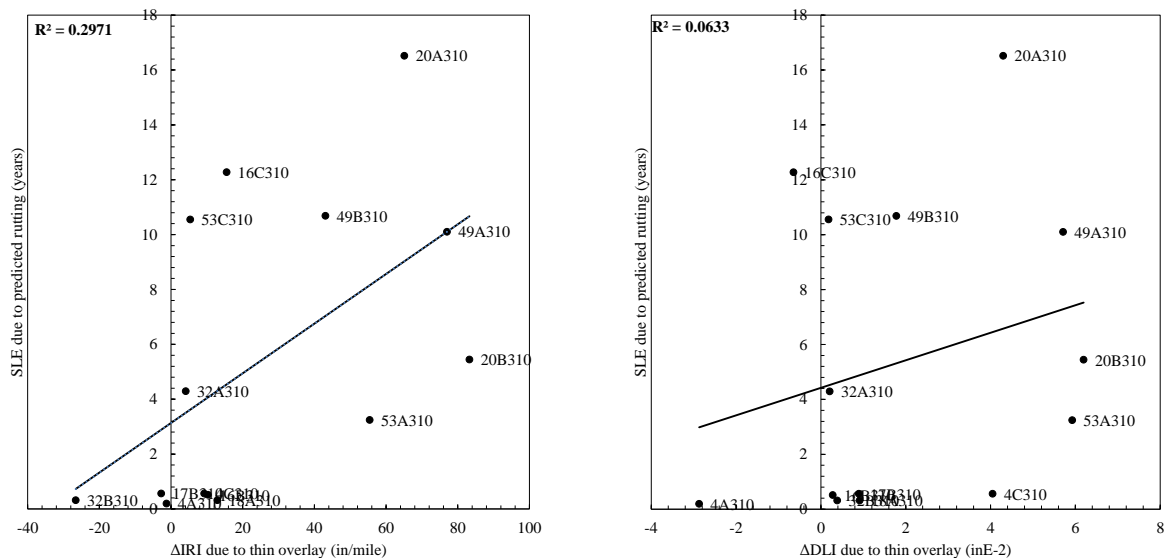
- There were no clear trends between profile-based indices and performance when evaluating predicted performance in terms of SLE due to alligator cracking, longitudinal cracking, and transverse cracking. The predicted performance of transverse and longitudinal cracks varied significantly between pavement sections, and many of the SLEs had unreasonably large positive and negative values. The predicted transverse

cracking values for each pavement section were zero or close to zero, regardless of change in the load spectra.

- The pavement sections experienced varying levels of predicted alligator and longitudinal cracking. Across all pavement sections, the magnitude of alligator cracking was very negligible, at most 1.8 percent after a 20-year design life. The predicted longitudinal cracking at the end of the same design life was highly variable, ranging from 0 to 400 feet per mile, but remains a less significant value when considering the average nationally calibrated threshold in MEPDG for 20-year-design life is 2000 feet per mile (33). These variations in performance led to an inconclusive range of SLEs from which no reasonable trends with respect change to profile index could be obtained.
- Thermal cracking is not a load related distress and is not expected to change as a result of changing the load spectra inputs in the MEPDG. Therefore, predicted performance in terms of transverse cracking is difficult to directly relate to the impact of thin overlay treatment.
- A significant variation in performance was observed in predicted SLE due to rutting. This variation may be due to a variety of construction and material related factors, including: traffic, mix design, pavement layer structure, and climate.

An attempt was made to group the pavement sections with similar characteristics, such as similar traffic levels (ranges of AADTT), similar overlay thicknesses (less than one inch and greater than one inch), similar structure (with base and without base), and climatic location (freeze and non-freeze). However, no clear trends were observed when relating cracking performance measures to a change in surface roughness index with respect to these identified groups.

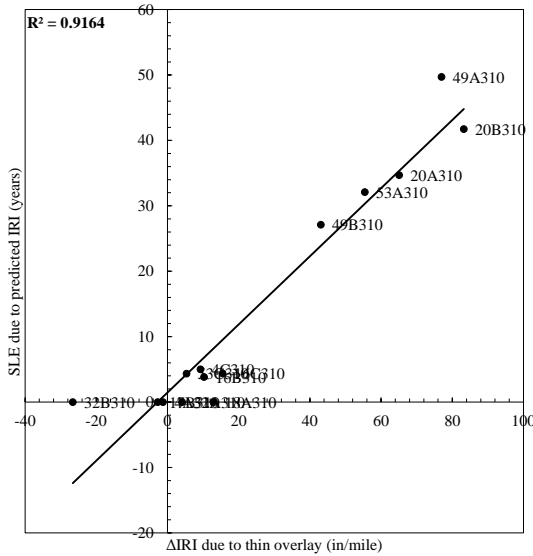
These observations suggest that it is more difficult to determine performance-based relationships between IRI and DLI for thin overlain pavements when considering the MEPDG predicted performance measures of cracking and rutting. There were no reasonable SLE values that could be concluded from observation of cracking performance, and Figure 6.12 shows only a weak correlation between change in roughness index and SLE due to rutting. As stated previously, Gillespie et. al (8) determined that gross vehicle weights and the maximum axle load on each vehicle combination have a direct impact on permanent deformation of asphalt pavements. Therefore, the change in rutting performance may not be accurately captured through a change in dynamic load spectra. However, it is difficult to consistently apply the proposed mechanistic-empirical procedure to constant GVWs. It is more appropriate to specify that the change in performance as a result of thin overlay is solely due to life extension as a result of predicted IRI.



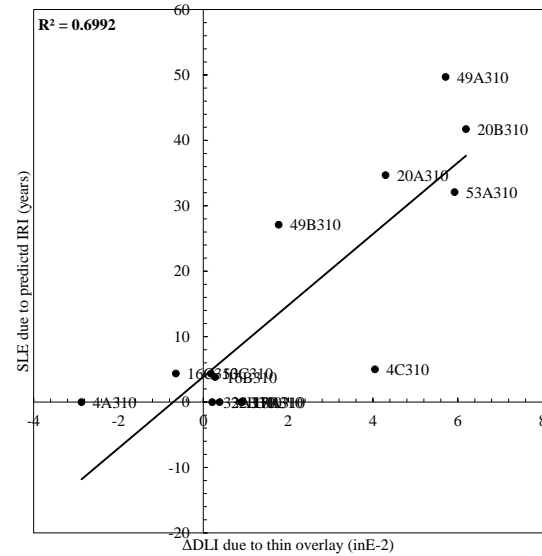
(a) Δ IRI vs SLE due to predicted rutting

(b) Δ DLI vs SLE due to predicted rutting

Figure 6.12: Effect of thin overlay on predicted rutting performance



(a) ΔIRI vs SLE due to predicted IRI

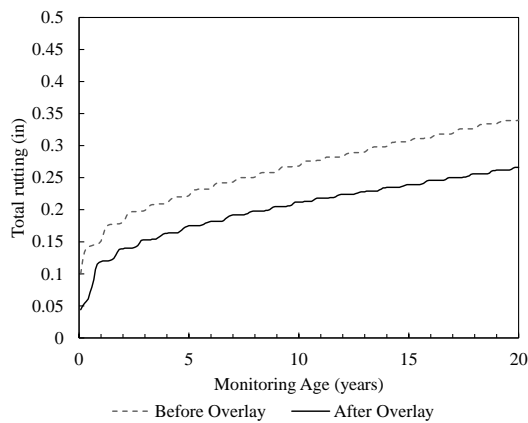


(b) ΔDLI vs SLE due to predicted IRI

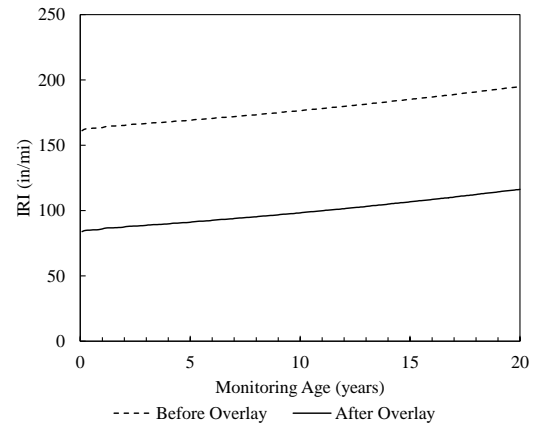
Figure 6.13: Effect of thin overlay on predicted roughness performance

In contrast to rutting, Figure 6.13 shows that the change IRI and DLI correlate well with the performance of thin overlain treatment due to predicted roughness, based on the relationship developed using the proposed mechanistic-empirical procedure. It is possible that with more exact representation of asphalt pavement properties (more directly Level 1 inputs from real-time construction), a more accurate performance-based relationship between the IRI and DLI and the other performance measures can be developed. In continuation of the example of effective and ineffective thin overlay treatment, the impact of change in pavement roughness, and thus a change in dynamic load, on predicted performance is presented in Figure 6.14, for sections 49-A310 and 32-B310. The effect of the reduction in profile roughness can be seen in Figures 6.14 a and b, as each reaches a lower level of predicted rutting and IRI measure at the end of the design life. In contrast, the performance measures of rutting and IRI increase as seen in Figures 6.14 c and d. Note that although sections such as 49-A310 exhibited an improvement in rutting performance due to a change in dynamic load spectra inputs, the overall distribution of predicted

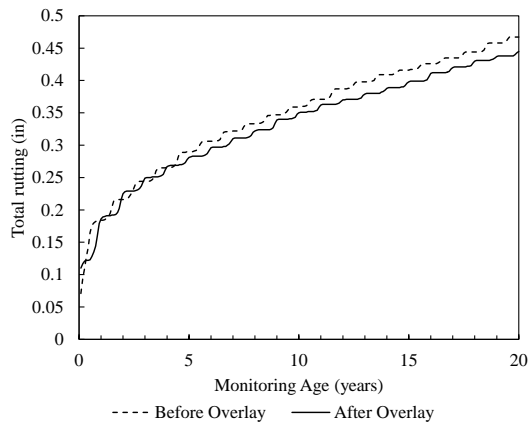
rutting performance was highly variable. It is likely that the change in rutting performance cannot be attributed to dynamic load, given the high discrepancies observed in predicted SLE due to rutting. However, it is more feasible that the change in SLE due to predicted IRI can be attributed to the change in dynamic loads, which can be amplified or reduced with respect to a change in pavement roughness.



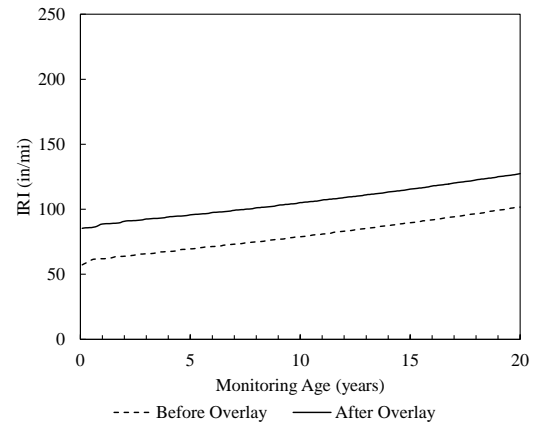
(a) 49-A310 rutting



(b) 32-B310 rutting



(c) 49-A310 IRI



(d) 32-B310 IRI

Figure 6.14: Comparison of effective and ineffective thin overlay treatment

CHAPTER 7: Summary, Conclusions, Recommendations

This chapter presents the summary of findings, conclusions, and recommendations for the proposed mechanistic-empirical analysis procedure as a means to evaluate the effect of diamond grinding and thin overlay treatments on roughness and predicted performance.

7.1 Summary of findings

In this study, a mechanistic-empirical procedure was developed and tested for relating the effect of change in pavement roughness, due to diamond grinding and thin overlay, on predicted pavement performance. This effect was quantified using established profile-based indices (IRI and DLI), and the performance was quantified with pavement service life extension (SLE) in terms of MEPDG-predicted performance measures. A summary of findings is given below:

1. The effect of diamond grinding on profile characteristics:
 - a. Grinding treatment generally improved surface smoothness as exhibited by a reduction in profile-based indices IRI and DLI for most of the pavement sections evaluated.
 - b. IRI and DLI appear to correlate well when describing this change in roughness with an R^2 value of 0.86.
 - c. The pavement sections that exhibited an increase in roughness (increase in IRI and DLI) after treatment show minimal change, or in some cases an increase, in profile PSD signal amplitude. This observation corresponds with the presence of surface irregularities that may amplify vehicle and axle bounce. The reverse was generally true for pavements that showed an improved surface smoothness after treatment.
2. The effect of thin overlay on profile characteristics:

- a. Thin overlay treatment generally improved surface smoothness as exhibited by a reduction in profile-based indices IRI and DLI for a majority of the sections evaluated.
 - b. Some disagreement between the changes in IRI and DLI was observed. The two indices remain somewhat correlated, though not as well as for diamond grinding treatment. The correlation coefficient R^2 was 0.66.
 - c. The pavement sections which exhibited an increase in roughness (increase in IRI and DLI) after treatment showed minimal change, or in some cases increase, in profile PSD signal amplitude. This suggests the presence of surface irregularities that may amplify vehicle body and axle bounce. The reverse was generally true for pavements that showed an improved surface smoothness after treatment. This is a similar observation as that on the effect of roughness change on profiles treated with diamond grinding.
3. The effect of diamond grinding on dynamic loads:
- a. Grinding generally reduced the dynamic axle loads, quantified by a measure of change in mean DLC of single and tandem axle loads, separately, before and after treatment.
 - b. The use of Class 9 load distributions was validated using Class 5, 9, and 12 distributions to show that there is only a small difference in change in mean DLC (2.6 to 7.6 percent difference).
 - c. IRI and DLI were both able to characterize the change in DLC, although with weak correlations with the change in single axle DLC ($R^2 = 0.274$ for DLI and R^2

= 0.198 for IRI) and in tandem axle DLC ($R^2 = 0.270$ for DLI and $R^2 = 0.279$ for IRI)

4. The effect of thin overlay on dynamic loads:
 - a. Thin overlay generally reduced the dynamic axle loads, quantified by a measure of change in mean DLC of single and tandem axle loads, separately, before and after treatment.
 - b. The use of Class 9 load distributions was validated using Class 5, 9, and 12 distributions to show there is only a minimal difference in change in mean DLC (10.5 to 13.6 percent difference). This difference is slightly larger than that of diamond grinding.
 - c. IRI was generally better than DLI in capturing the effect on DLC ($R^2 = 0.160$ for IRI and $R^2 = 0.02$ for DLI, for single axle; $R^2 = 0.246$ for IRI and $R^2 = 0.0627$ for DLI, for tandem axle). These correlations are lower than those found for diamond grinding treatments, suggesting that thin overlays are less effective in reducing dynamic loads.
5. The effect of diamond grinding on predicted SLE performance:
 - a. The MEPDG performance prediction resulted in the following ranges of SLE due to diamond grinding: -2.6 to 4.4 years (faulting), -0.8 to 14.4 years (fatigue cracking), and 0 to 36 years (IRI).
 - b. The predicted SLE due to IRI has a much greater range than that of SLE due to faulting or fatigue cracking. Eighty-eight percent of sections experienced an improvement of life greater than 1 year due to predicted roughness, compared to 38 percent for predicted faulting and 31 percent for predicted fatigue cracking.

- c. Sections that exhibited no cracking prior to treatment also exhibited no cracking after treatment, and this was present in both the monitored and predicted cracking performance.
 - d. Although there is a variation in the magnitude of SLE due to diamond grinding, it appears that a relationship can be developed between profile-based indices and predicted performance (i.e., faulting, fatigue cracking, and roughness.)
6. The effect of thin overlay on predicted SLE performance:
- a. The MEPDG performance prediction resulted in the following ranges of SLE due to diamond grinding: 0.2 to 16.5 years (rutting), 0 to 50 years (IRI).
 - b. The predicted performance of alligator cracking was negligible, with an observed maximum amount of alligator cracking of 2 percent at the end of a 20-year design life. Similarly, the predicted performance of longitudinal cracking highly varied, ranging from 0 to 400 foot per mile at the end of design life, the maximum value being negligible in comparison to the MEPDG nationally calibrated threshold of 2000 feet per mile. Due to these trends observed in alligator and longitudinal cracking, no conclusive trends could be obtained from the predicted SLE due to these performance measures.
 - c. The predicted transverse (thermal) cracking for each pavement section was zero or close to zero throughout the pavement design life. This is to be expected, as thermal cracking is non-load related and therefore should not be expected to be affected by variations in load spectra.
 - d. The potential for a relationship between the change in IRI and DLI versus SLE due to rutting exists, but with high variation in SLE magnitude. No clear trends

were observed despite grouping the pavement sections based on similar characteristics in terms of traffic, overlay thicknesses, structure, and climate.

- e. The profile based indices IRI and DLI were able to correlate better with the performance predictions in terms of SLE due to roughness, with $R^2 = 0.51$ for IRI and $R^2 = 0.39$ for DLI.

7.2 Conclusions

This study proposed and evaluated a procedure that uses a mechanistic-empirical approach for developing a performance-based relationship between roughness indices IRI and DLI and pavement performance. This was done for evaluating two preservation treatments that are designed to improve pavement surface smoothness: Diamond grinding of concrete pavements and thin overlay on asphalt pavements. To test this procedure, the monitored data before and after treatment were obtained from the LTPP database for 16 concrete pavement sections and 14 asphalt pavement sections.

The pavement profiles of these sections were used to calculate the change in roughness indices due to treatment (Δ IRI and Δ DLI) and evaluate characteristics pertaining to profile elevations and profile PSD signal that describe the effect of roughness-index change. These same profiles were used to simulate the dynamic response of Class 9 tractor semi-trailer axle load distributions, before and after treatment, using the TruckSim software. The effect of roughness change on dynamic loads was evaluated by determining the mean DLC of the dynamic load spectra for single and tandem axle loads. The resulting variations in dynamic load spectra were used as inputs to the MEPDG performance prediction software. The effect of the change in roughness on predicted pavement performance was determined by comparing the service life

extension (SLE) for the performance measures predicted by the software. The conclusions of applying the aforementioned analysis procedure are as follows:

- Diamond grinding and thin overlay generally improved surface smoothness as quantified by ΔIRI and ΔDLI . Surface smoothening generally resulted in a reduction of high amplitudes in the profile PSD signal which signifies a reduction in surface irregularities. ΔIRI and ΔDLI appear to correlate with each other well, and this correlation is stronger when evaluating roughness change due to diamond grinding compared to thin overlay.
- An increase in pavement roughness (ΔIRI and ΔDLI) generally resulted in an increase in dynamic load which was quantified using the change in mean DLC of single and tandem axles. However, a better correlation between roughness indices and DLC was found for sections treated with diamond grinding as compared to those treated with thin overlay. This suggests that thin overlay treatments were not as effective as diamond grinding in impacting the dynamic load.
- In terms of the impact of smoothening treatments on pavement performance, the majority of pavement sections showed that a reduction in both roughness and dynamic load yielded an extension of service life. However, the magnitudes of these SLE varied among sections, and between performance measures. In the case of diamond grinding, the change in dynamic load seemed to accurately reflect the SLE obtained from predicted cracking, faulting, and IRI. However, in the case of thin overlay treatment, the SLE ranges were inconclusive for all measures of cracking. Although the SLE due to rutting showed minimal correlation, the main contributor to the permanent deformation of asphalt pavements are gross vehicle weights of heavy vehicles. Therefore, the use of change in dynamic load spectra to predict the rutting performance of asphalt pavements is

not recommended. The SLE due to predicted IRI was much better correlated with a change in dynamic load. Therefore, the use of change in dynamic load spectra to predict the IRI performance of asphalt pavements is warranted.

- Among the sections treated with diamond grinding, it was observed that sections with lower SLE and worsening roughness had lower slab thicknesses, experienced higher AADTT levels, or were located in areas with low average annual wet days (potential of high slab temperature gradients could adversely impact performance). Among the sections treated with thin overlay, no clear trends were observed between pavement characteristics and performance. Certain performance measures predicted through MEPDG were negligible (alligator and longitudinal cracking) or nonexistent (transverse cracking), thus providing no conclusive SLE results. In general, the change in roughness indices, Δ IRI and Δ DLI, were able to better correlate with the performance of diamond ground pavements than that of thin overlain pavements.
- The mechanistic-empirical relationship proposed for predicting performance (service life extension) due to a known roughness-based index (Δ IRI and Δ DLI) showed good potential for developing performance-based relationships for preservation treatments known to impact pavement roughness (diamond grinding and thin overlay). For any given pavement preservation treatment, the potential for developing a performance-based relationship exists when using this procedure.

In current pavement quality assurance and management practice, there is a need to determine the impact of quality characteristics on the predicted performance of the pavement. There are currently few performance-related specifications for pavement preservation treatments, since it is difficult to obtain performance relationships for quality characteristics of treatments that largely

do not affect pavement structural capacity. However, roughness based indices (IRI and DLI) are examples of quality characteristics known to be related to the damage experienced by the pavement based on findings from truck-pavement interactions. As a result, the procedure proposed in this study can be used in real-time project applications for predicting the performance of preservation treatments known to affect pavement roughness, i.e. diamond grinding and thin overlay treatments. Developing relationships between quality characteristics and pavement performance is an important and necessary step as part of developing performance-related specifications in pavement preservation.

7.3 Recommendations

Several recommendations to further evaluate and expand the findings from this study are presented below:

- The number of sections evaluated in this study were shortlisted from a large portion of the sections known to be treated with diamond grinding and thin overlay treatment in the LTPP database. Therefore, it is desirable to expand the analysis using additional pavement sections. In doing so, the following considerations should be made:
 - The proposed mechanistic-empirical procedure can be applied to a series of pavement sections within a single project or region to minimize the impact of environmental and traffic variations. Furthermore, it is desirable to include pavements that are treated only with diamond grinding or thin overlay to ensure the change in predicted performance can largely be attributed to the treatment.
 - The scarcity of pavement profiles before and after treatment and problems with formatting of the profile measurements in the LTPP database, severely limited the number of pavement sections to be evaluated. Many pavement sections were not

evaluated simply due to lack of available profiles. The use of modern profilers and profile measurement techniques should eliminate this issue when applying the mechanistic-empirical procedure for current practice.

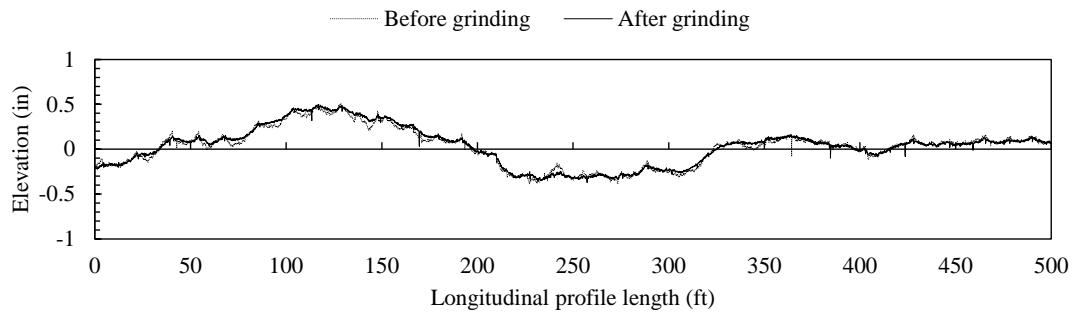
- When applying the procedure in this study to actual pavement sections, it is necessary to obtain as many Level 1 inputs as possible for input into MEPDG/Pavement ME analysis software.
 - Local calibration of the MEPDG/Pavement ME software must also be performed for the pavement sections evaluated. Nationally calibrated averages were used in this study since the pavement sections selected were located across the United States. However, in seeking to eliminate the effect of environment by studying sections in generally one location, local calibration is possible and necessary for accurate performance prediction.
 - Input details pertaining to asphalt mix design and aggregate gradations are especially important and may serve to accurately predict cracking performance measures for thin overlay treatments, a source of variation found in this study. Comprehensive inputs into MEPDG/Pavement ME software will further validate the performance prediction results and allow for the development of performance-based relationships between roughness indices and service life extension due to treatment.
 - Upon obtaining a comprehensive list of construction, traffic, material, and environmental properties for each section, it is possible to perform multiple regression analysis to determine which site factors are statistically significant in impacting pavement performance. The elimination of factors tied to location

(traffic and climate) will serve to increase the accuracy of findings obtained from multiple regression.

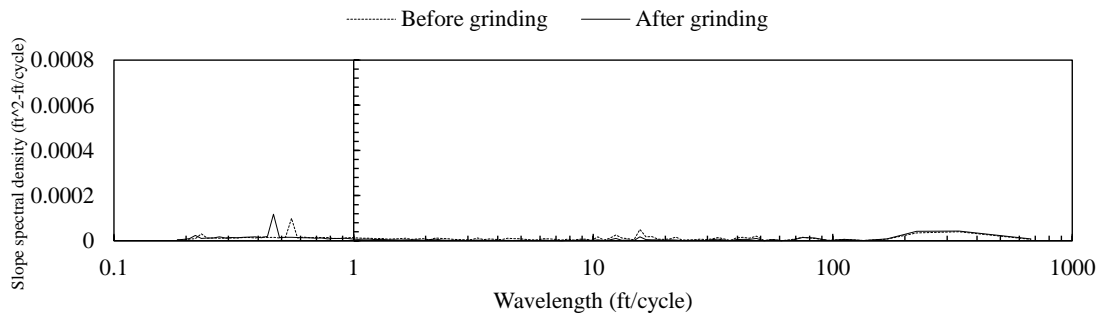
Upon developing performance-based relationships using the above proposed recommendations for a series of pavement sections in one location, the potential for development of a performance-related specification (PRS) for pavement smoothing treatments exists. A key step in developing PRS is establishing performance-based relationships between an acceptance quality characteristic (such as IRI or DLI) and pavement performance (SLE). It is necessary to quantify the impact of a treatment such as diamond grinding or thin overlay, not just on roughness, but also on performance. Service life extension is an easily relatable quantification in practice, since an increase or decrease in pay award can be tied to an improvement or a decline in service life. A state highway agency can apply the mechanistic-empirical procedure proposed in this report to develop PRS unique to pavements within the state. This should help in developing a more effective and comprehensive pavement preservation program.

APPENDICES

Appendix A Concrete pavement profile elevations and PSD

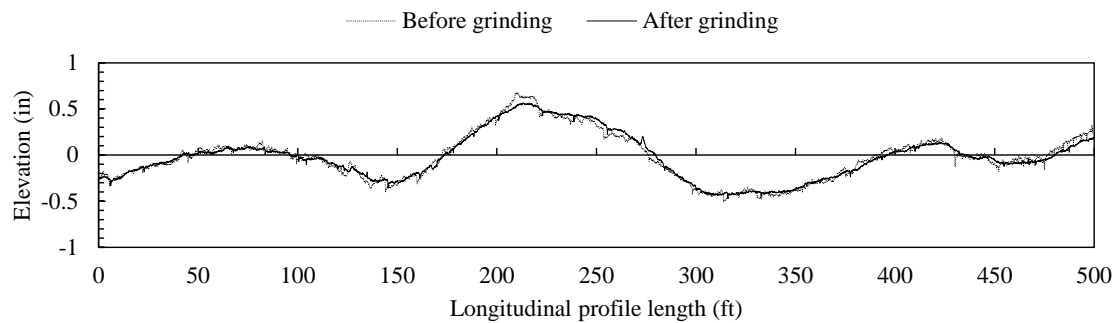


(a) Profile elevations before and after grinding

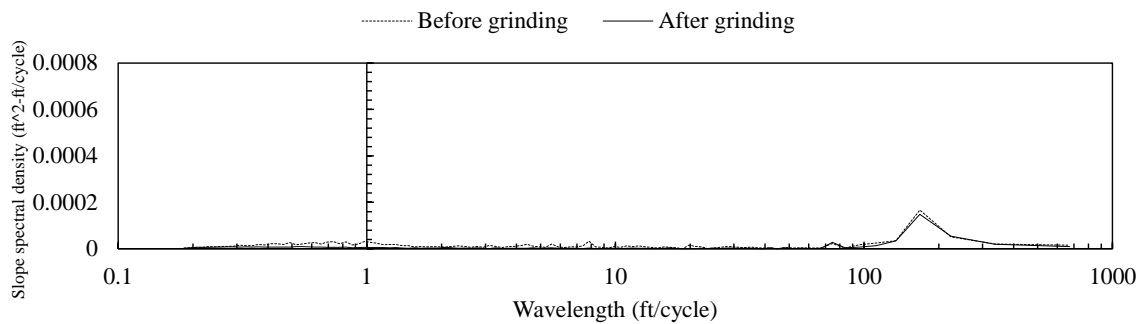


(b) PSD before and after grinding

Figure A.1: 6-3010 profile analysis results

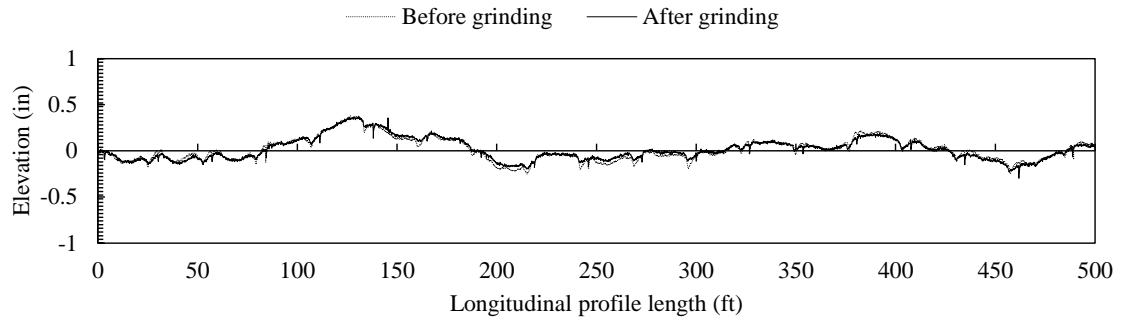


(a) Profile elevations before and after grinding

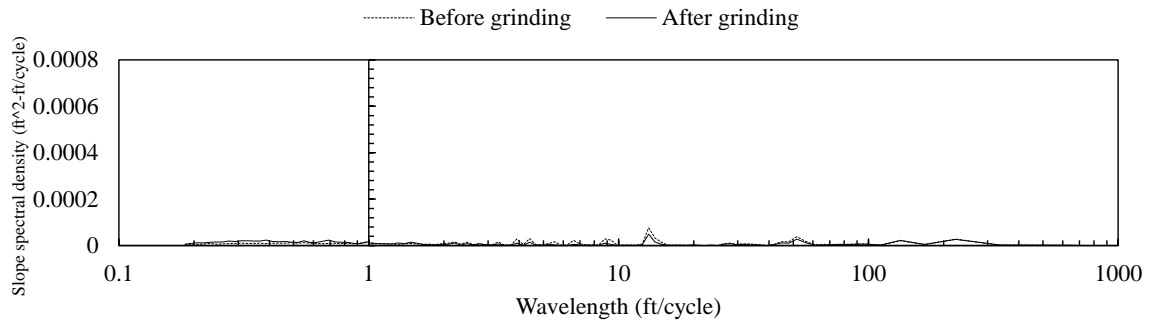


(b) PSD before and after grinding

Figure A.2: 13-3017 profile analysis results

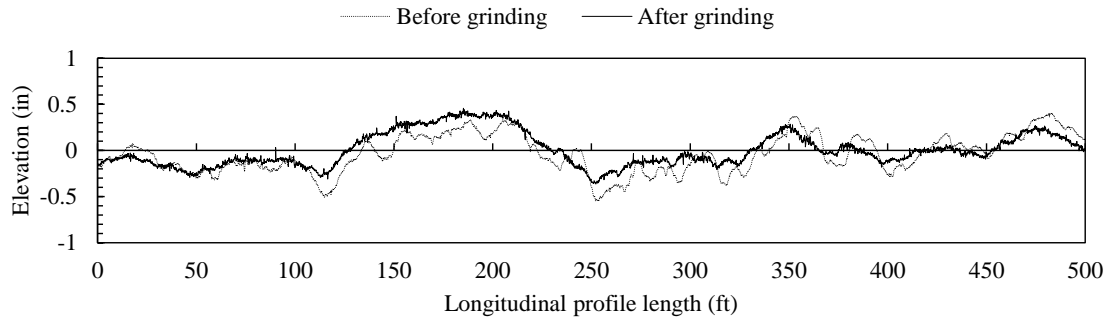


(a) Profile elevations before and after grinding

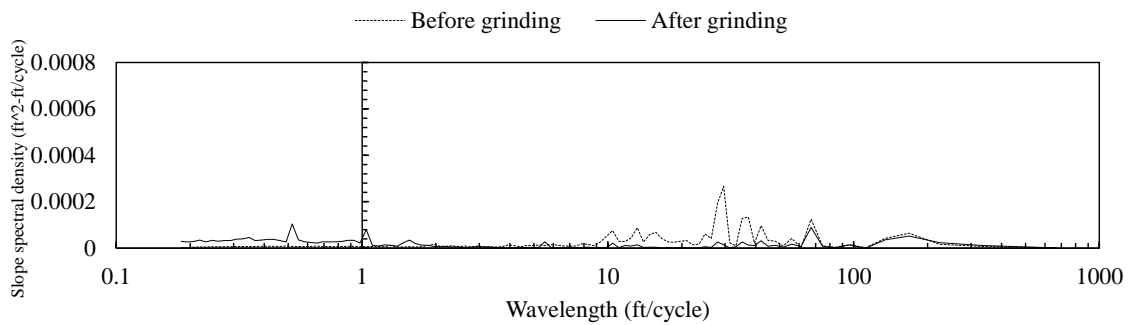


(b) PSD before and after grinding

Figure A.3: 27-4050 profile analysis results

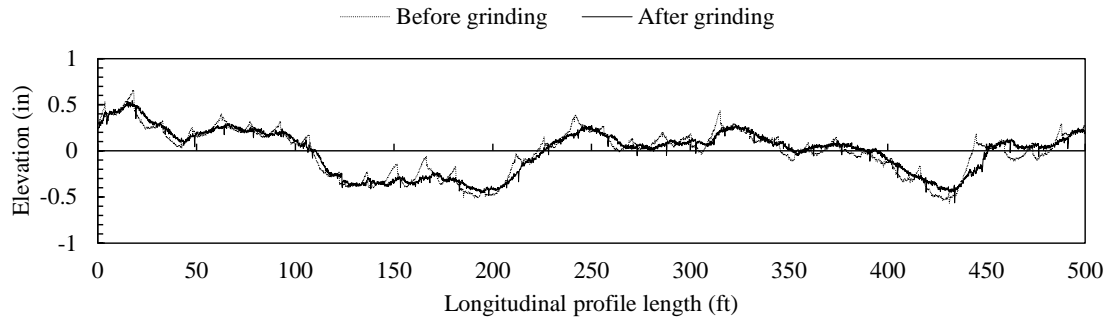


(a) Profile elevations before and after grinding

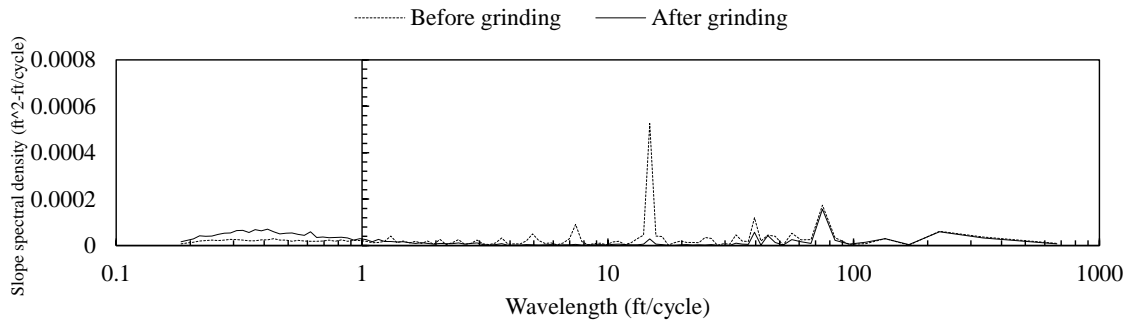


(b) PSD before and after grinding

Figure A.4: 42-3044 profile analysis results

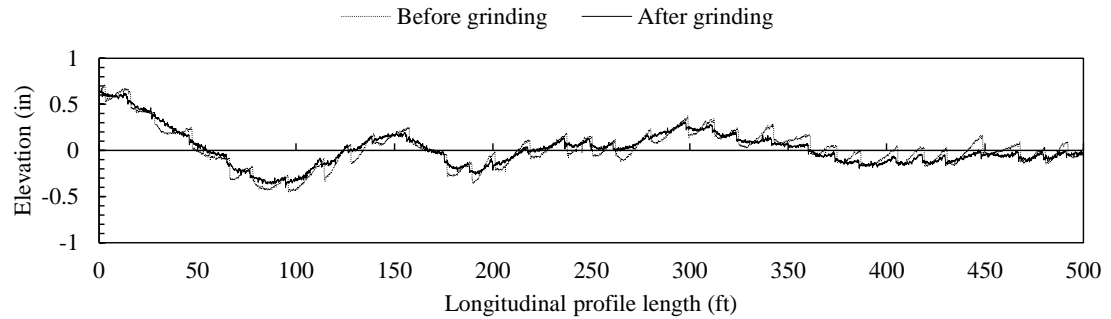


(a) Profile elevations before and after grinding

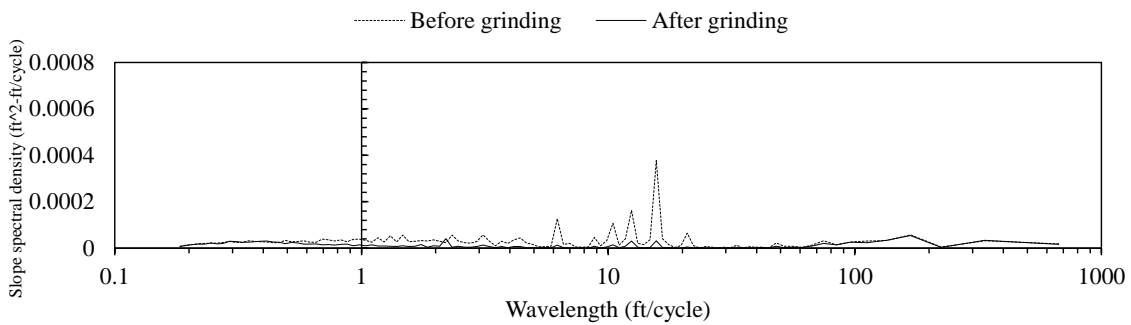


(b) PSD before and after grinding

Figure A.5: 46-3010 profile analysis results

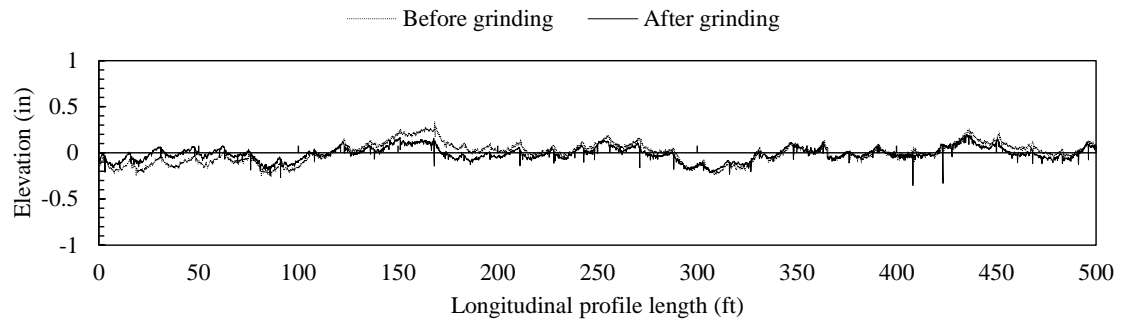


(a) Profile elevations before and after grinding

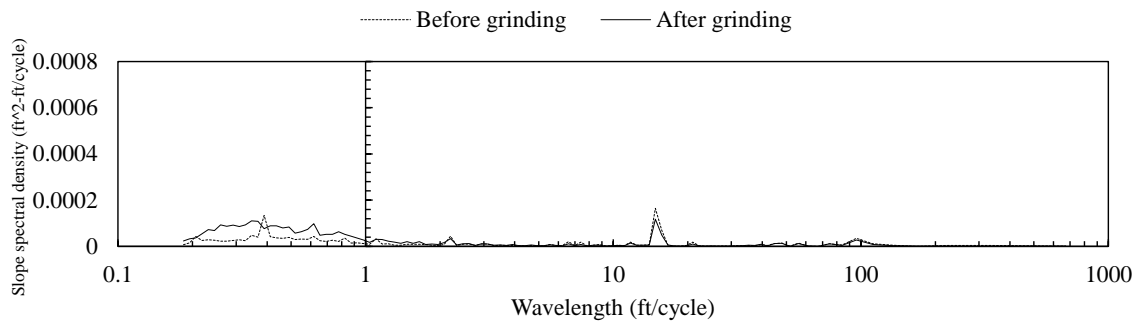


(b) PSD before and after grinding

Figure A.6: 55-3009 profile analysis results

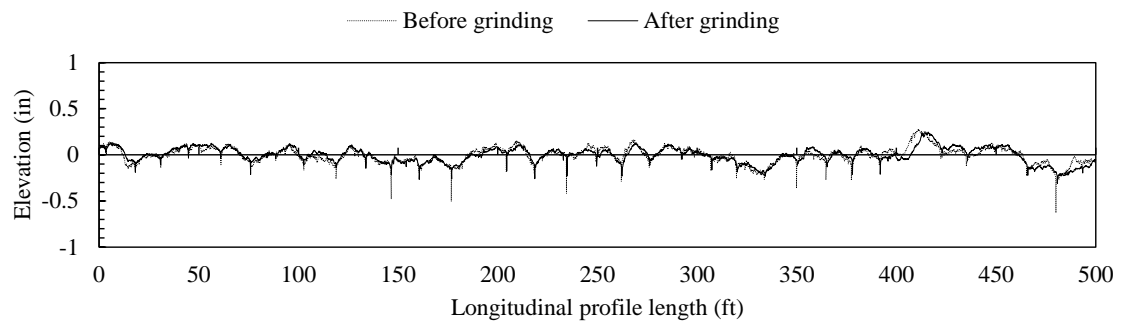


(a) Profile elevations before and after grinding

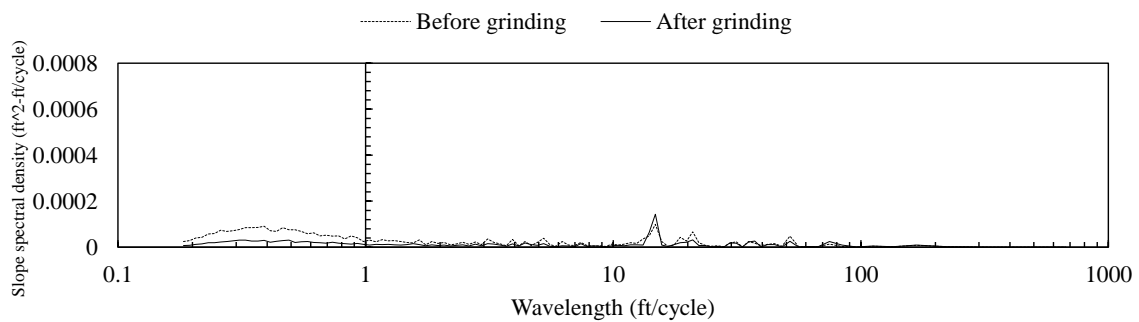


(b) PSD before and after grinding

Figure A.7: 4-7614 profile analysis results

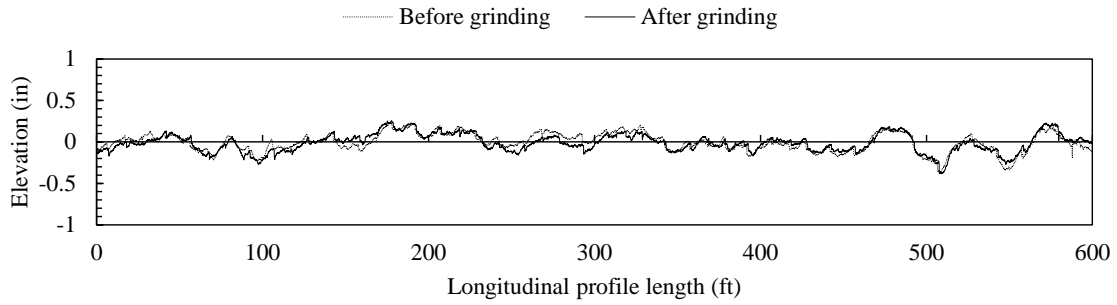


(a) Profile elevations before and after grinding

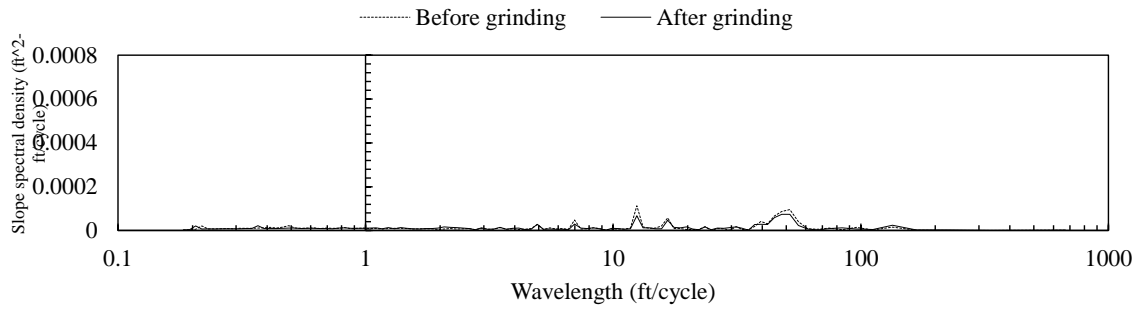


(b) PSD before and after grinding

Figure A.8: 16-3017 profile analysis results

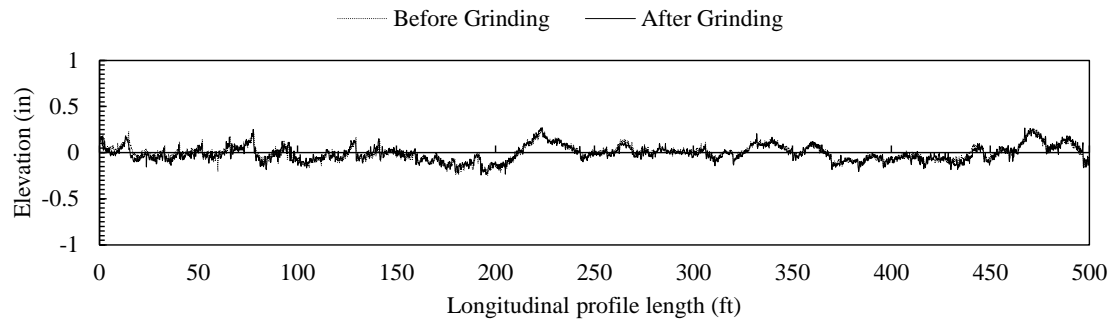


(a) Profile elevations before and after grinding

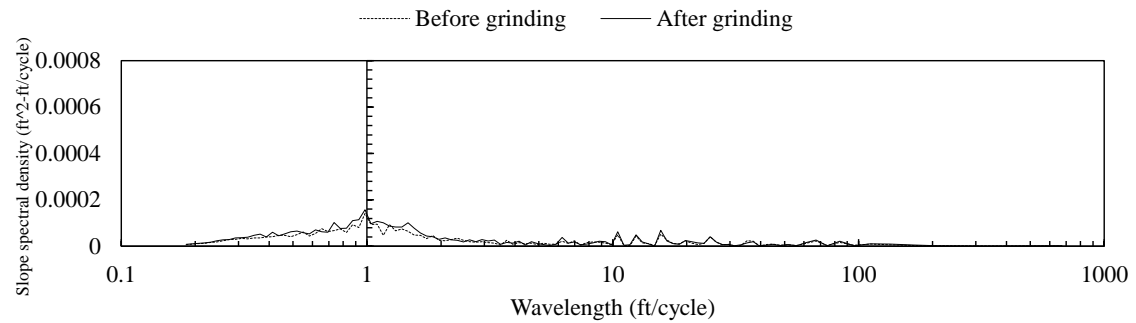


(b) PSD before and after grinding

Figure A.9: 49-C431 profile analysis results

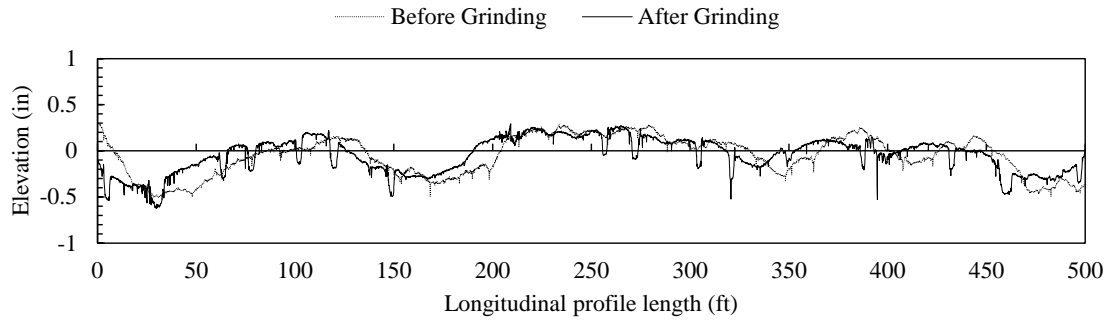


(a) Profile elevations before and after grinding

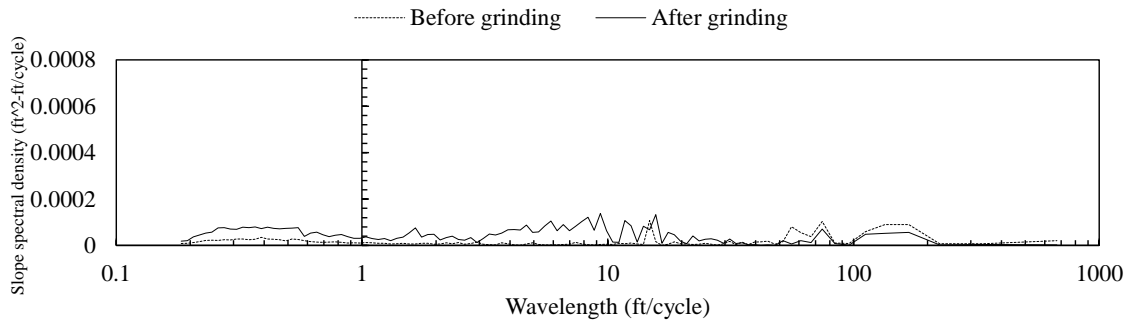


(b) PSD before and after grinding

Figure A.10: 8-3032 profile analysis results

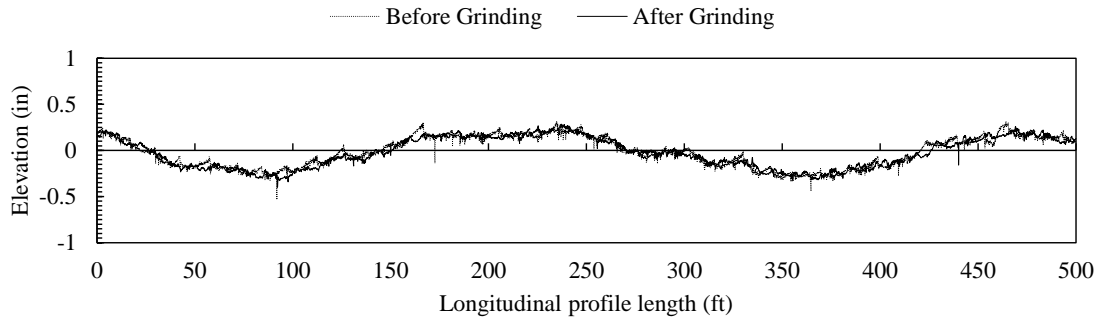


(a) Profile elevations before and after grinding

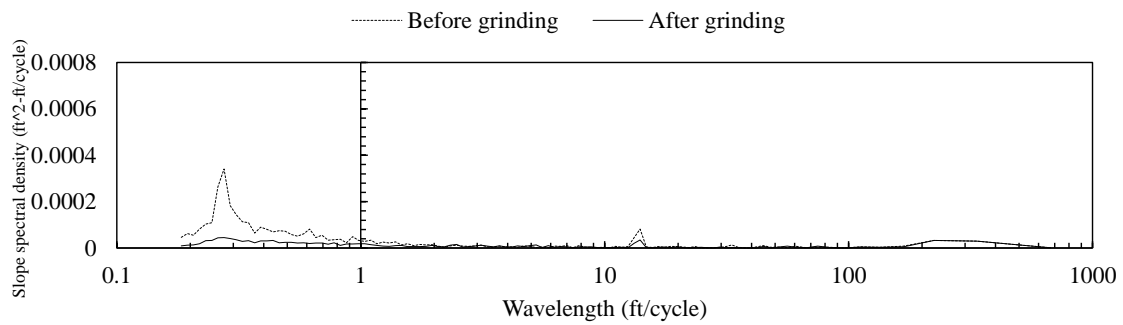


(b) PSD before and after grinding

Figure A.11: 27-3009 profile analysis results

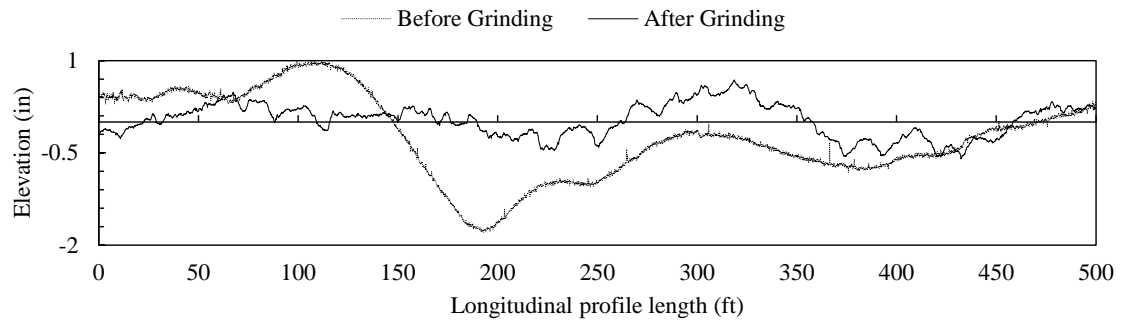


(a) Profile elevations before and after grinding

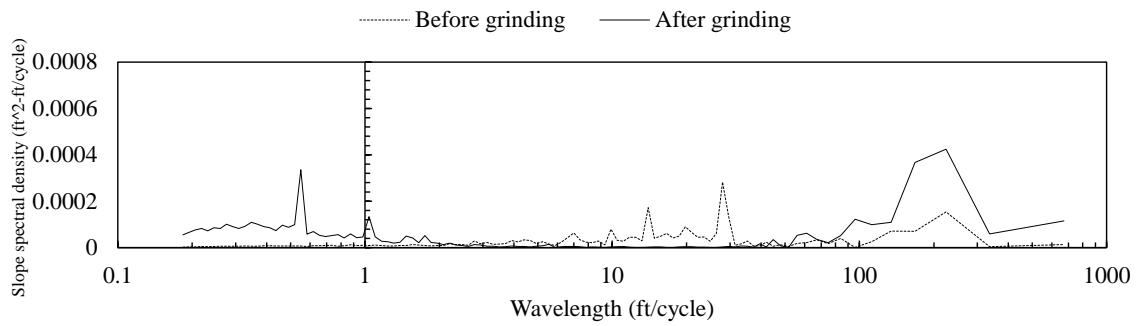


(b) PSD before and after grinding

Figure A.12: 38-3006 profile analysis results

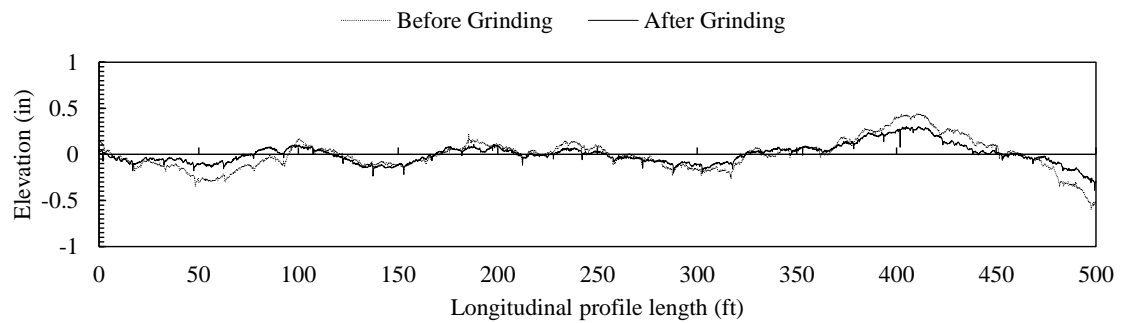


(a) Profile elevations before and after grinding

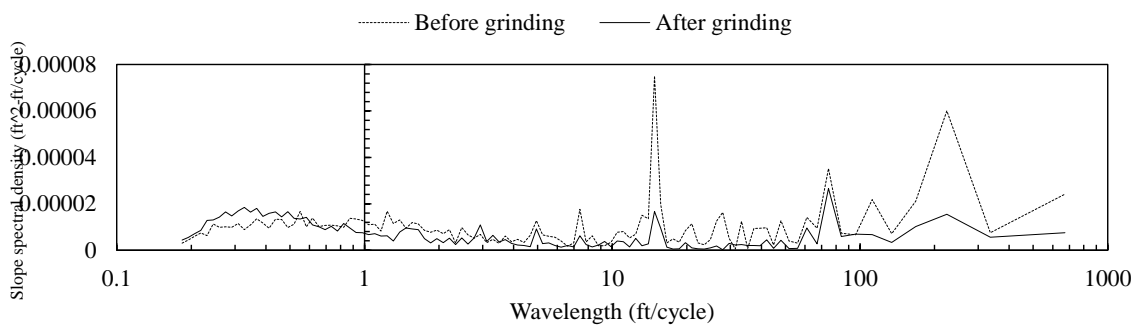


(b) PSD before and after grinding

Figure A.13: 42-9027 profile analysis results

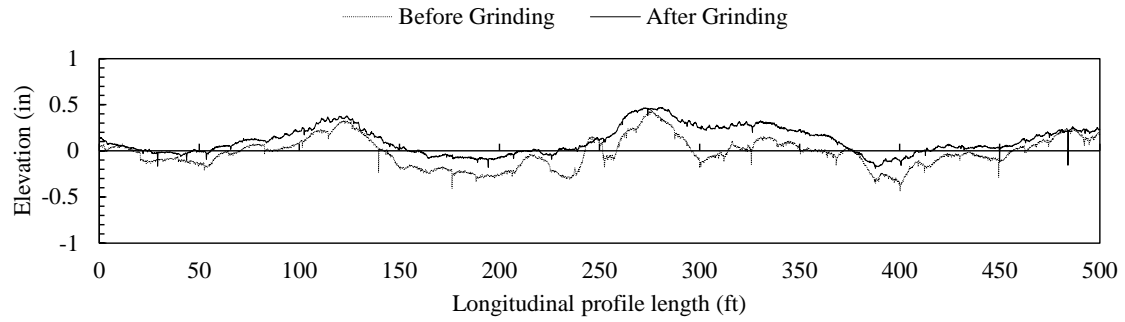


(a) Profile elevations before and after grinding

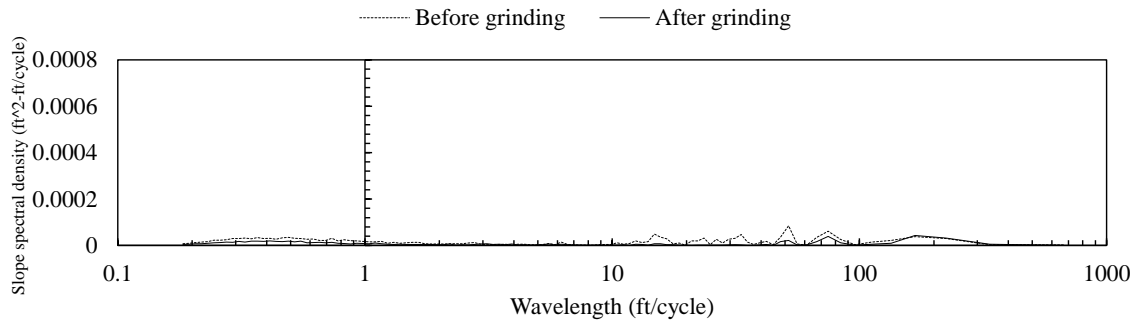


(b) PSD before and after grinding

Figure A.14: 20-3015 profile analysis results

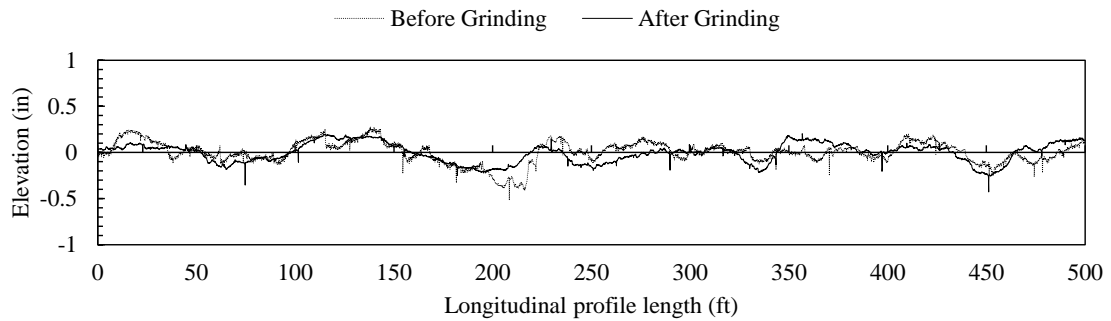


(a) Profile elevations before and after grinding

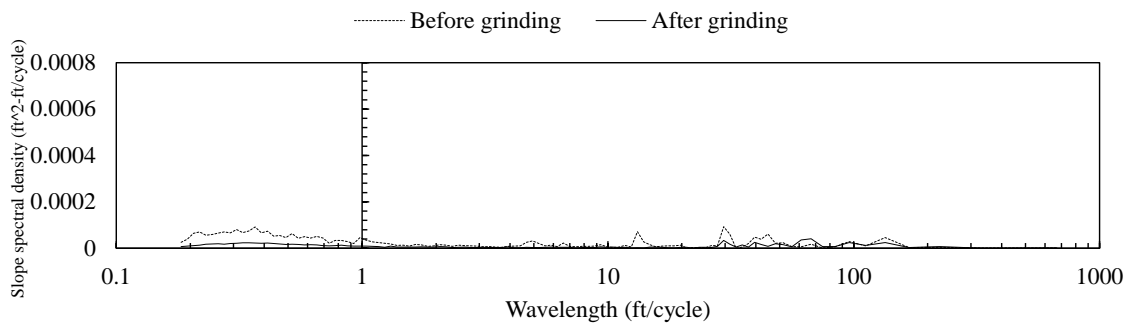


(b) PSD before and after grinding

Figure A.15: 31-3028 profile analysis results



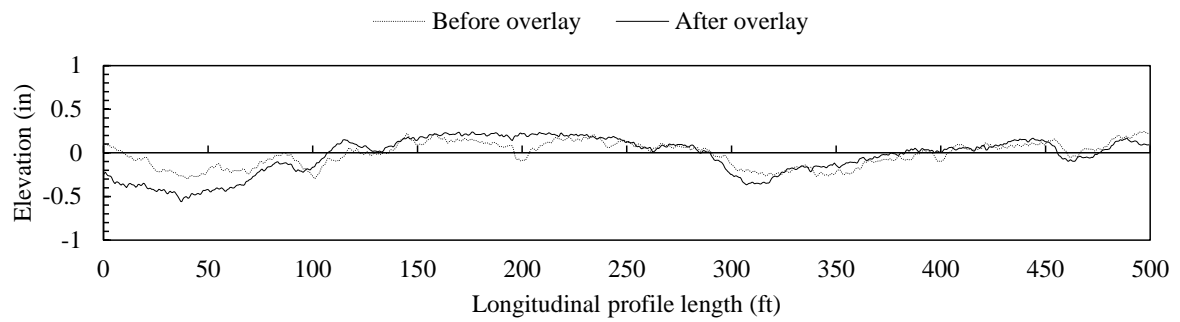
(a) Profile elevations before and after grinding



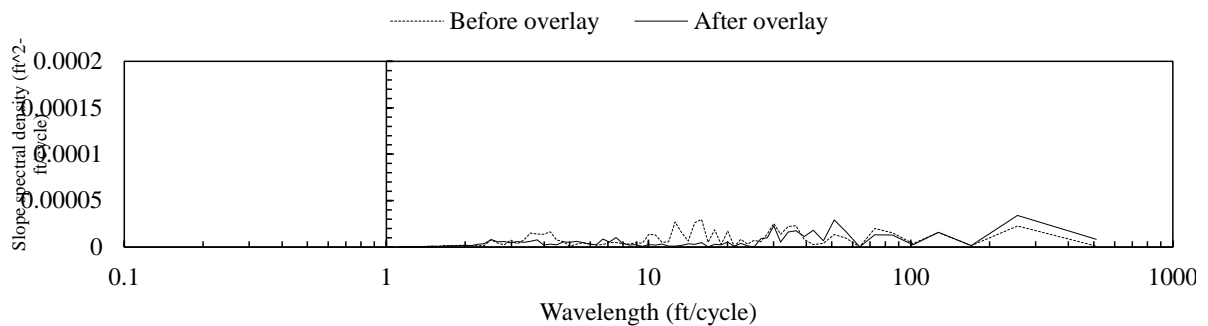
(b) PSD before and after grinding

Figure A.16: 39-9006 profile analysis results

Appendix B Asphalt pavement profile elevations and PSD

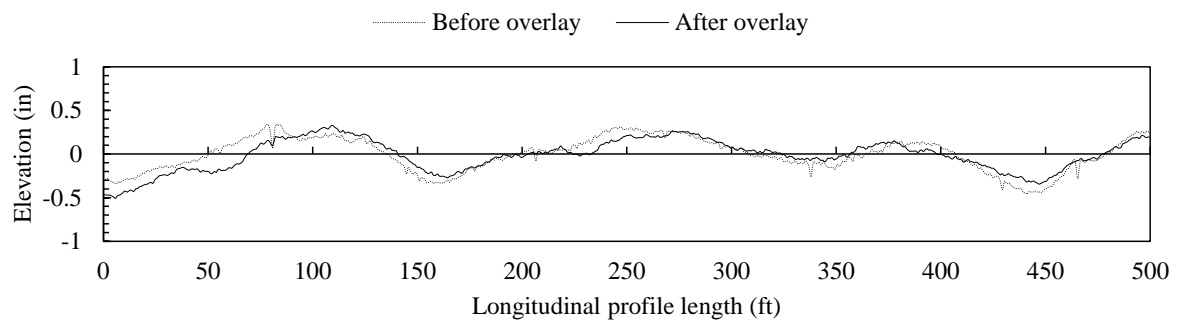


(a) Profile elevations before and after overlay

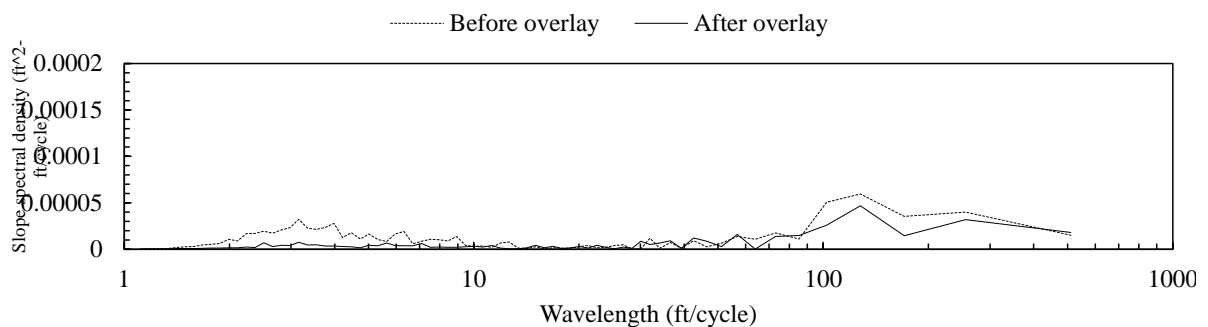


(b) PSD before and after overlay

Figure B.1: 16-B310 profile analysis results

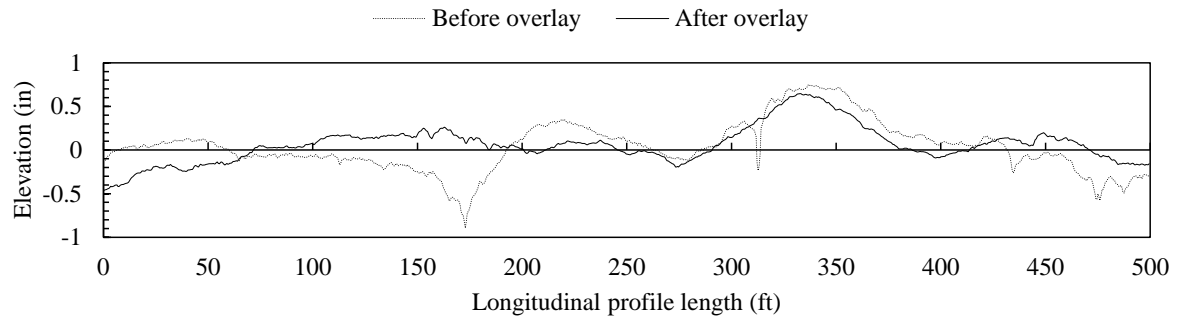


(a) Profile elevations before and after overlay

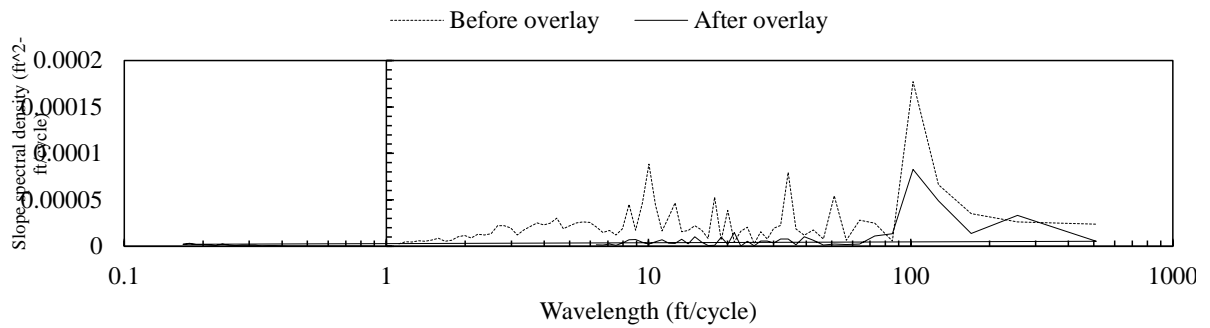


(b) PSD before and after overlay

Figure B.2: 16-C310 profile analysis results

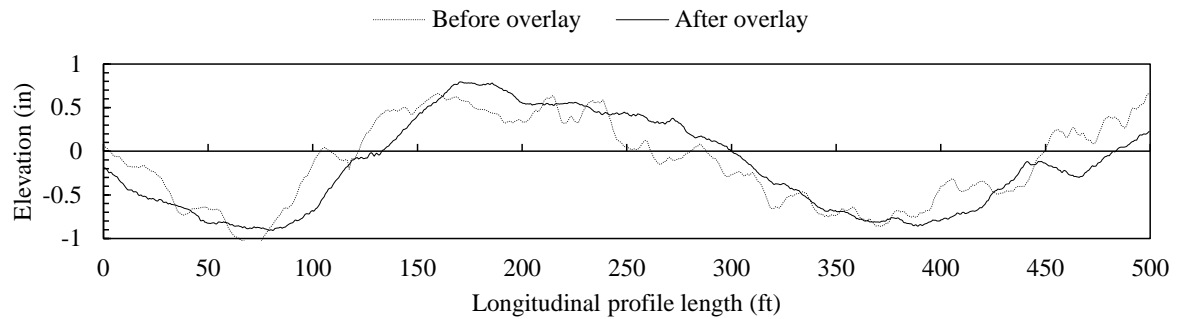


(a) Profile elevations before and after overlay

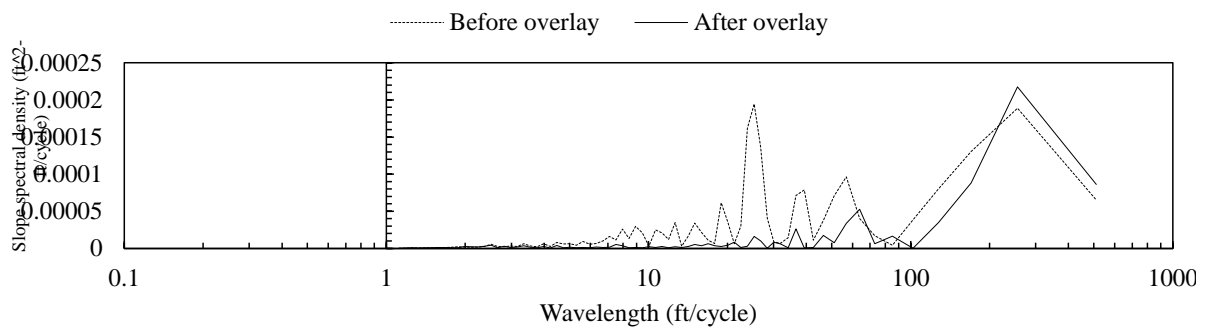


(b) PSD before and after overlay

Figure B.3: 53-A310 profile analysis results

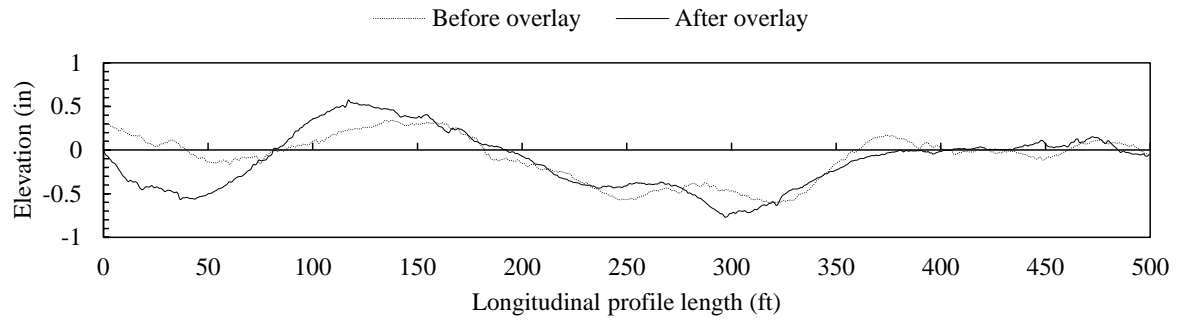


(a) Profile elevations before and after overlay

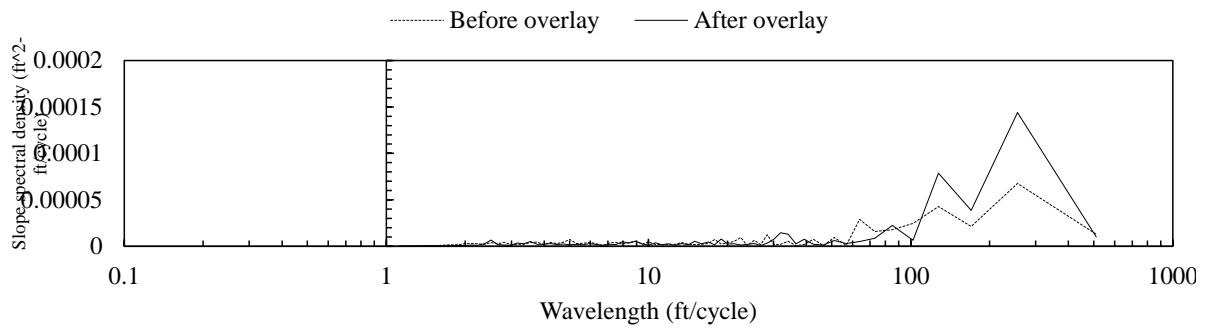


(b) PSD before and after overlay

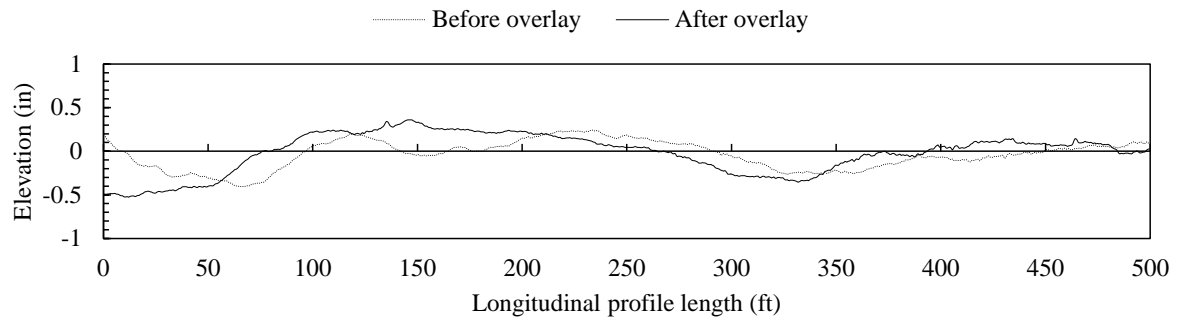
Figure B.4: 20-B310 profile analysis results



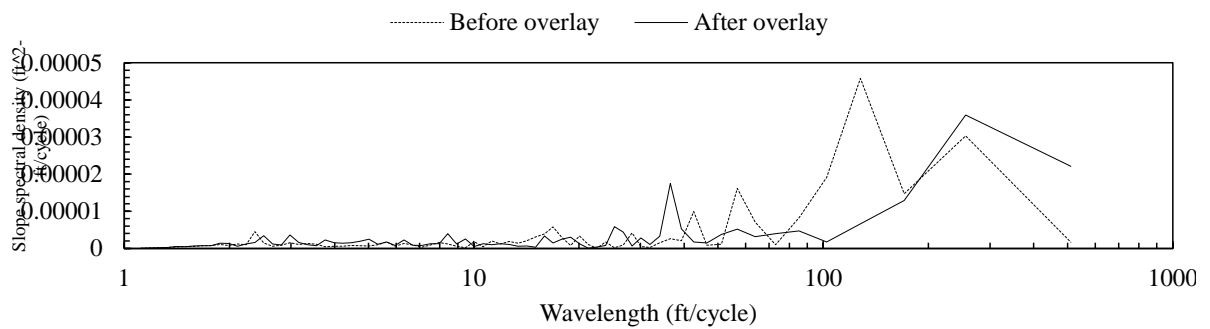
(a) Profile elevations before and after overlay



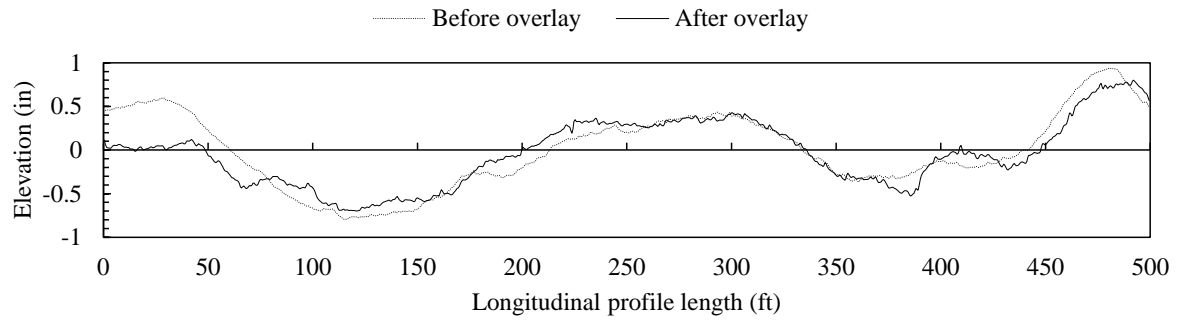
(b) PSD before and after overlay
Figure B.5: 4-C310 profile analysis results



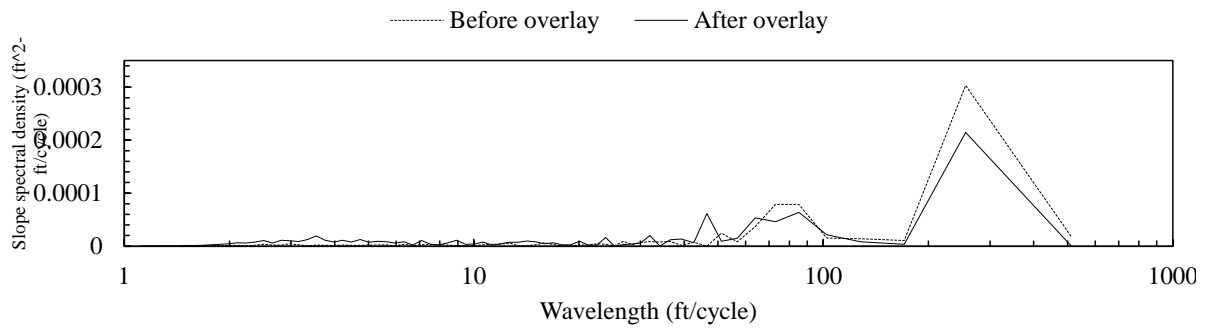
(a) Profile elevations before and after overlay



(b) PSD before and after overlay
Figure B.6: 4-A310 profile analysis results

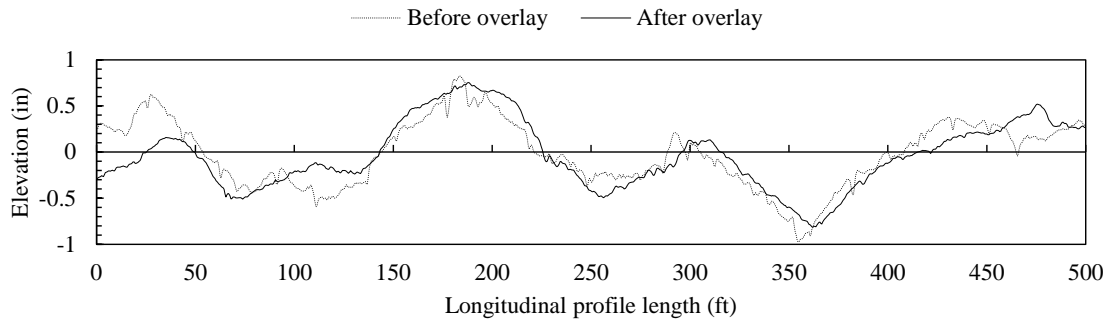


(a) Profile elevations before and after overlay

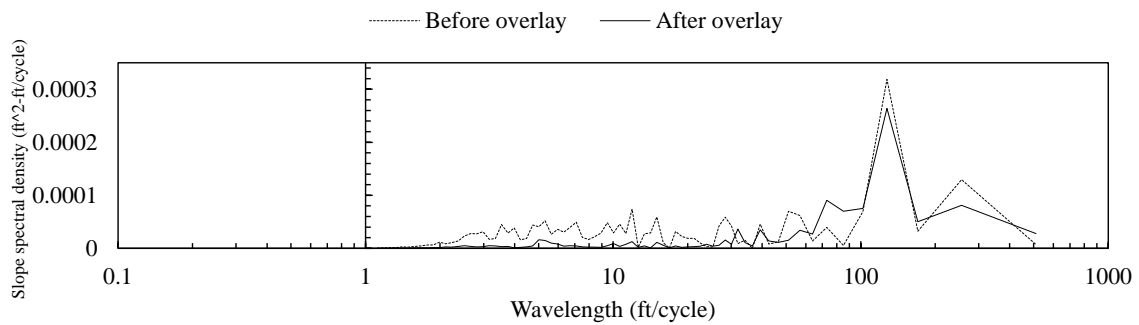


(b) PSD before and after overlay

Figure B.7: 32-B310 profile analysis results

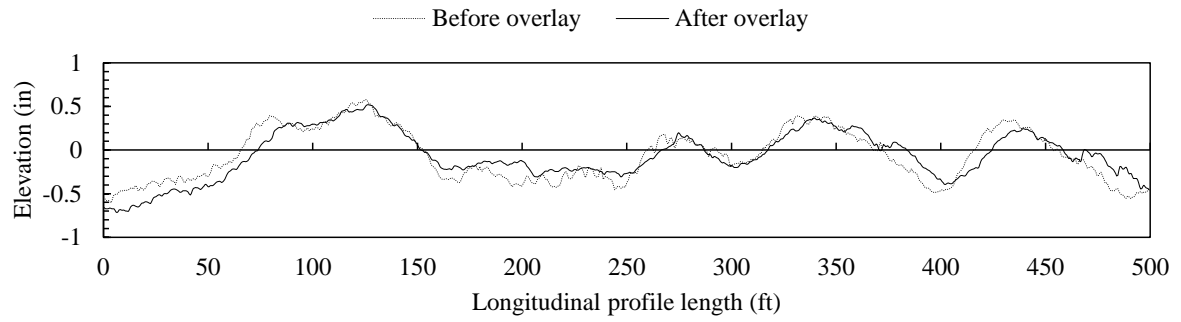


(a) Profile elevations before and after overlay

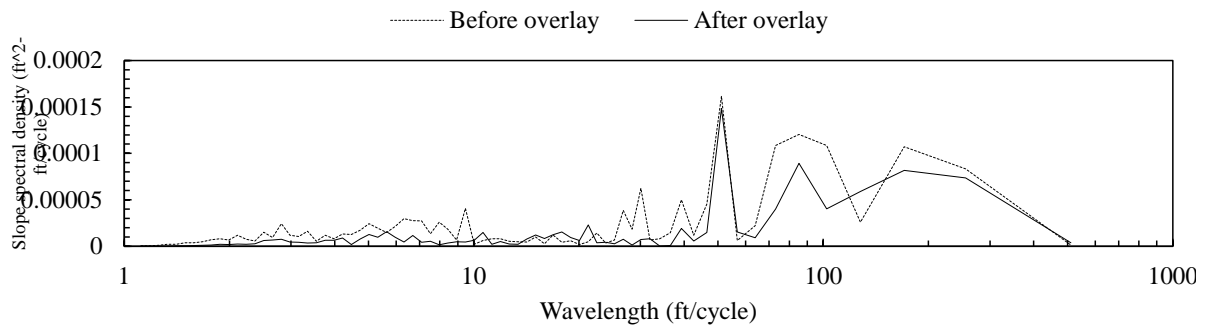


(b) PSD before and after overlay

Figure B.8: 49-A310 profile analysis results

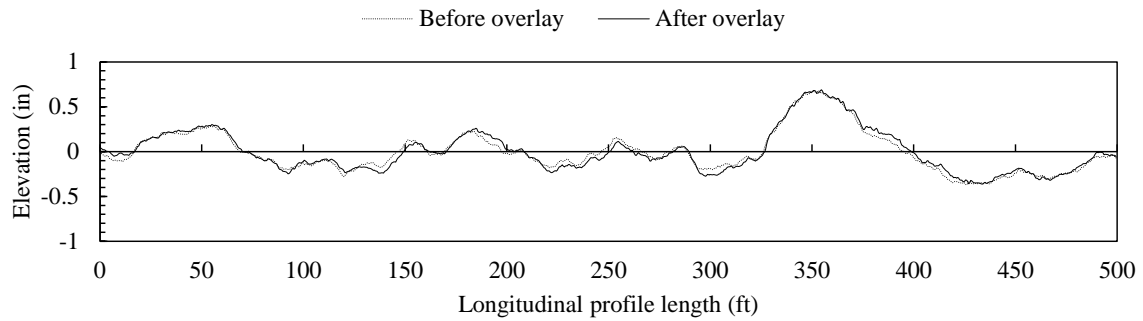


(a) Profile elevations before and after overlay

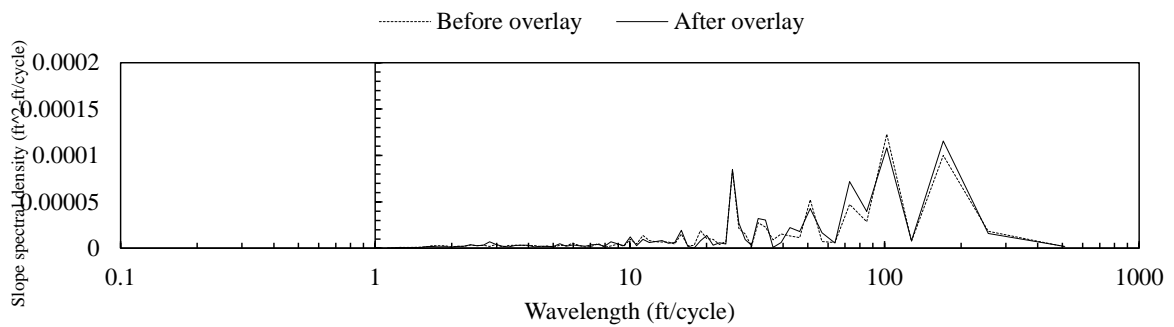


(b) PSD before and after overlay

Figure B.9: 49-B310 profile analysis results

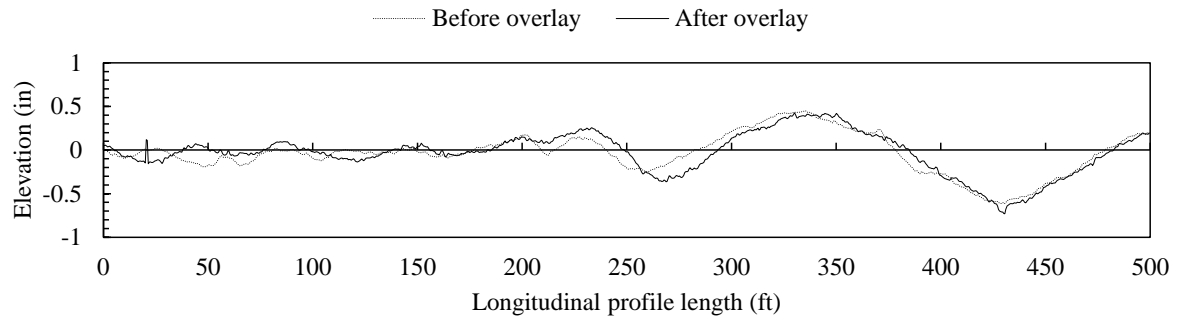


(a) Profile elevations before and after overlay

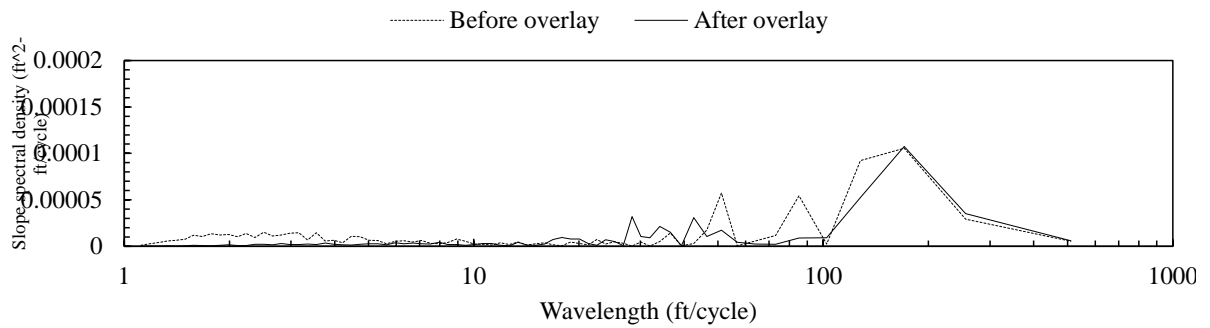


(b) PSD before and after overlay

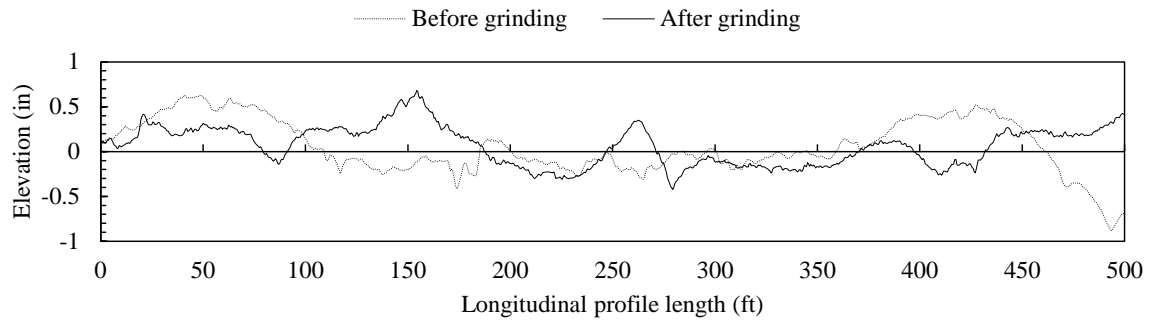
Figure B.10: 17-B310 profile analysis results



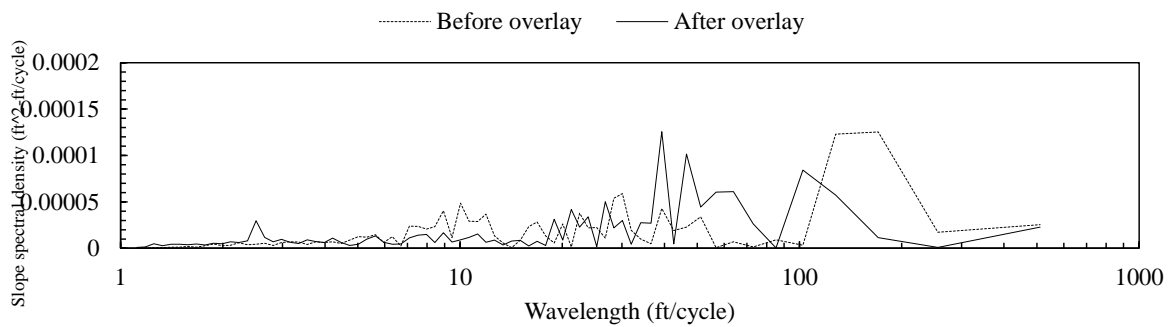
(a) Profile elevations before and after overlay



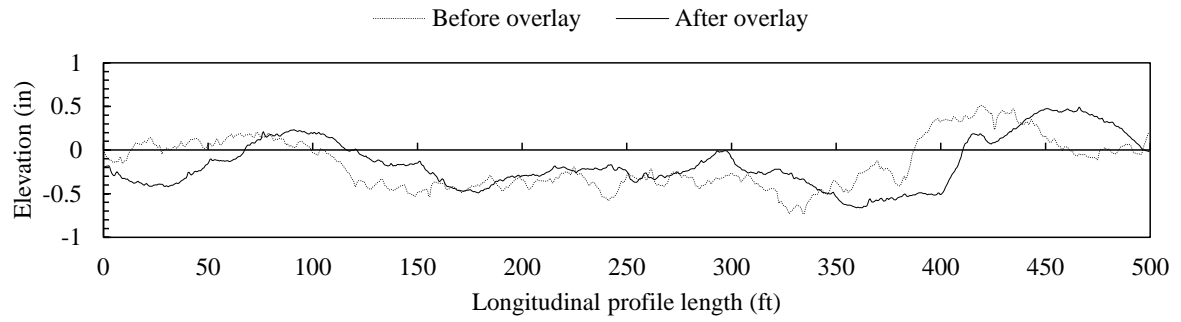
(b) PSD before and after overlay
Figure B.11: 53-C310 profile analysis results



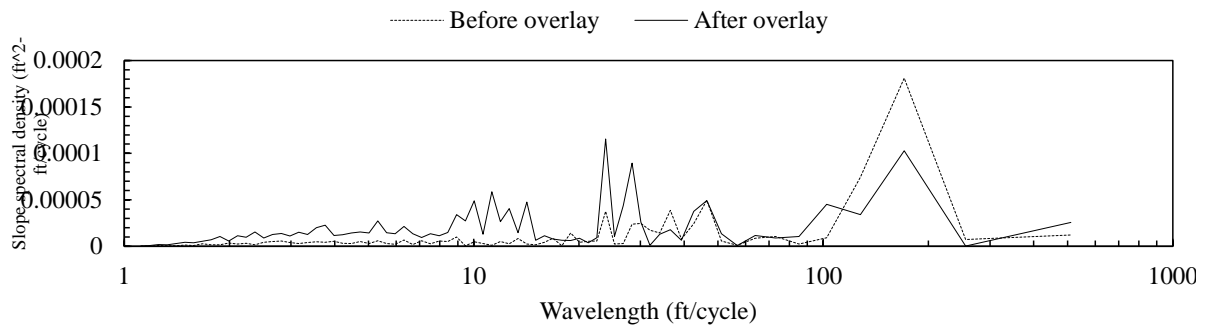
(a) Profile elevations before and after overlay



(b) PSD before and after overlay
Figure B.12: 18-A310 profile analysis results

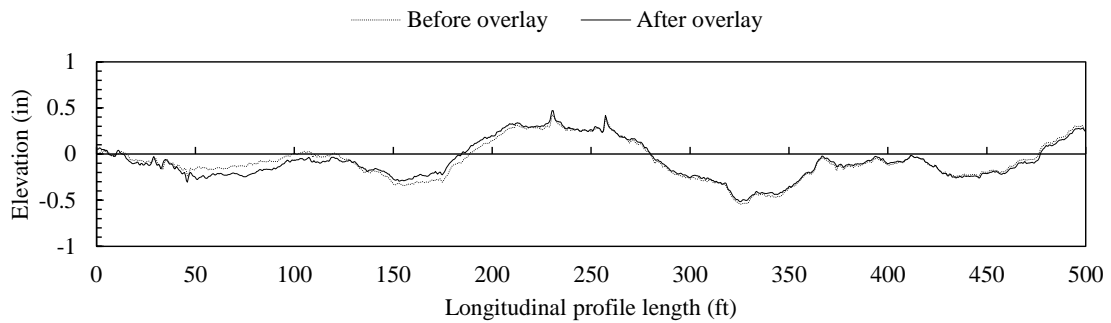


(a) Profile elevations before and after overlay

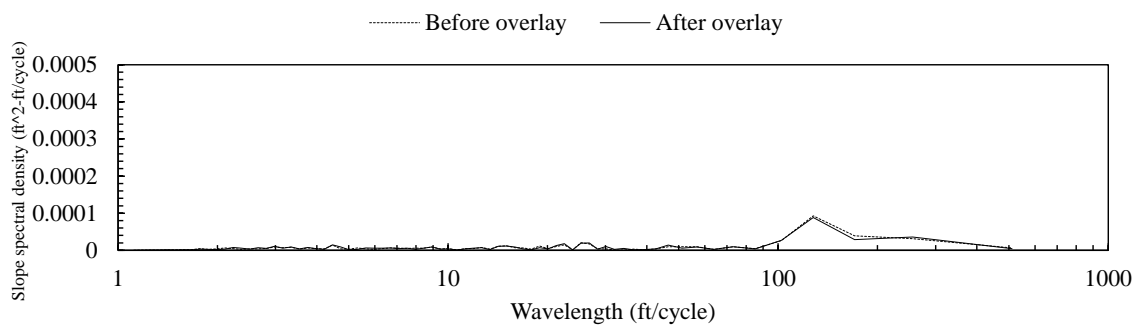


(b) PSD before and after overlay

Figure B.13: 20-A310 profile analysis results



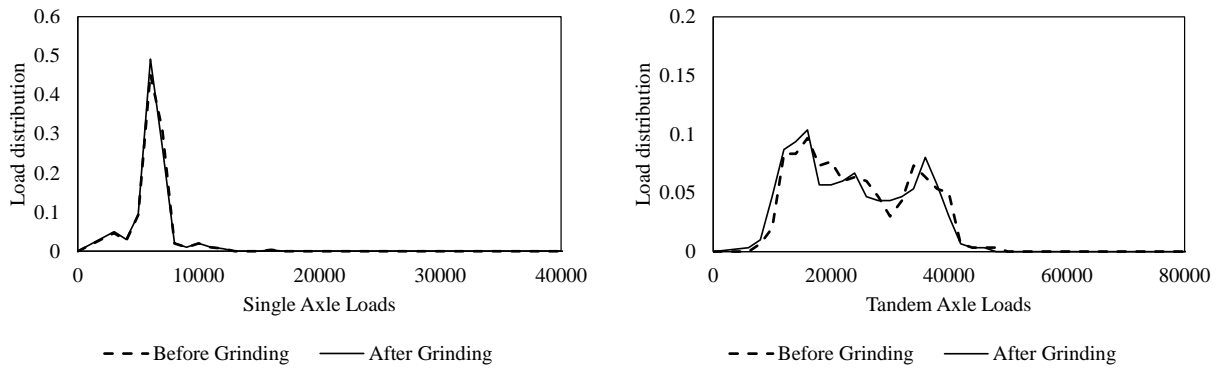
(a) Profile elevations before and after overlay



(b) PSD before and after overlay

Figure B.14: 32-A310 profile analysis results

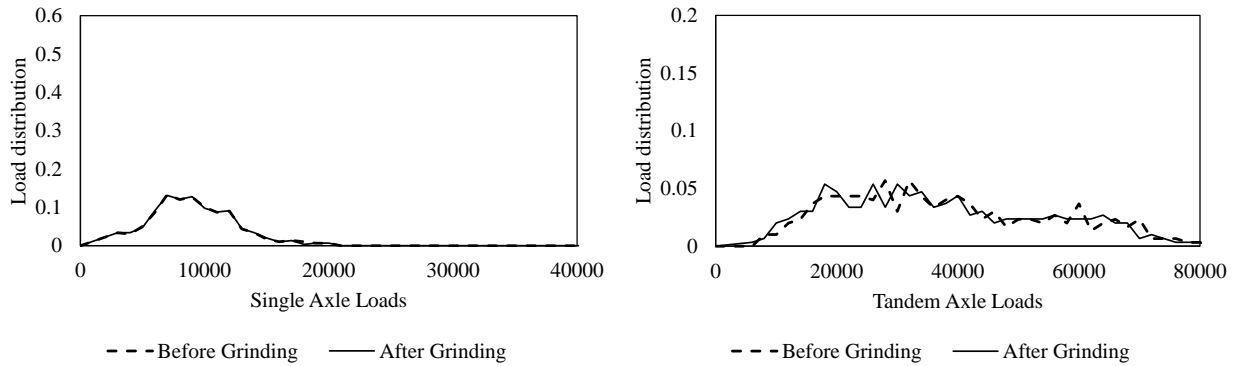
Appendix C Concrete pavement dynamic axle load spectra



(a) Single axle loads

(b) Tandem axle loads

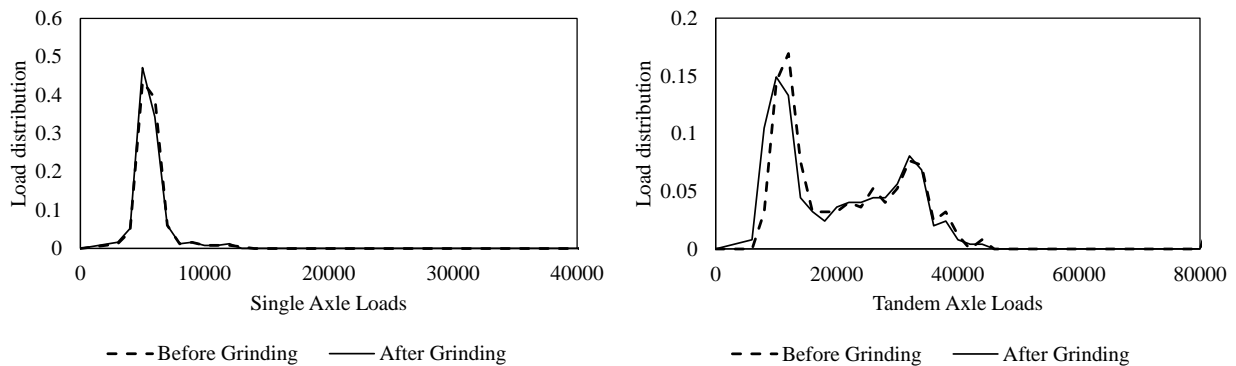
Figure C.1: 6-3010 95th percentile axle load spectra



(a) Single axle loads

(b) Tandem axle loads

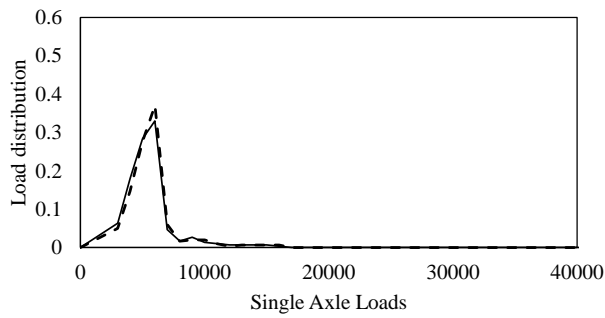
Figure C.2: 13-3017 95th percentile axle load spectra



(a) Single axle loads

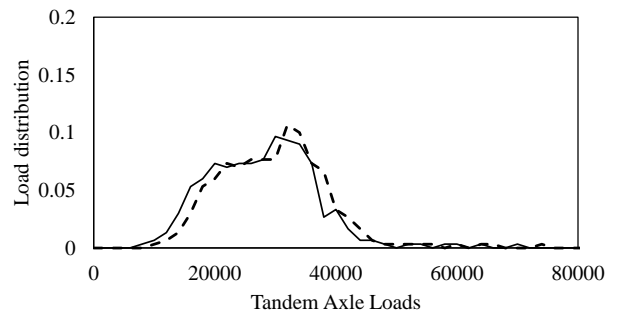
(b) Tandem axle loads

Figure C.3: 27-4050 95th percentile axle load spectra



-- Before Grinding — After Grinding

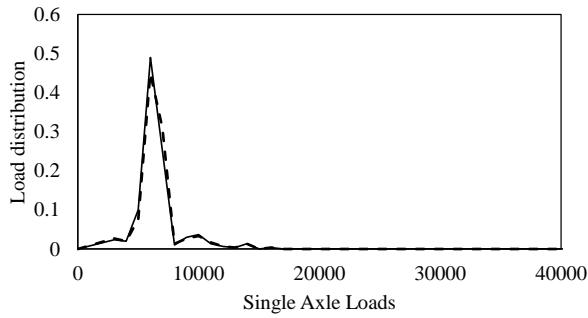
(a) Single axle loads



-- Before Grinding — After Grinding

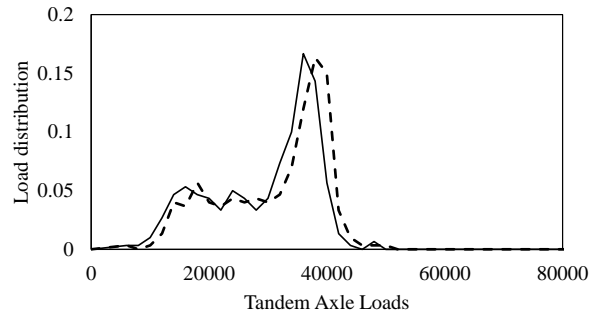
(b) Tandem axle loads

Figure C.4: 42-3044 95th percentile axle load spectra



-- Before Grinding — After Grinding

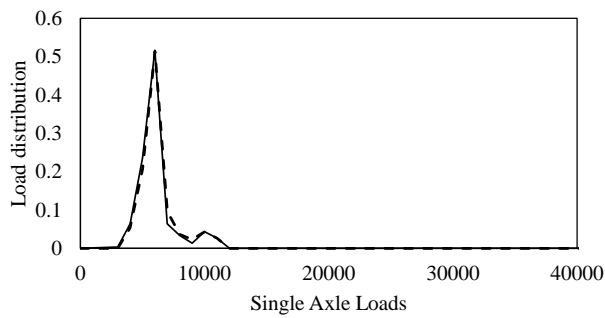
(a) Single axle loads



-- Before Grinding — After Grinding

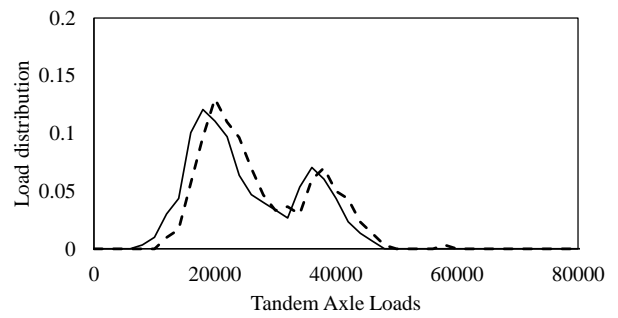
(b) Tandem axle loads

Figure C.5: 46-3010 95th percentile axle load spectra



-- Before Grinding — After Grinding

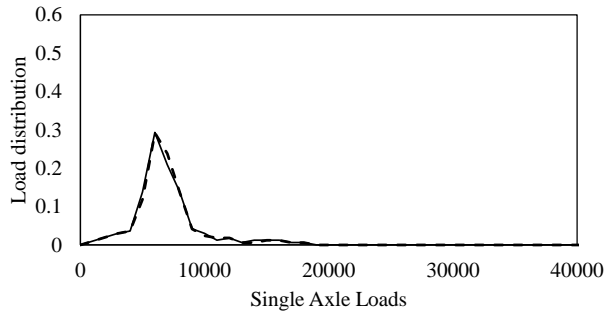
(a) Single axle loads



-- Before Grinding — After Grinding

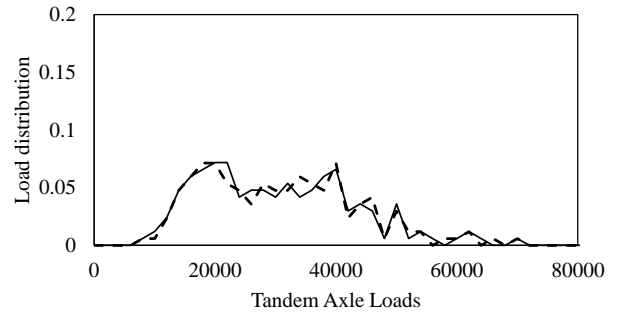
(b) Tandem axle loads

Figure C.6: 55-3009 95th percentile axle load spectra



-- Before Grinding — After Grinding

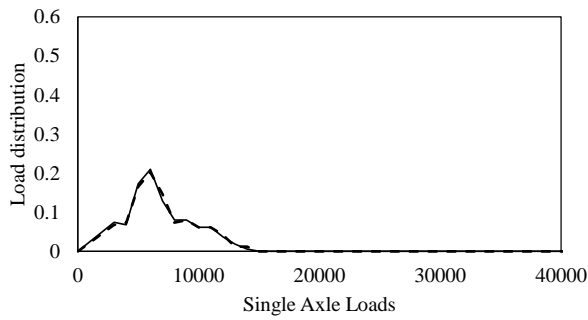
(a) Single axle loads



-- Before Grinding — After Grinding

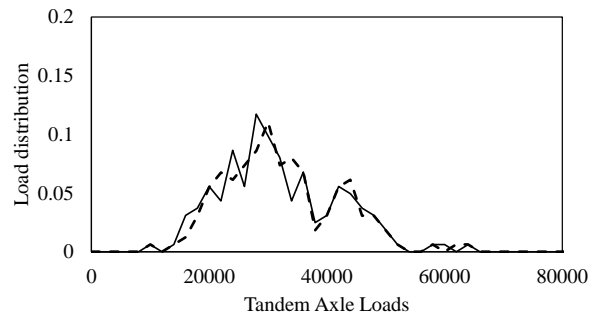
(b) Tandem axle loads

Figure C.7: 4-7614 95th percentile axle load spectra



-- Before Grinding — After Grinding

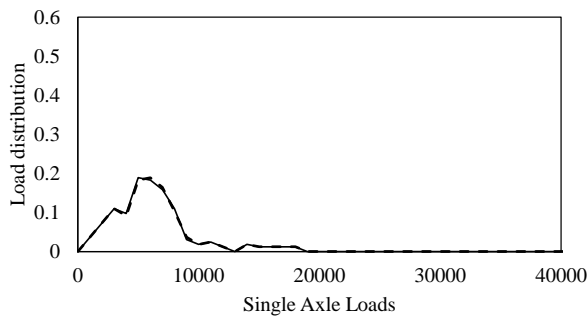
(a) Single axle loads



-- Before Grinding — After Grinding

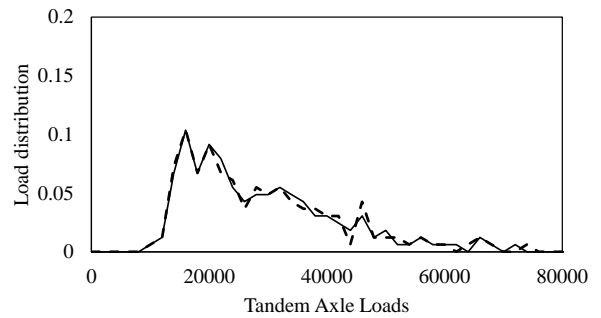
(b) Tandem axle loads

Figure C.8: 16-3017 95th percentile axle load spectra



-- Before Grinding — After Grinding

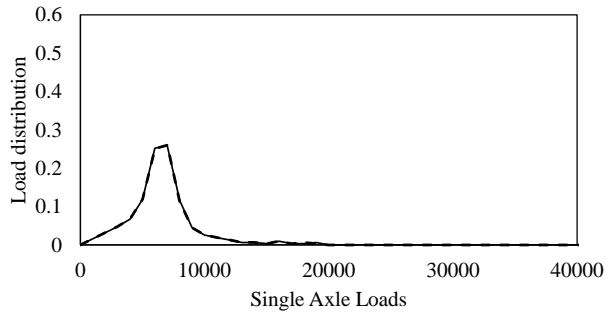
(a) Single axle loads



-- Before Grinding — After Grinding

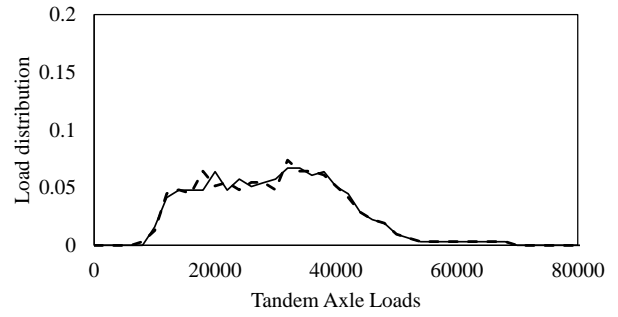
(b) Tandem axle loads

Figure C.9: 49-C431 95th percentile axle load spectra



-- Before Grinding — After Grinding

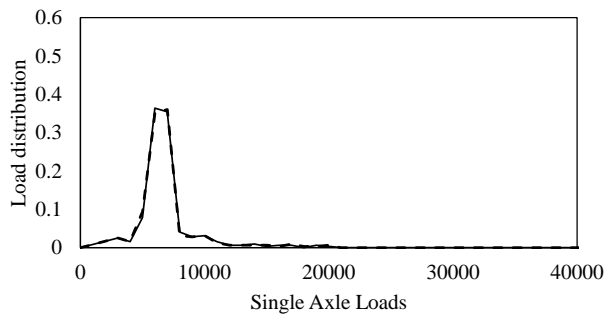
(a) Single axle loads



-- Before Grinding — After Grinding

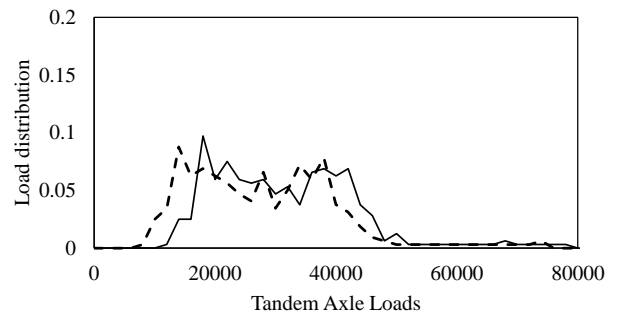
(b) Tandem axle loads

Figure C.10: 8-3032 95th percentile axle load spectra



-- Before Grinding — After Grinding

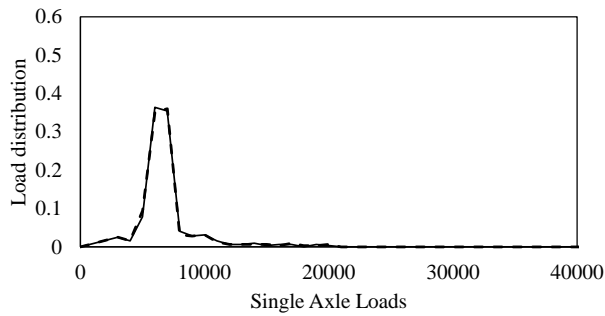
(a) Single axle loads



-- Before Grinding — After Grinding

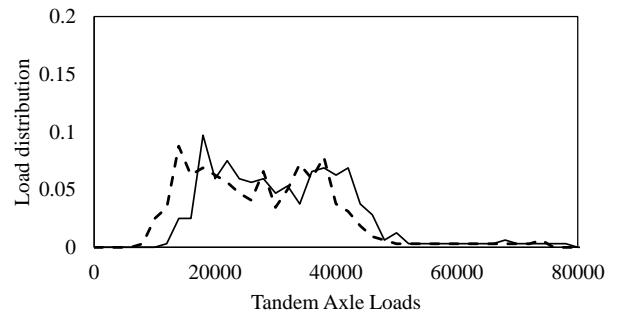
(b) Tandem axle loads

Figure C.11: 27-3009 95th percentile axle load spectra



-- Before Grinding — After Grinding

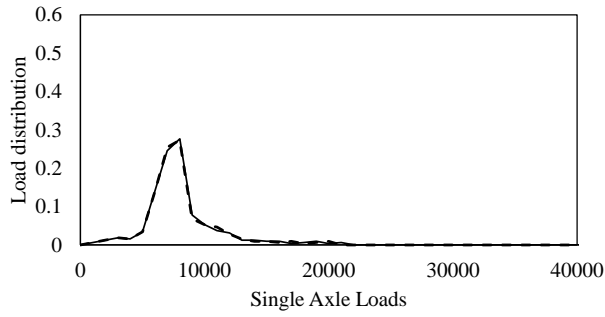
(a) Single axle loads



-- Before Grinding — After Grinding

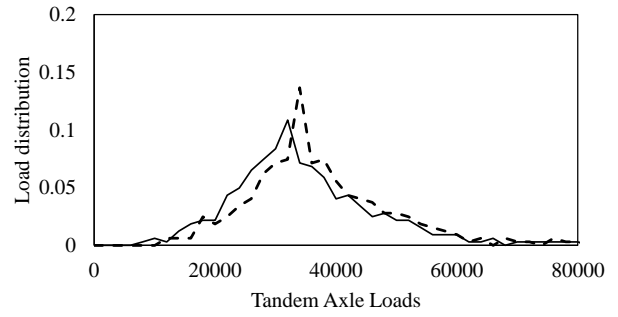
(b) Tandem axle loads

Figure C.12: 38-3006 95th percentile axle load spectra



-- Before Grinding — After Grinding

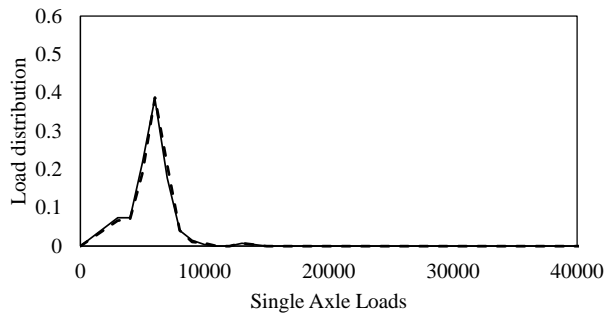
(a) Single axle loads



-- Before Grinding — After Grinding

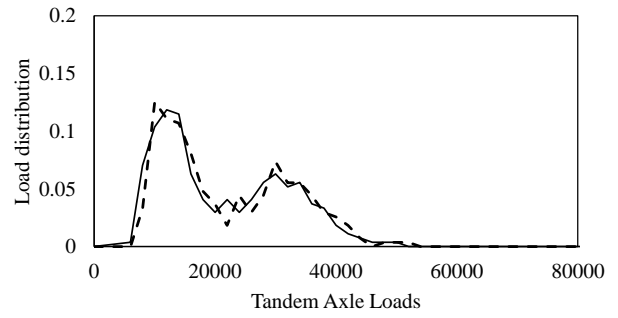
(b) Tandem axle loads

Figure C.13: 42-9027 95th percentile axle load spectra



-- Before Grinding — After Grinding

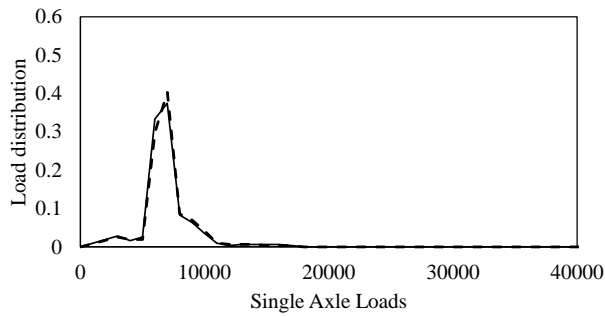
(a) Single axle loads



-- Before Grinding — After Grinding

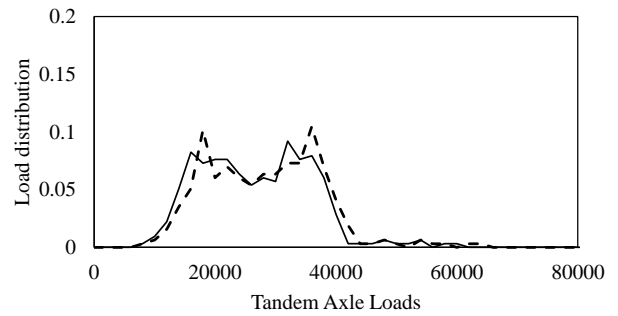
(b) Tandem axle loads

Figure C.14: 31-3028 95th percentile axle load spectra



-- Before Grinding — After Grinding

(a) Single axle loads

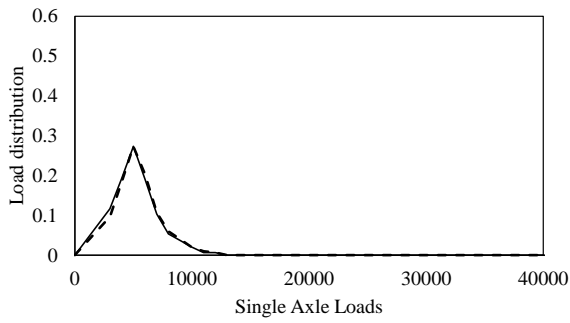


-- Before Grinding — After Grinding

(b) Tandem axle loads

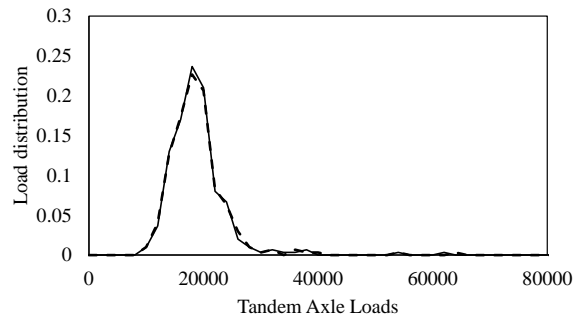
Figure C.15: 39-9006 95th percentile axle load spectra

Appendix D Asphalt pavement dynamic axle load spectra



-- Before Thin OL — After Thin OL

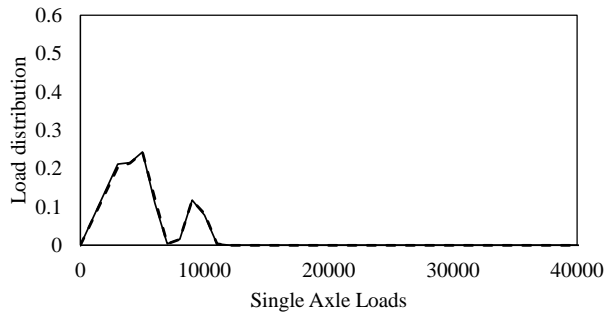
(a) Single axle loads



-- Before Thin OL — After Thin OL

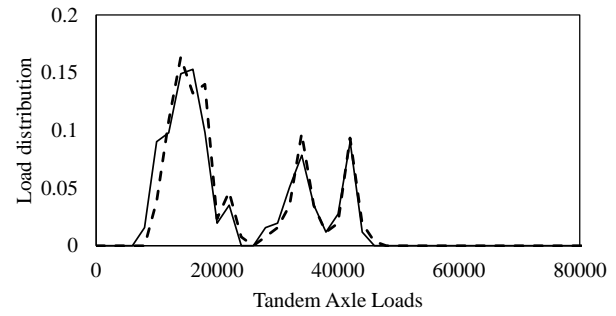
(b) Tandem axle loads

Figure D.1: 16-B310 95th percentile axle load spectra



-- Before Thin OL — After Thin OL

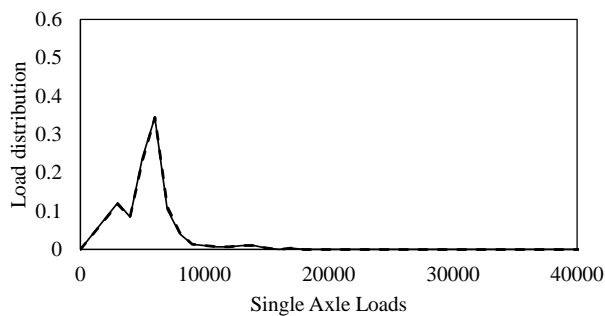
(a) Single axle loads



-- Before Thin OL — After Thin OL

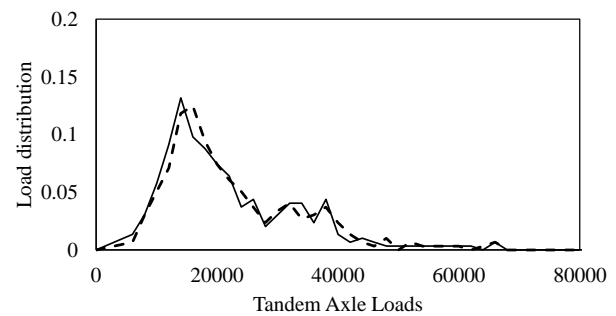
(b) Tandem axle loads

Figure D.2: 16-C310 95th percentile axle load spectra



-- Before Thin OL — After Thin OL

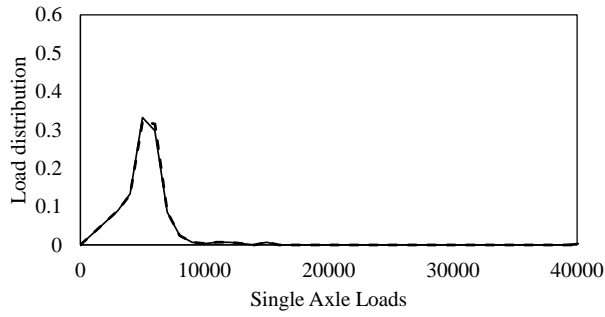
(a) Single axle loads



-- Before Thin OL — After Thin OL

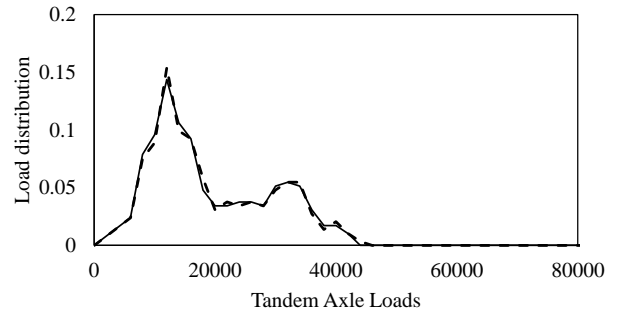
(b) Tandem axle loads

Figure D.3: 53-A310 95th percentile axle load spectra



-- Before Thin OL — After Thin OL

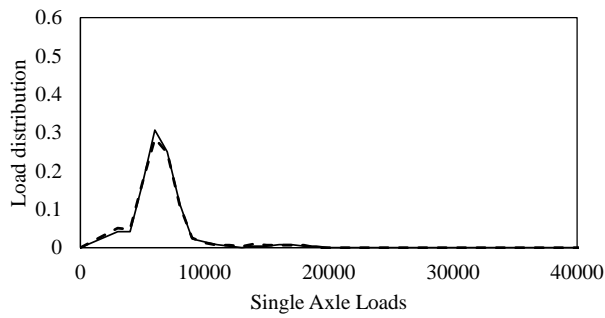
(a) Single axle loads



-- Before Grinding — After Grinding

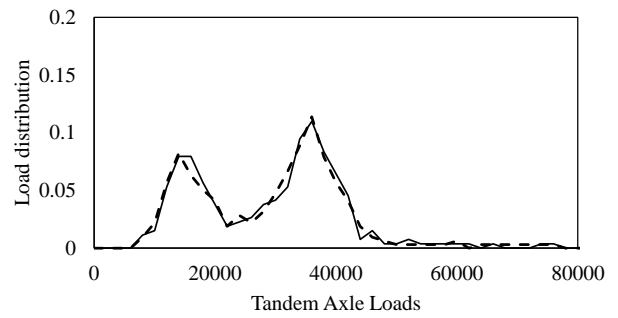
(b) Tandem axle loads

Figure D.4: 20-B310 95th percentile axle load spectra



-- Before Thin OL — After Thin OL

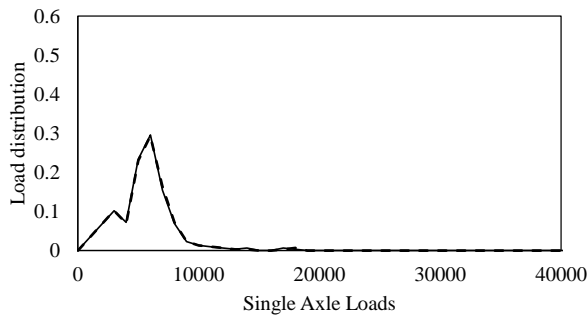
(a) Single axle loads



-- Before Thin OL — After Thin OL

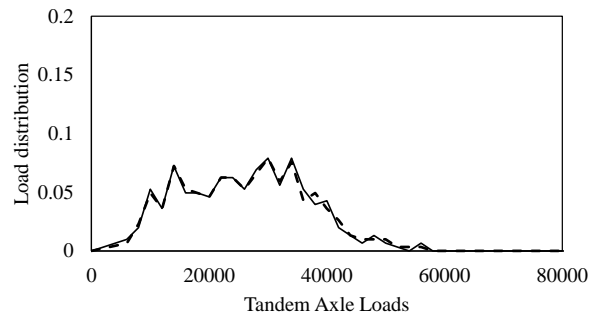
(b) Tandem axle loads

Figure D.5: 4-C310 95th percentile axle load spectra



-- Before Thin OL — After Thin OL

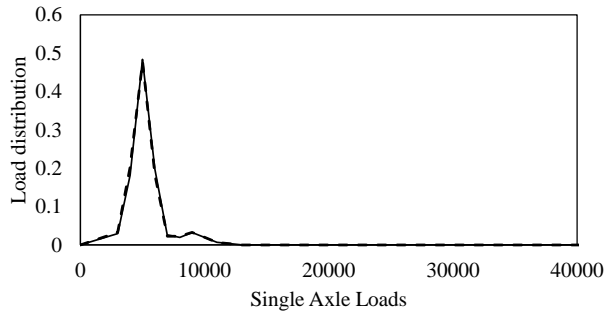
(a) Single axle loads



-- Before Thin OL — After Thin OL

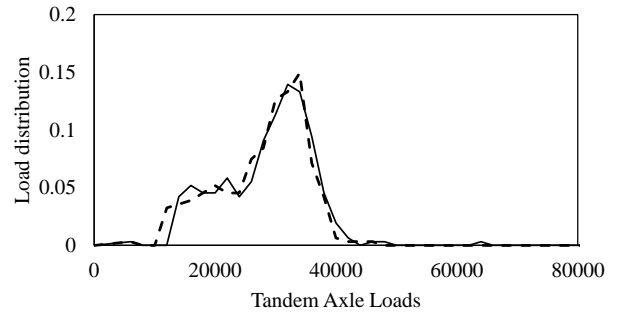
(b) Tandem axle loads

Figure D.6: 4-A310 95th percentile axle load spectra



-- Before Thin OL — After Thin OL

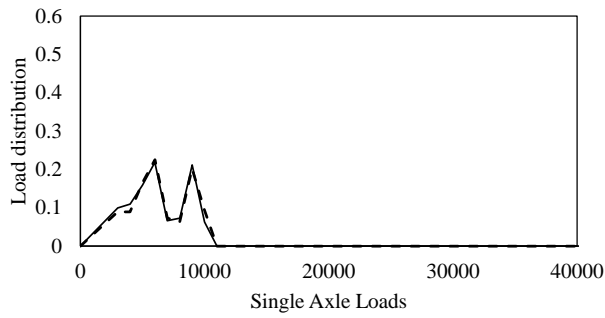
(a) Single axle loads



-- Before Thin OL — After Thin OL

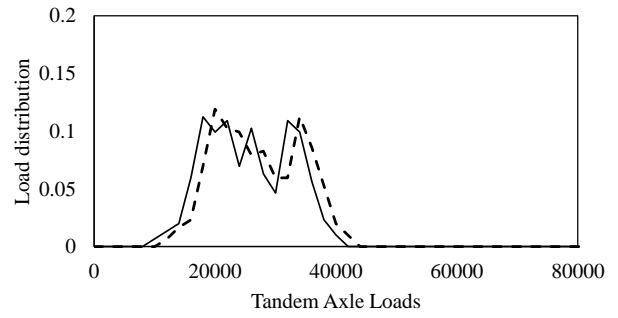
(b) Tandem axle loads

Figure D.7: 32-B310 95th percentile axle load spectra



-- Before Thin OL — After Thin OL

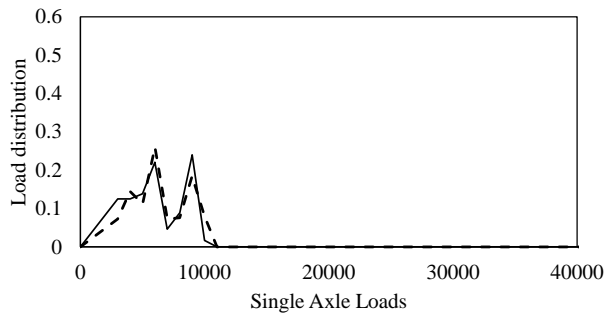
(a) Single axle loads



-- Before Grinding — After Grinding

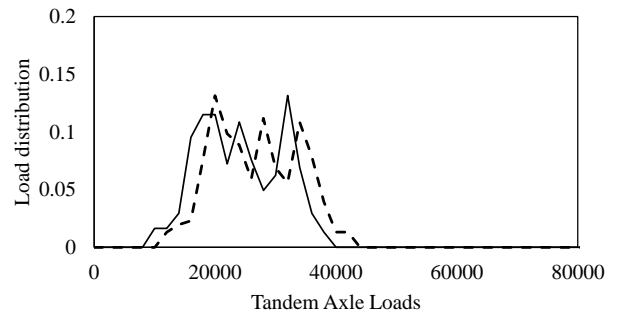
(b) Tandem axle loads

Figure D.8: 49-A310 95th percentile axle load spectra



-- Before Thin OL — After Thin OL

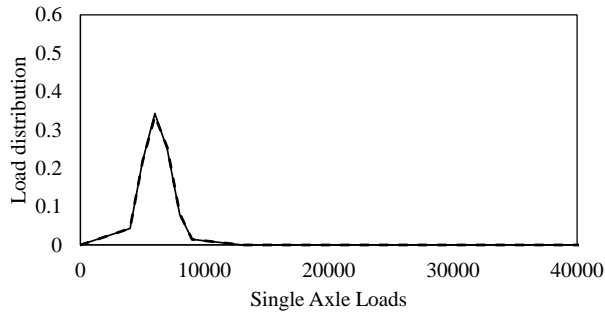
(a) Single axle loads



-- Before Thin OL — After Thin OL

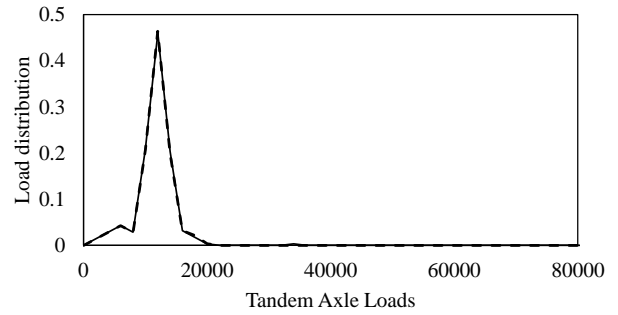
(b) Tandem axle loads

Figure D.9: 49-B310 95th percentile axle load spectra



-- -- Before Thin OL — After Thin OL

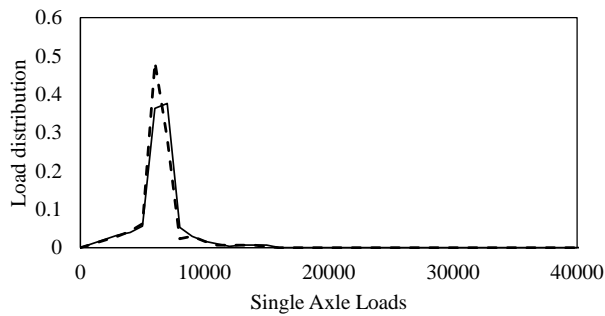
(a) Single axle loads



-- -- Before Thin OL — After Thin OL

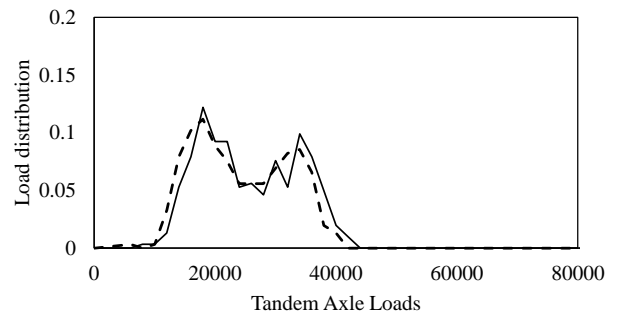
(b) Tandem axle loads

Figure D.10: 17-B310 95th percentile axle load spectra



-- -- Before Thin OL — After Thin OL

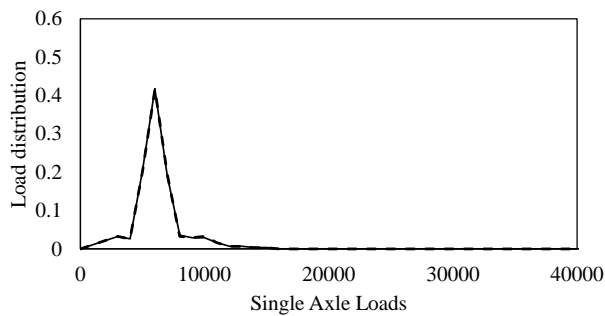
(a) Single axle loads



-- -- Before Thin OL — After Thin OL

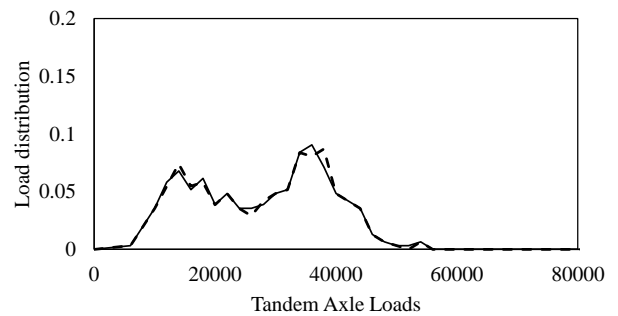
(b) Tandem axle loads

Figure D.11: 53-C310 95th percentile axle load spectra



-- -- Before Thin OL — After Thin OL

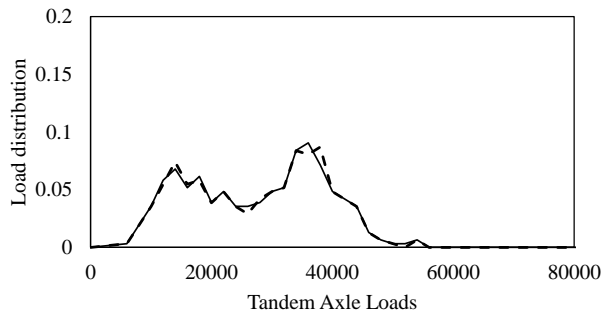
(a) Single axle loads



-- -- Before Thin OL — After Thin OL

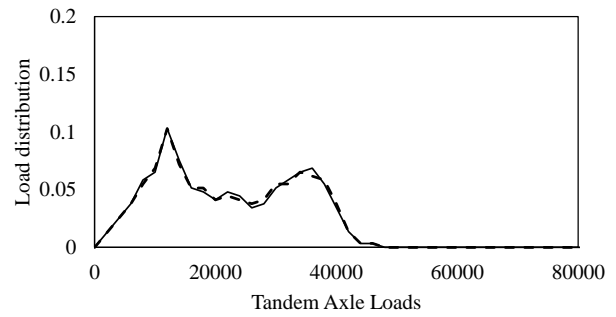
(b) Tandem axle loads

Figure D.12: 18-A310 95th percentile axle load spectra



-- -- Before Thin OL — After Thin OL

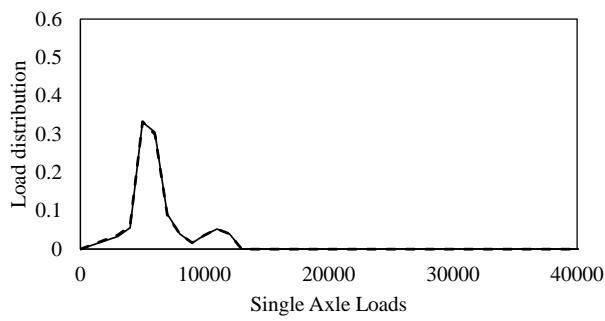
(a) Single axle loads



-- -- Before Thin OL — After Thin OL

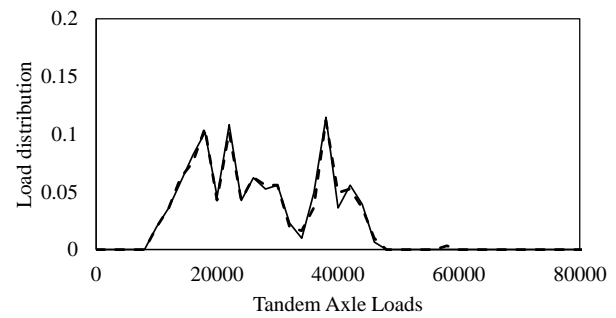
(b) Tandem axle loads

Figure D.13: 20-A310 95th percentile axle load spectra



-- -- Before Thin OL — After Thin OL

(a) Single axle loads

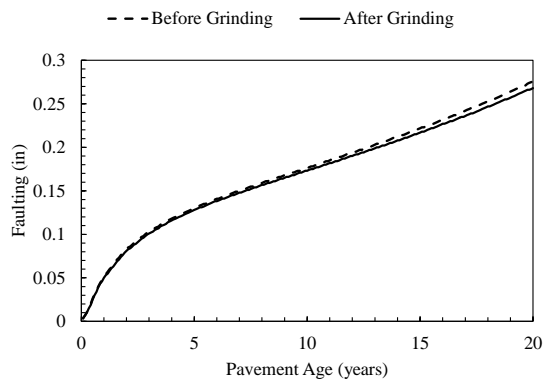


-- -- Before Thin OL — After Thin OL

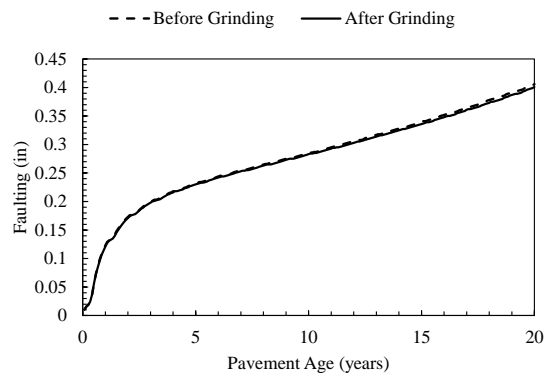
(b) Tandem axle loads

Figure D.14: 32-A310 95th percentile axle load spectra

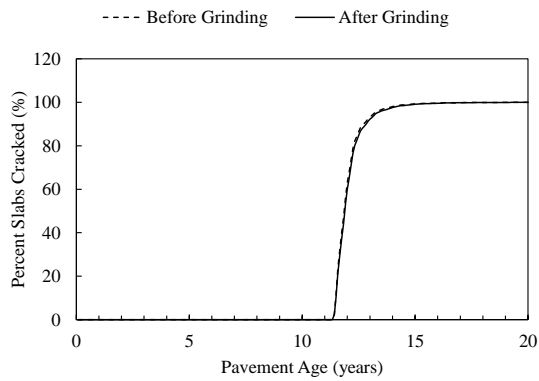
Appendix E Concrete pavement predicted performance



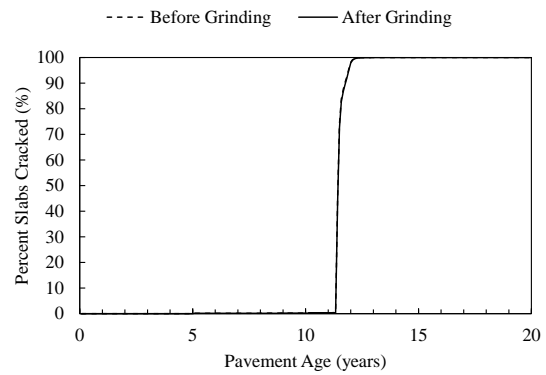
(a) Predicted faulting



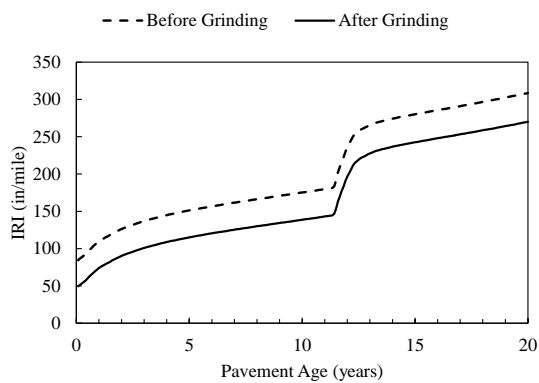
(a) Predicted faulting



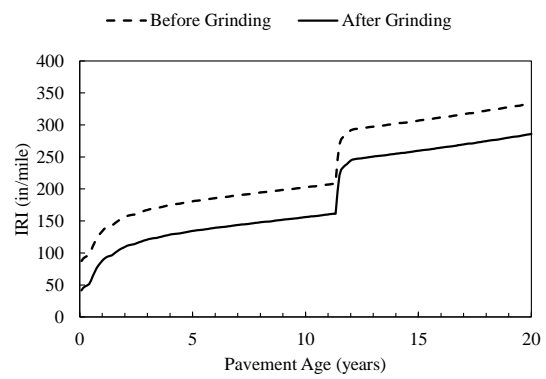
(b) Predicted cracking



(b) Predicted cracking



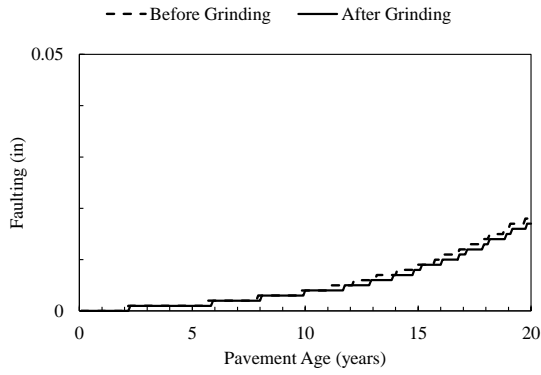
(c) Predicted IRI



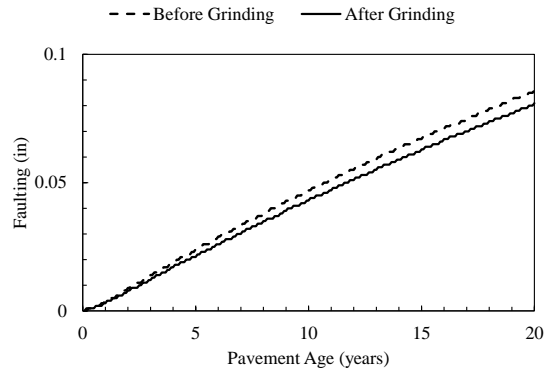
(c) Predicted IRI

Figure E.1: 6-3010 predicted performance

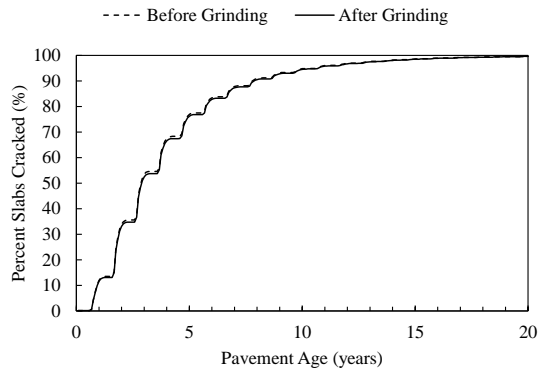
Figure E.2: 13-3017 predicted performance



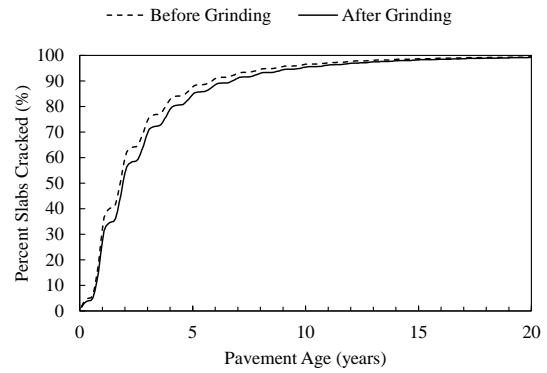
(a) Predicted faulting



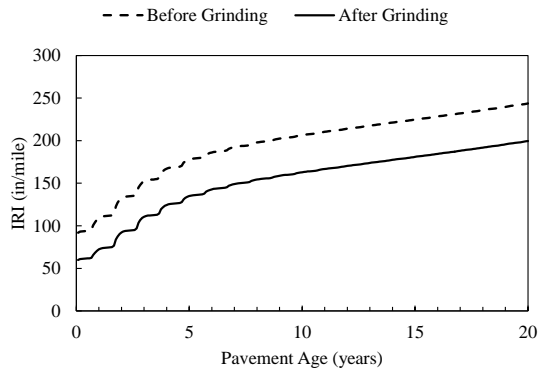
(a) Predicted faulting



(b) Predicted cracking

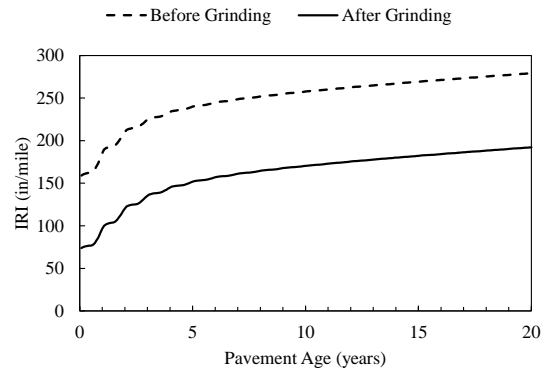


(b) Predicted cracking



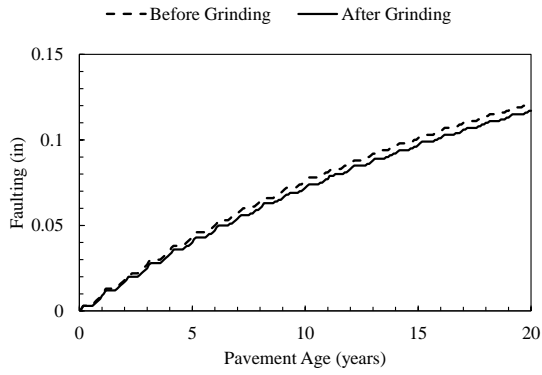
(c) Predicted IRI

Figure E.3: 27-4050 predicted performance

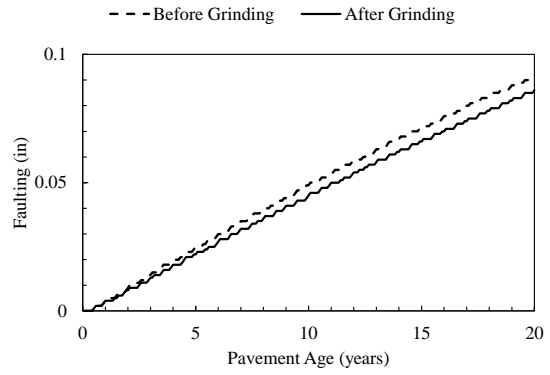


(c) Predicted IRI

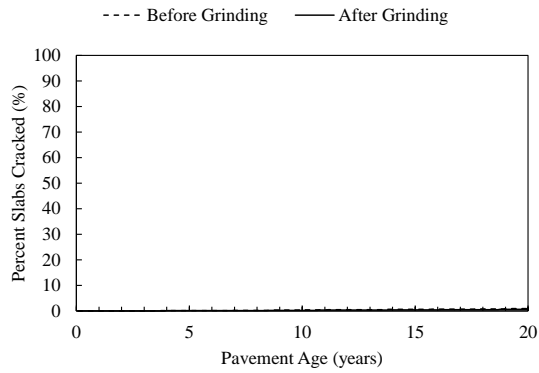
Figure E.4: 42-3044 predicted performance



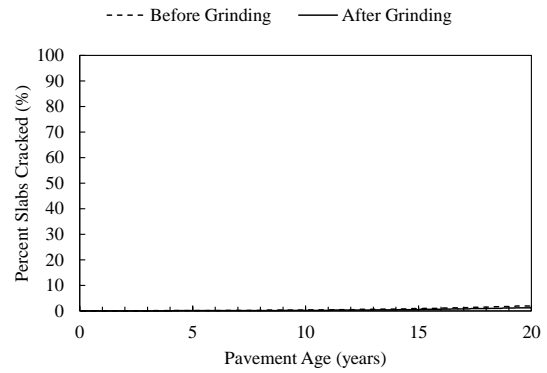
(a) Predicted faulting



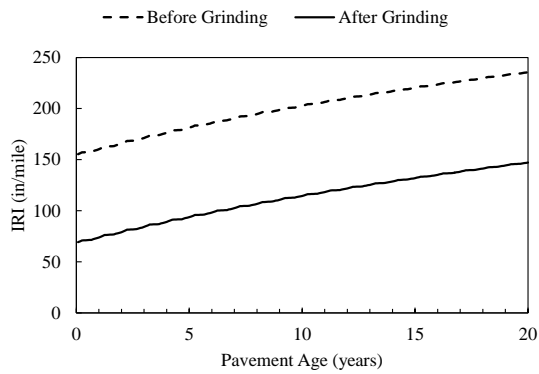
(a) Predicted faulting



(b) Predicted cracking

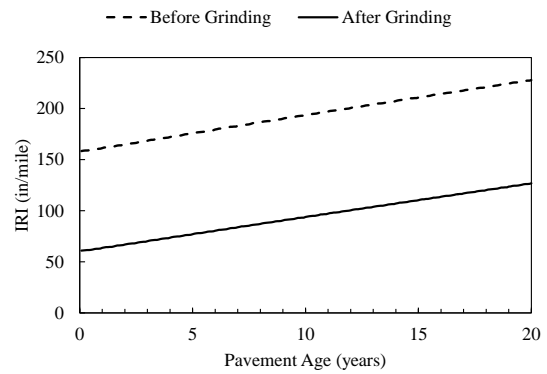


(b) Predicted cracking



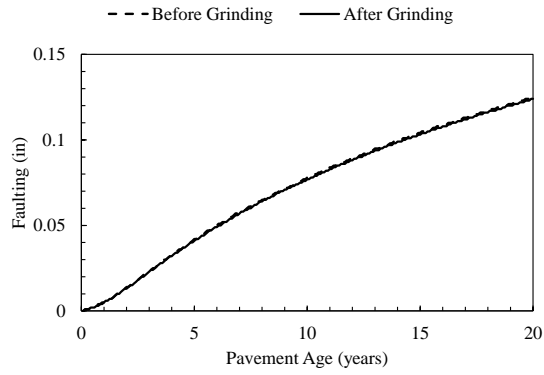
(c) Predicted IRI

Figure E.5: 46-3010 predicted performance

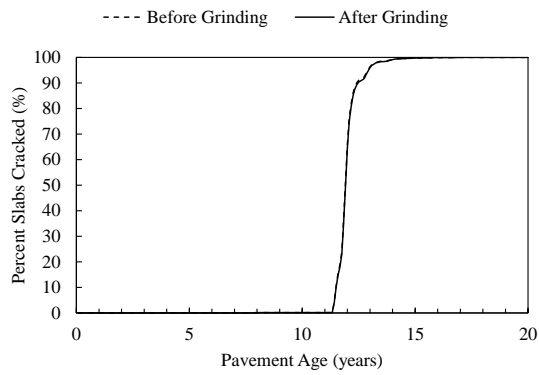


(c) Predicted IRI

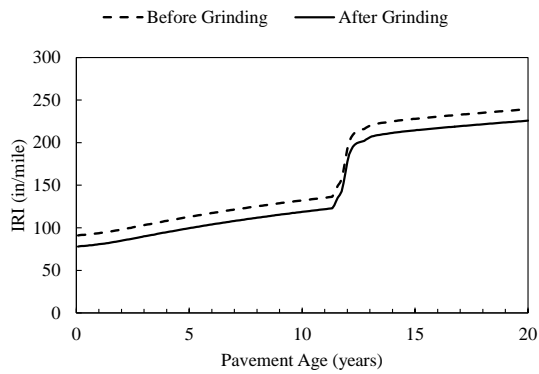
Figure E.6: 55-3009 predicted performance



(a) Predicted faulting

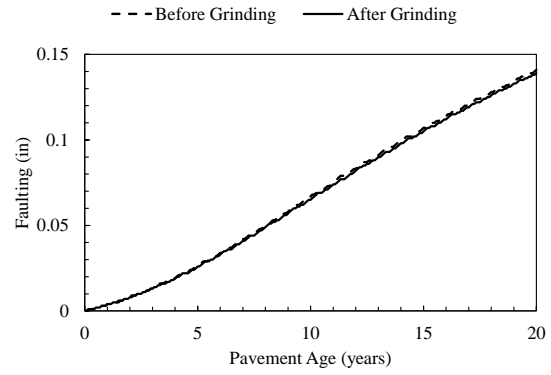


(b) Predicted cracking

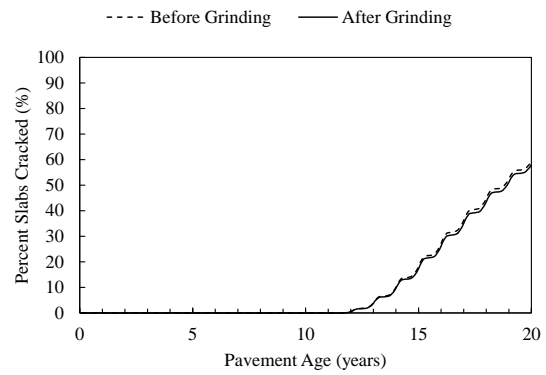


(c) Predicted IRI

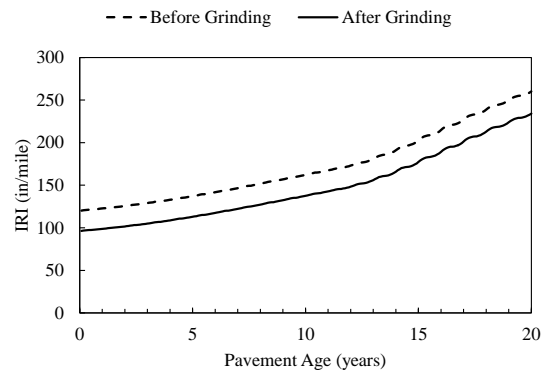
Figure E.7: 4-7614 predicted performance



(a) Predicted faulting

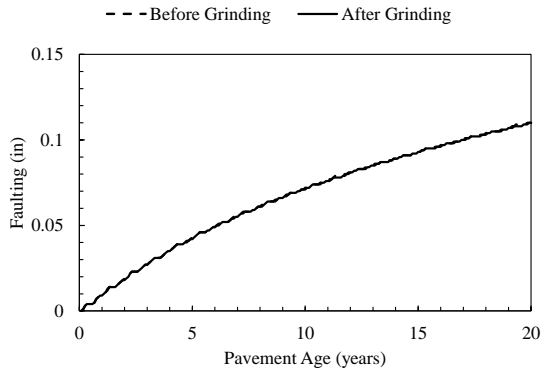


(b) Predicted cracking

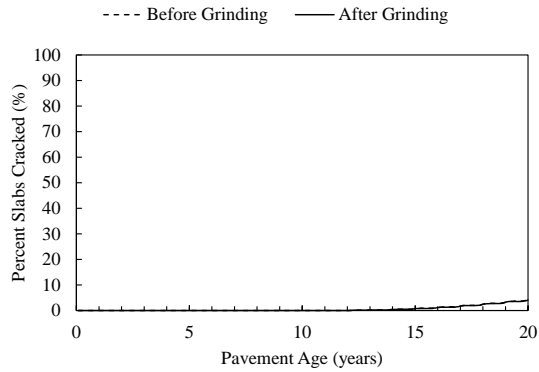


(c) Predicted IRI

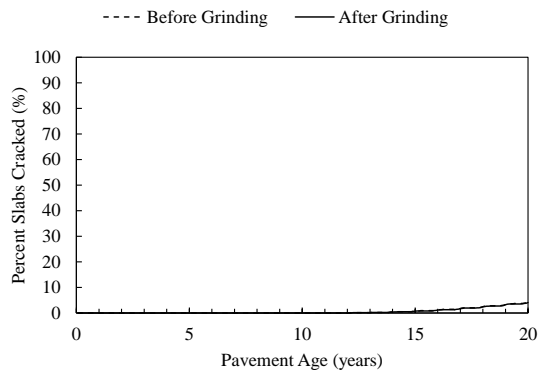
Figure E.8: 16-3017 predicted performance



(a) Predicted faulting

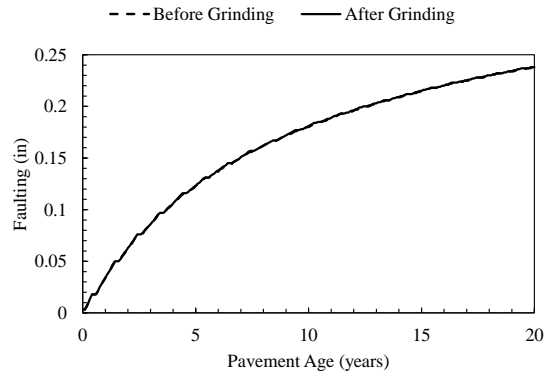


(b) Predicted cracking

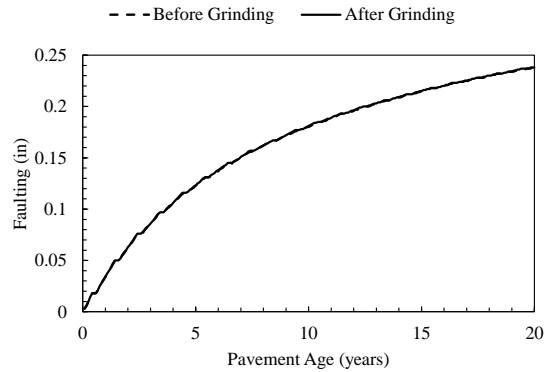


(c) Predicted IRI

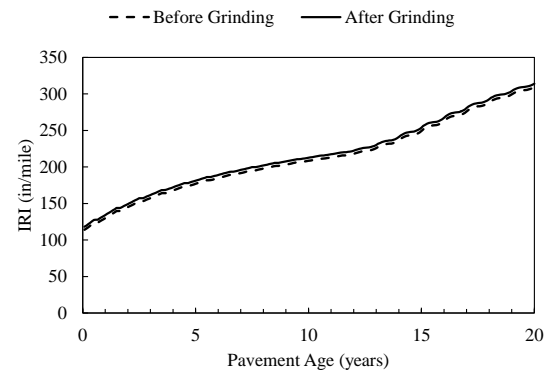
Figure E.9: 49-C431 predicted performance



(a) Predicted faulting

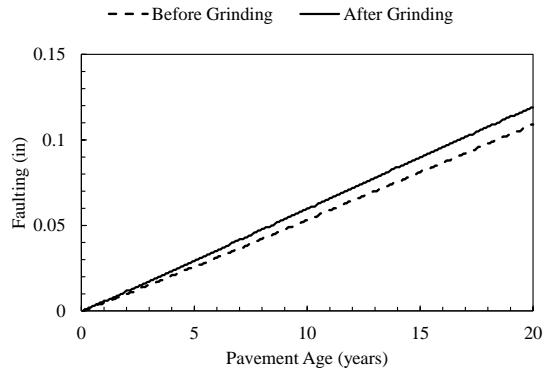


(b) Predicted cracking

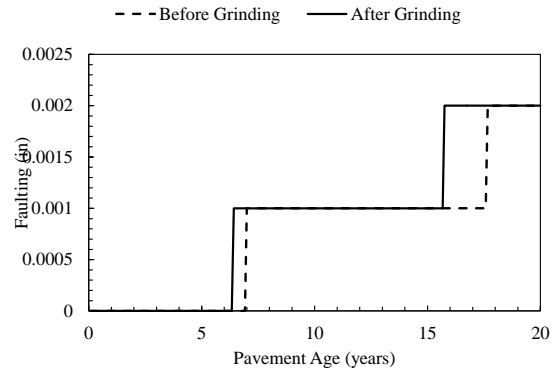


(c) Predicted IRI

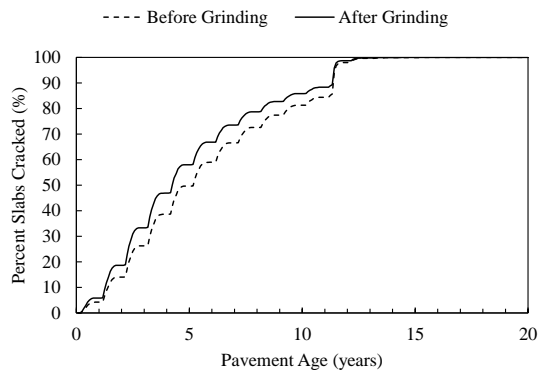
Figure E.10: 8-3032 predicted performance



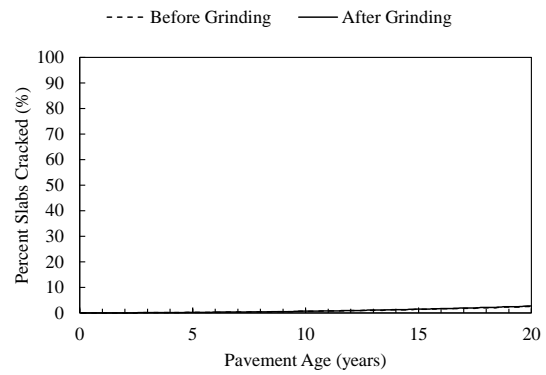
(a) Predicted faulting



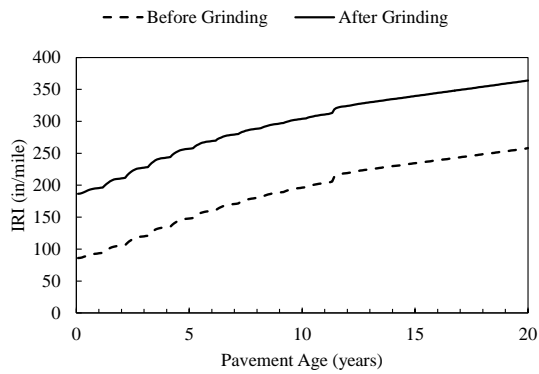
(a) Predicted faulting



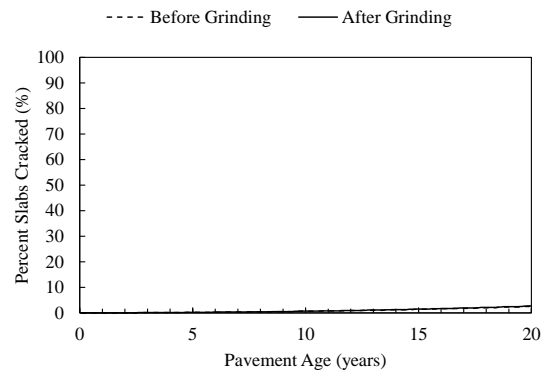
(b) Predicted cracking



(b) Predicted cracking



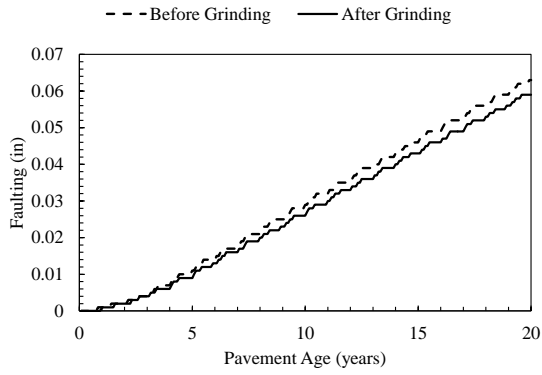
(c) Predicted IRI



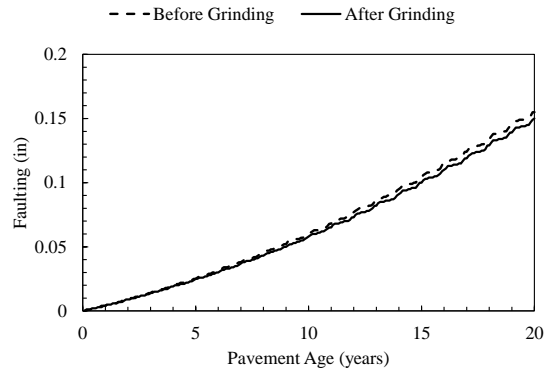
(c) Predicted IRI

Figure E.11: 27-3009 predicted performance

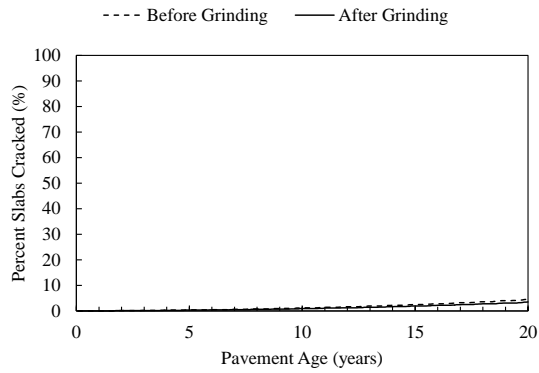
Figure E.12: 38-3006 predicted performance



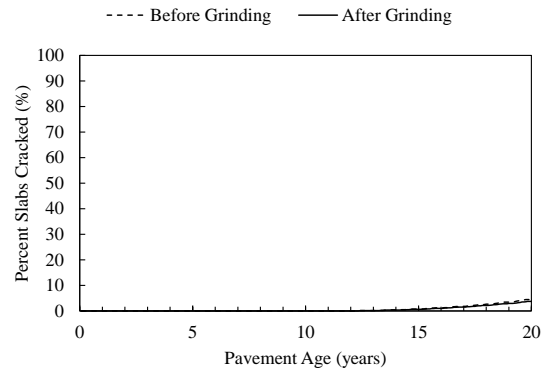
(a) Predicted faulting



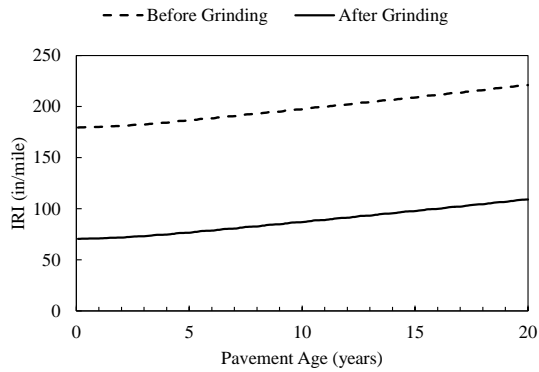
(a) Predicted faulting



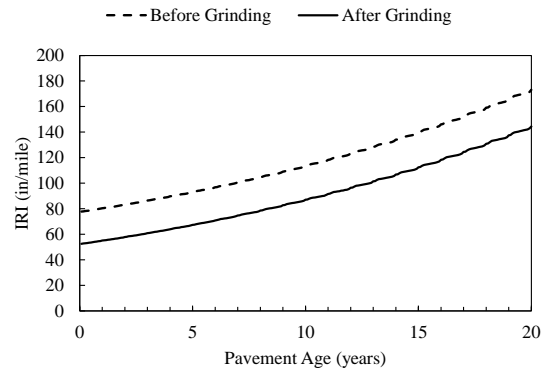
(b) Predicted cracking



(b) Predicted cracking



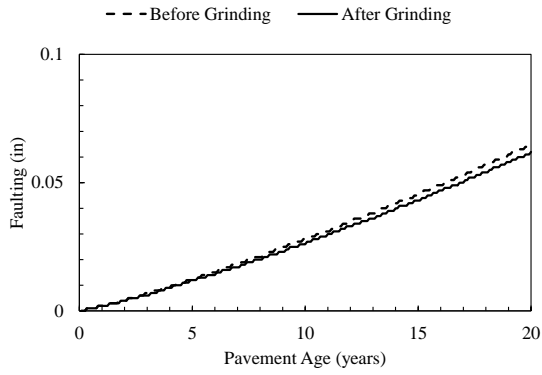
(c) Predicted IRI



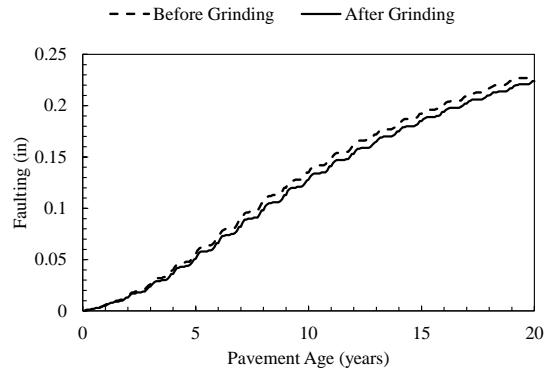
(c) Predicted IRI

Figure E.13: 42-9027 predicted performance

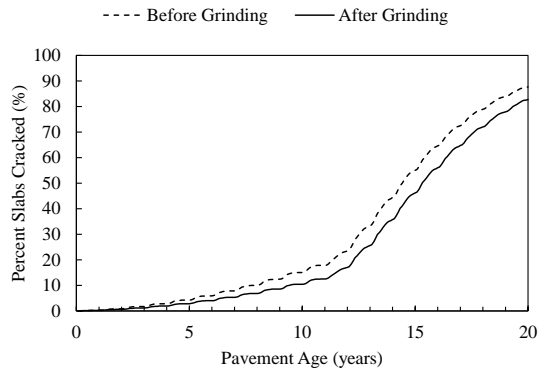
Figure E.14: 20-3015 predicted performance



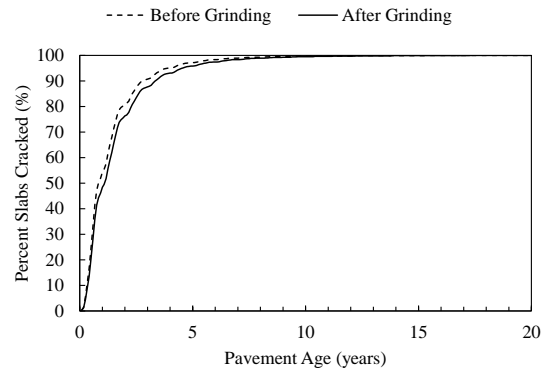
(a) Predicted faulting



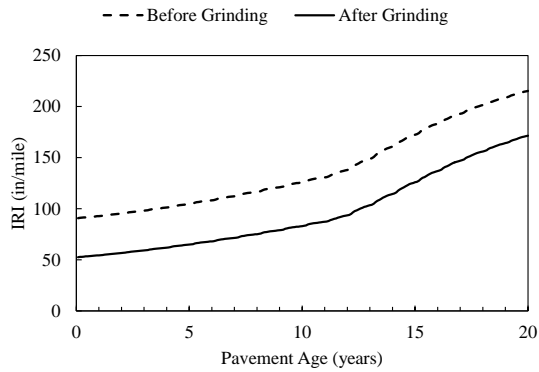
(a) Predicted faulting



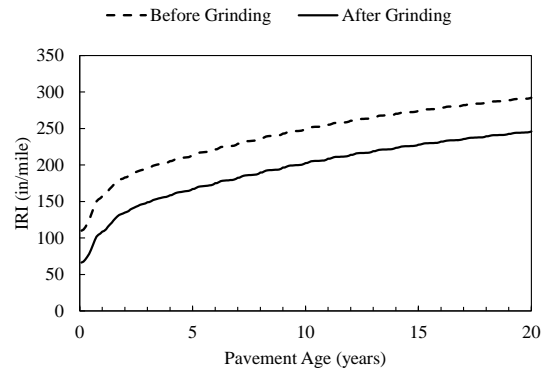
(b) Predicted cracking



(b) Predicted cracking



(c) Predicted IRI

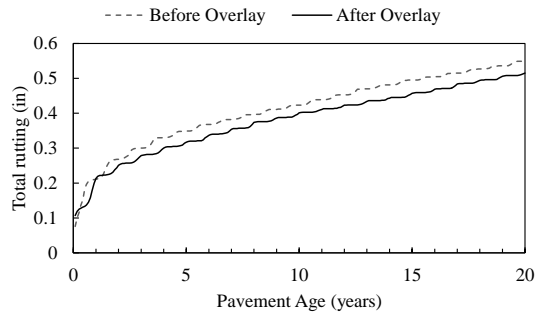


(c) Predicted IRI

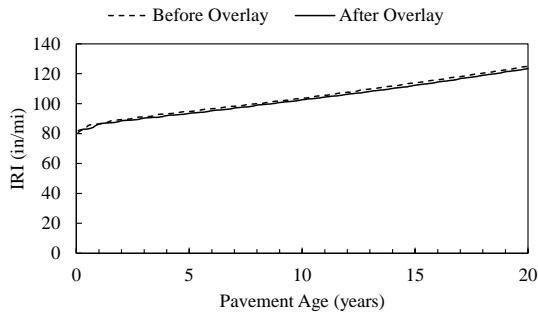
Figure E.15: 31-3028 predicted performance

Figure E.16: 39-9006 predicted performance

Appendix F Asphalt pavement predicted performance

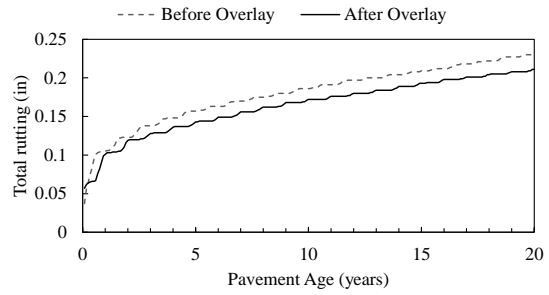


(a) Predicted rutting

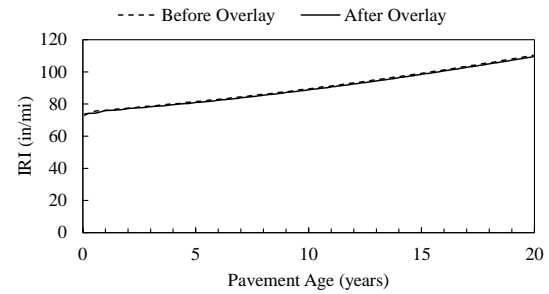


(b) Predicted IRI

Figure F.1: 16-B310 predicted performance

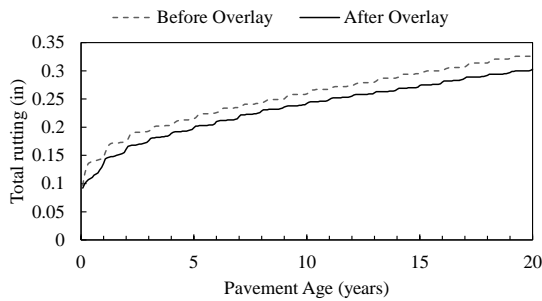


(a) Predicted rutting

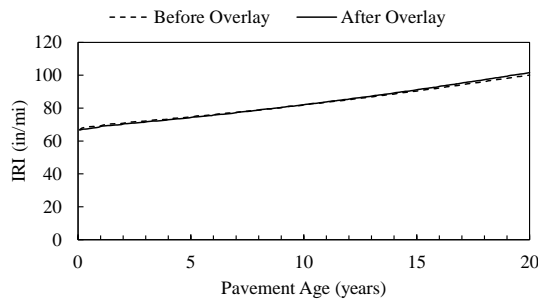


(b) Predicted IRI

Figure F.2: 16-C310 predicted performance

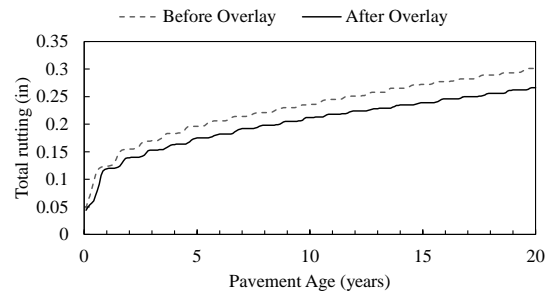


(a) Predicted rutting

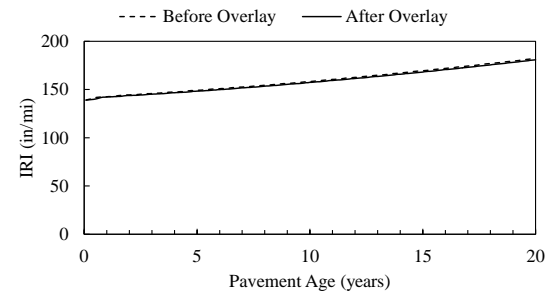


(b) Predicted IRI

Figure F.3: 53-A310 predicted performance

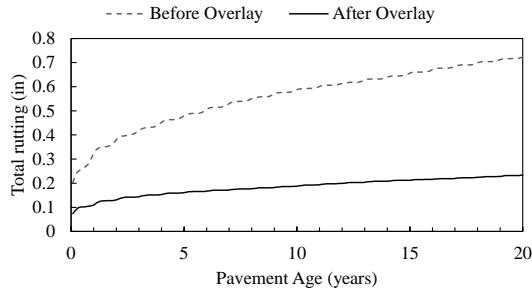


(a) Predicted rutting

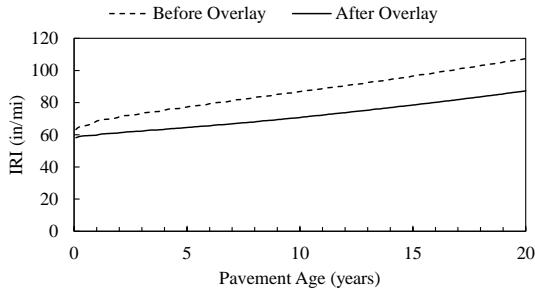


(b) Predicted IRI

Figure F.4: 20-B310 predicted performance

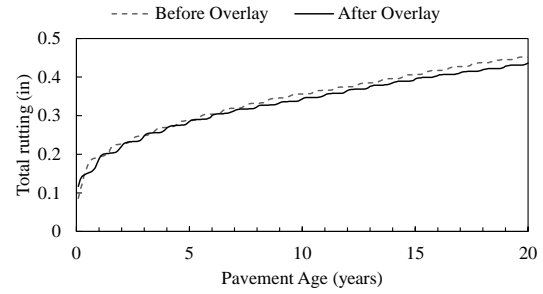


(a) Predicted rutting

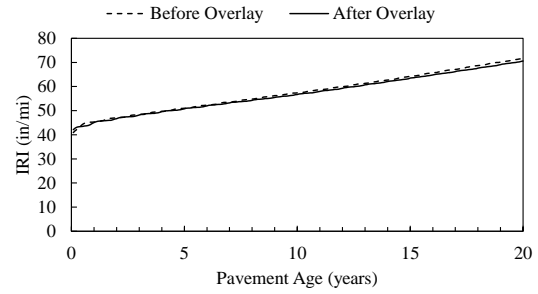


(b) Predicted IRI

Figure F.5: 4-C310 predicted performance

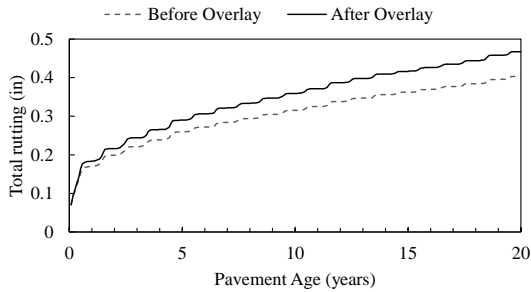


(a) Predicted rutting

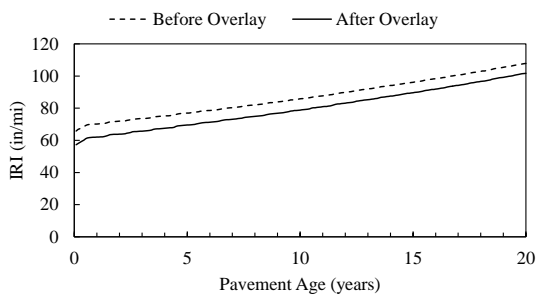


(b) Predicted IRI

Figure F.6: 4-A310 predicted performance

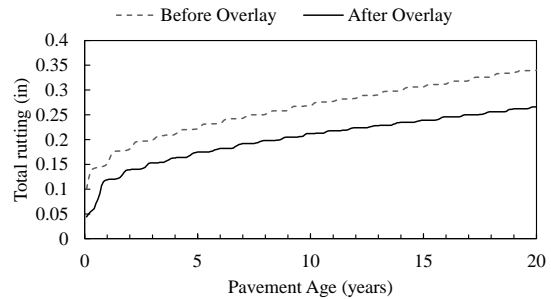


(a) Predicted rutting

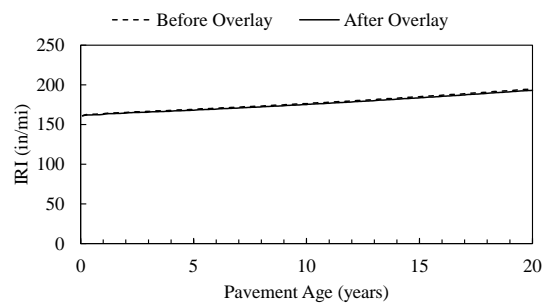


(b) Predicted IRI

Figure F.7: 32-B310 predicted performance

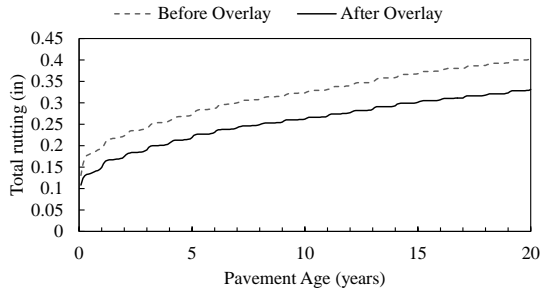


(a) Predicted rutting

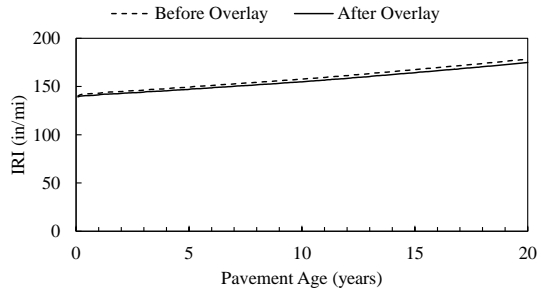


(b) Predicted IRI

Figure F.8: 49-A310 predicted performance

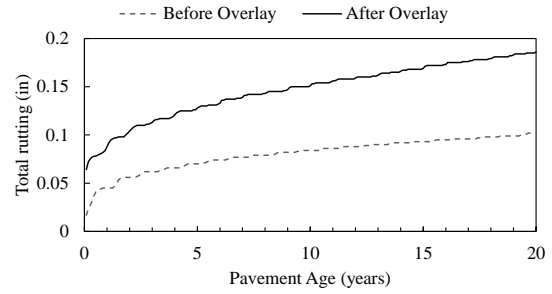


(a) Predicted rutting

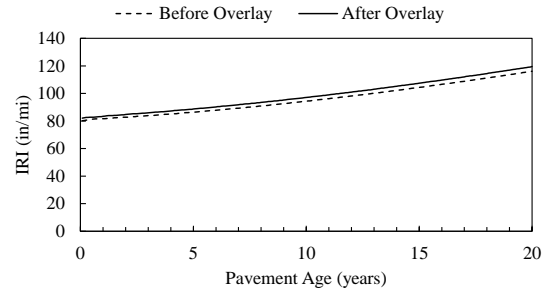


(b) Predicted IRI

Figure F.9: 49-B310 predicted performance

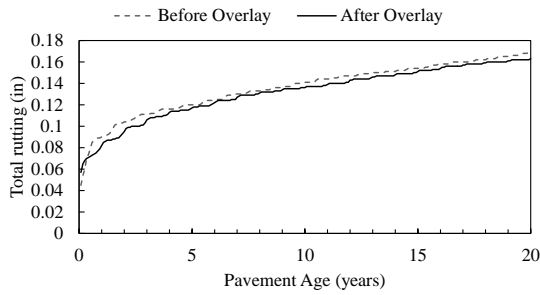


(a) Predicted rutting

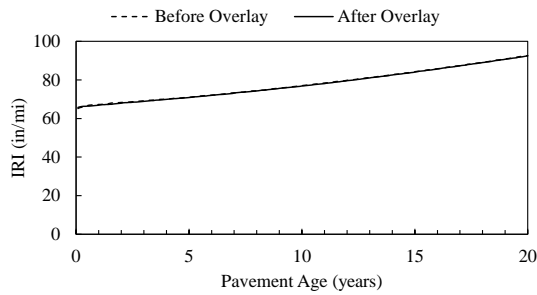


(b) Predicted IRI

Figure F.10: 17-B310 predicted performance

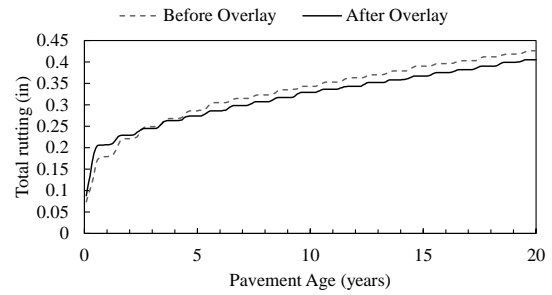


(a) Predicted rutting

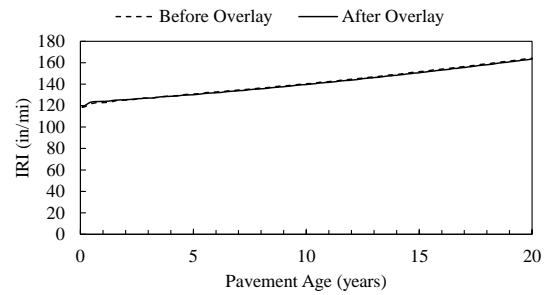


(b) Predicted IRI

Figure F.11: 53-C310 predicted performance

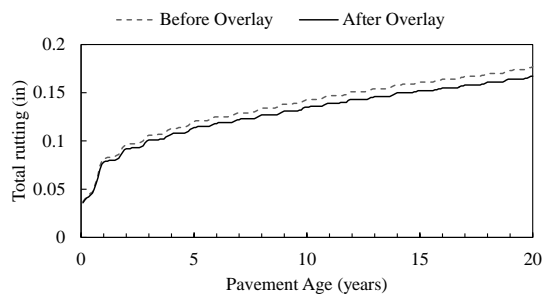


(a) Predicted rutting

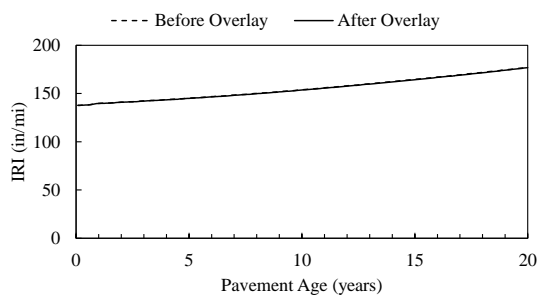


(b) Predicted IRI

Figure F.12: 18-A310 predicted performance

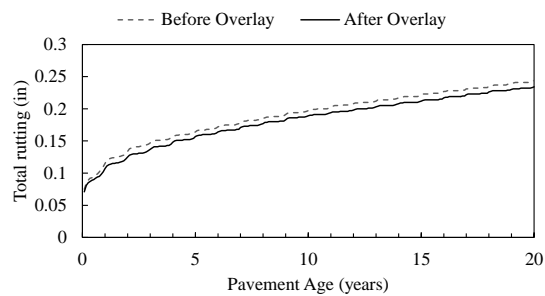


(a) Predicted rutting

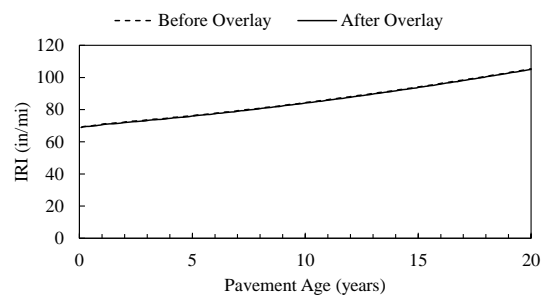


(b) Predicted IRI

Figure F.13: 20-A310 predicted performance



(a) Predicted rutting



(b) Predicted IRI

Figure F.14: 32-A310 predicted performance

REFERENCES

REFERENCES

1. Tighe, S., Gransberg, D., "Sustainable Pavement Maintenance and Preservation Practices: A Review of Current Practice," pp. 1-14, 2011.
2. Cheng, D. T., S.; Hicks, R., "Improving Pavement Management System by Adding Pavement Preservation Component."
3. Scott, S., T. Ferragut, S. Anderson, I. Damjanovic, G. Huber, J. Katafanas, K. McGhee, M. Sprinkel, C. Ozyilirim, B. Diefenderfer, D. Merrit, D. Dawood, K. Molenaar, M. Loulakis, D. White, and V. Schaeffer, "Performance Specifications for Rapid Highway Renewal," S2-R07-RR-1, 2014.
4. Scott, S., L. Konrath, and T. Ferragut, "Framework for Performance Specifications," S2-R07-RR-3, 2014.
5. J. L. Burati, R. M. W., C. S. Hughes, H. S. Hill, "Optimal Procedures for Quality Assurance Specifications," 2003.
6. J.L. Burati, R. M. W., C.S. Hughes, and H.S. Hill, "Evaluation of Procedures for Quality Assurance Specifications," 2004.
7. Sayers, M. W. and S. M. Karamihas, *The Little Book of Profiling - Basic Information about Measuring and Interpreting Road Profiles*, 1998.
8. Gillespie, T. D., S. M. Karamihas, D. Cebon, M. W. Sayers, M. A. Nasim, W. Hansen, and N. Ehsan, "Effects of Heavy Vehicle Characteristics on Pavement Response and Performance," Project 1-25, 1992.
9. Chatti, K. and I. Zaabar, "Estimating the Effects of Pavement Condition on Vehicle Operation Costs," NCHRP Report 720, 2012.
10. Smith, K. L., L. Titus-Glover, and L. D. Evans, "Pavement Smoothness Index Relationships," Federal Highway Administration FHWA-RD-02-057, 2002.

11. Ksaibati, K., R. McNamara, W. Miley, and J. Armaghani, "Pavement Roughness Data Collection and Utilization," 99-0257, 1999.
12. Chatti, K. and D. Lee, "A Profile Based Truck Dynamic Load Index (DLI)," in *7th International Symposium on Heavy Vehicle Weights & Dimensions*, 2002.
13. Geiger, D., "Pavement Preservation Definitions." Federal Highway Administration, 2005.
14. Peshkin, D., K. L. Smith, A. Wolters, J. Krtulovich, J. Moulthrop, and C. Alvarado, "Guidelines for the Preservation of High-Traffic Roads," S2-R26-RR-2, 2011.
15. Wang, Z., "Analysis of Effectiveness of Pavement Preservation Using Long-Term Pavement Performance Data," Rutgers State University of New Jersey 2013.
16. Cuelho, E., R. Mokwa, and M. Akin, "Preventive Maintenance Treatments of Flexible Pavements: A Synthesis of Highway Practice," Montana Department of Transportation 2006.
17. Wu, Z., J. L. Groeger, A. L. Simpson, and R. G. Hicks, "Performance Evaluation of Various Rehabilitation and Preservation Treatments," 2010.
18. Cebon, D., "Theoretical Road Damage Due to Dynamic Tyre Forces of Heavy Vehicles Part 2: Simulated Damage Caused by a Tandem-Axle Vehicle," *Proc.I.Mech.E.*, vol. 202, pp. 109-117, 1988.
19. FHWA, "Heavy Vehicle Travel Information System Field Manual," in *Field Vehicle Classes with Definitions*: U.S. Department of Transportation, 2001.
20. Ullidtz, P. and B. K. Larsen, "Mathematical Model for Predicting Pavement Performance," *Transportation Research Record*, pp. 44-55, 1983.
21. Papagiannakis, A. T., "Impact of Roughness-Induced Dynamic Load on Flexible Pavement Performance," presented at First International Symposium on Surface Characteristics, Pennsylvania State University, 1988, pp.

22. Monismith, C. L., "Modern Pavement Design Technology Including Dynamic Load Conditions," *Society of Automotive Engineers*, pp. 33-52, 1988.
23. O'Connell, S., "Analyses of Moving Dynamic Loads on Highway Pavements Part I: Vehicle Response," presented at International Symposium on Heavy Vehicle Weights and Dimensions, Kelowna, British Columbia, 1986, pp. 363-380.
24. Cebon, D., "Examination of the Road Damage Caused by Three Articulated Vehicles," presented at 10th IAVSD Symposium on the Dynamics of Vehicles on Roads and on Tracks, Prague, Swets and Zeitlinger, 1987, pp. 65-76.
25. Cebon, D. and C. B. Winkler, "A Study of Road Damage Due to Dynamic Wheel Loads Using a Load Measuring Mat," SHRP-ID/UFR-91-518, 1991.
26. Gillespie, T. D. and M. W. Sayers, "A Multibody Approach with Graphical User Interface for Simulating Truck Dynamics," 1999-01-3705, 1999.
27. *TruckSim v3.2 Reference Manual*. Ann Arbor, Michigan: Mechanical Simulation Corporation, 1995.
28. Carey, W. N. and P. E. Irick, "The Pavement Serviceability Concept," *Highway Research Board Bulletin* 250, pp. 40-58, 1960.
29. Sayers, M. W., T. D. Gillespie, and C. A. V. Queiroz, "The International Road Roughness Experiment: A Basis for Establishing a Standard Scale for Road Roughness Measurements," presented at 65th Annual Meeting of the Transportation Research Board, Washington, D.C., 1986, pp.
30. Ksaibati, K., R. McNamera, W. Miley, and J. Armaghani, "Pavement Roughness Data Collection and Utilization," *Transportation Research Record* 1655, 1999.
31. OECD, "Dynamic Loading of Pavements," Road Transport Research, Paris 1992.
32. Cebon, D., *Handbook of Vehicle-Road Interaction*. Lisse, Netherlands: Swets & Zeitlinger, 1999.

33. "Guide for Mechanistic-Empirical Design of New and Rehabilitated Pavement Structures," American Research Association, Inc. NCHRP 1-37A, 2004.
34. Elkins, G., T. Thompson, A. Simpson, and B. Ostrom, "Long-Term Pavement Performance Information Management System Pavement Performance Database User Guide," Federal Highway Administration FHWA-RD-03-088, 2013.
35. Perera, R. W. and S. D. Kohn, "Quantification of Smoothness Index Differences Related to LTPP Equipment Type," Soil and Materials Engineers, Inc., Federal Highway Administration FHWA-HRT-05-054, 2005.
36. Merritt, D. K., G. K. Chang, and J. L. Rutledge, "Best Practices for Achieving and Measuring Pavement Smoothness, A Synthesis of State-of-Practice," FHWA/LA.14/550, 2015.